A Steady-state And Dynamic Model Of The Iron Blast Furnace.

A STEADY-STATE AND DYNAMIC MODEL OF THE IRON BLAST FURNACE

by

John Donald Oakey

A Dissertation

Presented to the Graduate Faculty

of Lehigh University

in Candidacy for the Degree of

Doctor of Philosophy

in

Metallurgy and Materials Science

Lehigh University

1970

CERTIFICATE OF APPROVAL

Approved and recommended for acceptance as a dissertation in partial fulfillment of the requirements for the degree of Doctor of Philosophy.

15 August 1970
(date)

Walter C. Hahn, Jr.
Professor in Charge

Stephen K. Jarby
Professor in Charge

Accepted, 15 August 1970
(date)

Special committee directing the doctoral work of Mr. John D. Oakey

Walter C. Hahn, Jr.
Co-Chairman

Stephen K. Jarby
Co-Chairman

Edward L. Resteth Jr

Alan W. Pense

W. E. Schmeiser

ACKNOWLEDGEMENTS

The author extends his sincere appreciation to Dr. Walter C. Hahn and Dr. Stephen K. Tarby, associate professors of Metallurgy and Materials Science at Lehigh University, for their unending encouragement and technical guidance and advice concerning the analysis of this work, and for their critical review of the manuscript. Gratitude is extended to Professors Alan W. Pense and William E. Schiesser and Dr. Edward Restelli for their advice and comments as members of the committee directing this investigation.

The author is also grateful to the National Science Foundation and the Lehigh Chemical-Metallurgy Program whose financial support made this work possible.

Deepest thanks are due to the author's family for their support and encouragement through many years of schooling. In particular, the author is deeply indebted to the unfailing patience and encouragement of his wife whose smiles throughout the course of this work served to ease many trying times.

TABLE OF CONTENTS

LIST OF FIGURES

LIST OF TABLES

ABSTRACT

A mathematical model of the iron blast furnace was constructed to predict the behavior of the furnace in steady-state operation as well as the time response of the furnace to step-changes in furnace operating parameters. The model is a completely general model, requiring no prior knowledge of furnace operation. Previous models have required large quantities of actual operating data from which furnace "characteristics" must be determined, and none could satisfactorily determine the temperatures and compositions of the slag and metal. The only information required in this simulation is the physical dimensions of the furnace, the flow rates, chemical compositions, and physical characteristics of the charge materials, and the conditions of the hot blast.

The temperatures and compositions of the slag and liquid metal phases were determined on the basis of the assumption that slag-metal equilibrium distribution is achieved for silicon, manganese, and sulfur in the furnace hearth. The agreement between model predictions and reported results with actual operating data is excellent.

The stack and bosh regions of the furnace were simulated based on the process dynamics of the operation-considering the kinetics of the important chemical reactions and the rates of heat transfer. In combination with the hearth model predictions on the steady-state operation of the furnace showed excellent agreement with the reported operating results.

A finite-difference approach was employed to introduce time for the dynamic model. Step changes in both flame temperature and blast moisture were introduced. For both cases tested the model indicates to the furnace operator that a new "steady-state" would be reached by the furnace in approximately 2 casts or 8 hours.

INTRODUCTION

Pig iron is the term applied generally to the metallic product of the iron blast furnace and is the intermediate form through which almost all iron passes in the manufacture of steel. In addition to being an intermediary between iron ore and steel, pig iron is also used in foundries for the manufacture of a wide variety of iron castings. The importance of pig iron to our technology can be seen in the fact that over 65,000,000 tons of pig iron are produced in the United States alone each year.

During the past half a century there has been a drastic change in the method of converting pig iron into steel. The pneumatic Bessemer process yielded to the open-hearth process, which in turn has given way to the widespread use of the very rapid basic oxygen furnace (BOF). Now, the longevity of the BOF may be shortened greatly by more continuous steel-making processes which are receiving increasing study and attention in the steel industry today.

Through the same period of time the iron blast furnace has remained supreme as the method of reducing iron ores to produce pig iron, and despite numerous attempts to develop alternative processes which replace the blast furnace as an iron producer or produce steel directly from the ore, iron blast furnaces still pierce the skyline of all our major steelmaking cities.

FURNACE CONSTRUCTION AND DESIGN

The blast furnace (see Fig. 1), itself, in which the pig iron

is produced is essentially a large stack with a crucible or hearth at the bottom of the stack in which the molten pig iron and slag are collected. The stack of the furnace is in the form of a truncated cone with steep sides. This cone consists of a welded steel shell inside of which are numerous layers of refractory brick. Inserted in the stack are cooling plates which are water cooled. The hearth or crucible at the bottom of the furnace is constructed of many layers of carbon brick surrounded by a hearth jacket of steel for support. The hearth area is externally cooled by the use of water-cooled cast iron segments called staves. Two openings in the hearth, a slag notch and an iron notch, permit the removal of the liquid slag and pig iron.

The hot air blast is introduced into the furnace through a series of cast copper, water-cooled nozzles known as tuyeres which are located at intervals around the furnace circumference at the top of the hearth. These tuyeres are supplied with hot air by the bustle pipe, a large refractory-lined pipe, which completely encircles the furnace just above the tuyeres.

The physical dimensions of the iron blast furnace are quite impressive, being greater than 130 feet from the base of the hearth to the charging equipment at the top of the stack, while the inside hearth diameters, especially on the new Japanese furnaces, are well in excess of 30 feet.

The blast furnace also has a number of pieces of auxiliary equipment associated with it. A series of brick-lined stoves is

Figure 1

A schematic diagram of the blast furnace showing the typical dimensions of the modern furnaces of today.

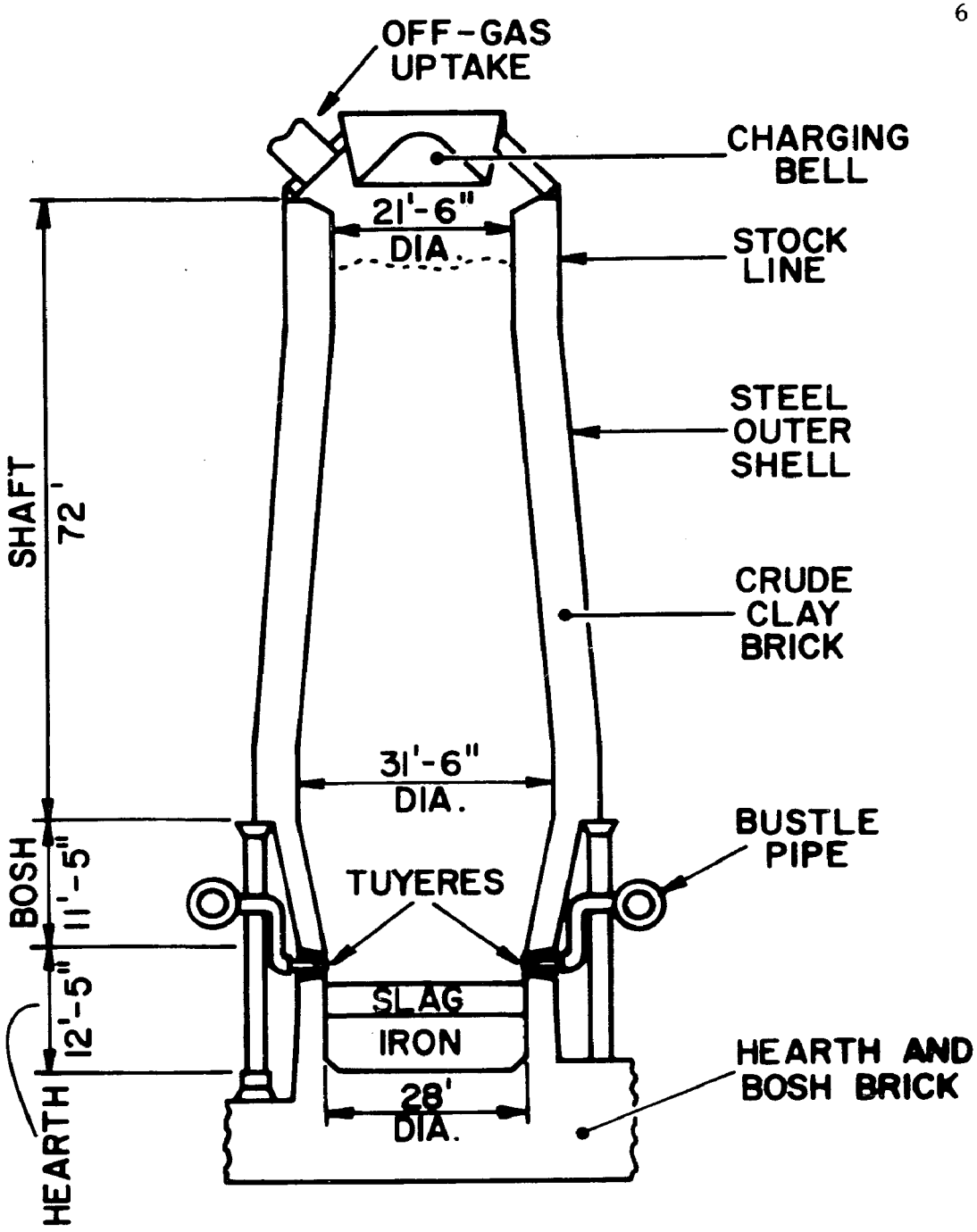
OFF-GAS
UPTAKE
CHARGING
BELL
21'-6"
DIA.
STOCK
LINE
STEEL
OUTER
SHELL
SHAFT
72'
CRUDE
CLAY
BRICK
31'-6"
DIA.
BUSTLE
PIPE
BOSH
11'-5"
TUYERES
SLAG
IRON
12'-5"
HEARTH
HEARTH AND
BOSH BRICK
28'
DIA.

utilized to heat the incoming air to produce the hot blast, large generating and blowing equipment is necessary to supply the great quantities of blast required by the furnace, dust catching and gas-cleaning equipment remove the dust and larger particles that are carried along with the gas exiting at the top of the furnace, and hoisting and weighing equipment for loading the skip cars and discharging their contents into the furnace are also required.

INCREASED FURNACE PRODUCTIVITY

A modern blast furnace and its auxiliary equipment costs in excess of $60,000,000 for its construction. Because of the high demand for pig iron, the almost prohibitive cost of erecting additional furnace facilities, and with no favorable alternative production methods on the horizon, it behooves the world's iron and steel producers to extract the maximum output of pig-iron from each and every furnace that is presently standing or on the drawing board.

The basic design and method of operation of these furnaces has remained constant for a great many years (the process was actually carried out to some extent over 500 years ago), but the productivity of the individual furnace has been dramatically increased through technical and engineering developments. The average furnace, in 1920, produced in the neighborhood of 350 tons of hot metal a day, while today's modern furnaces can produce in excess of 3000 tons of molten pig iron in a 24 hour period.

This increased productivity has been the result of numerous

refinements in furnace operation such as screened and sized burden materials, beneficiated and self-fluxing burden materials, high top-gas pressure operation, increased blowing rates for the hot air blast along with higher blast temperatures, and various other types of blast modifications such as steam, oil, natural gas, and coal injection at the tuyeres and oxygen enrichment of the blast.

As a result of the increased productivity of the furnace has come increasing complexity of the furnace operation due to the introduction of many new operating variables and parameters which must be controlled. The increased complexity of furnace operation has placed greater pressure on the furnace operator to run his furnace under the best working conditions and to exploit all the advantages of the new operating techniques to extract the utmost from his furnace.

THE BLAST FURNACE OPERATION

The iron blast furnace operates on a counter-current principle with solid materials charged into the furnace at the top of the furnace stack and the heated air blast injected into the furnace through the numerous tuyeres at the top of the hearth. (For more detailed discussion of the blast furnace operation see References 1-4). The heated blast entering the furnace combines with the hot coke in front of the tuyeres, liberating much heat and producing a highly reducing atmosphere. These very hot, reducing gases flow upward from the tuyeres into the stack heating the descending charge materials and reducing the iron oxides. The counter-current

operation permits the colder solid materials to extract considerable heat from the hotter ascending gases, and hence the blast furnace is, thermally, a relatively efficient metallurgical process. The gas exiting at the top of the furnace has some calorific value and is used later for preheating the air blast for the blast furnace and for other plant purposes. However, the use of expensive metallurgical coke to produce low-grade fuel gases is not an economical venture.

BLAST FURNACE CHARGE MATERIALS

The solid materials charged at the top of the stack include iron-bearing materials, coke, and limestone and/or dolomite. The iron-bearing materials may be any combination of raw iron ores, sinter, pellets, mill-scale, open-hearth slags, and some iron and steel scrap. Sinter and pellets are being used at an ever increasing rate as they allow greater throughput of iron. The function of the iron-bearing materials is obvious in that they supply the element iron which makes up approximately 93% by weight of the resulting pig iron.

The coke, being approximately 85% or better carbon by weight, combines with the heated air blast in front of the tuyeres, forming CO, producing a very large amount of heat for heating the charged solids, and a very reducing atmosphere for reducing the iron oxides. Coke also supplies the large amount of carbon which dissolves in the molten iron, amounting to between 4 and 5% of the pig iron by weight.

The limestone and/or dolomite act as fluxes, supplying the basic oxides, CaO and MgO, which help to produce a slag which is

sufficiently fluid and of the proper chemistry. Fluidity is vital to insure a free running slag when tapped from the furnace hearth and to prevent entrapment of molten iron droplets. The slag chemical composition controls the final composition of the metal, CaO and MgO in particular providing some degree of control of the sulfur content in the molten iron.

Although the furnace is a continuously operating process with the solid materials and hot air blast being fed to the furnace without interruption, the slag and metal are not allowed to run from the furnace continuously but are "tapped" at time intervals ranging upward from four hours.

CHEMICAL REACTIONS IN THE FURNACE

Since the entire objective of the iron blast furnace is to produce molten pig iron, the iron oxides entering the furnace must be reduced to elemental iron which is eventually converted to the molten state. A considerable percentage of the reduction of the iron oxides occurs in the stack portion of the furnace with the reduction brought about by the CO and H_2 in the ascending stream of gases.

The typical oxide of iron that is charged to the furnace is hematite or Fe_2O_3, although small amounts of iron may enter as Fe_3O_4 or FeO. Hematite is reduced by CO in steps or stages in the following sequence.

(1) $1/2\ Fe_2O_3 + 1/6\ CO \rightarrow 1/3\ Fe_3O_4 + 1/6\ CO_2$

(2) $1/3\ Fe_3O_4 + 1/3\ CO \rightarrow FeO + 1/3\ CO_2$ (above 570°C)

(3) $FeO + CO \rightarrow Fe + CO_2$,

with the overall net reaction being

(4) $1/2\ Fe_2O_3 + 3/2\ CO \rightarrow Fe + 3/2\ CO_2$.

Reaction (2) is marked above 570°C because above this temperature the wustite (FeO) form is the oxide with the lowest oxygen potential, that is the oxide requiring the gas of the greatest reducing power to reduce it to iron. Likewise, Fe_3O_4 is the oxide with the lowest oxygen potential below 570°C, and if the reduction were carried out below 570°C the sequence of oxides would be

(5) $Fe_2O_3 \rightarrow Fe_3O_4 \rightarrow Fe$.

If a gas is provided which will reduce the oxides of the lowest oxygen potential, it will reduce all other oxides present according to the sequences shown above. The reduction of Fe_2O_3 to Fe by CO (reaction 4) is slightly exothermic (liberates heat).

The same sequences of iron oxides are also produced by H_2 reduction, but in this case the overall heat effect is endothermic, meaning heat must be supplied in order for the reaction to proceed. The percentage of H_2 in the ascending gas stream is very small and the total amount of iron oxide reduction in the blast furnace by H_2 is very small relative to the amounts of reduction by CO. However, in recent years with the injection of fuel oils and larger amounts of moisture in the blast, the amount of H_2 in the gas stream is greater and the amount of H_2 reduction is also greater.

If equilibrium were attained between iron, iron oxide, CO, and

CO_2 in the blast furnace, the ratio of CO/CO_2 in the top gas would be approximately 0.65. In practice the gases coming off the top of blast furnaces have CO/CO_2 ratios in the range of 1.0 to 3.0, indicating that the gas is very much more reducing than the predicted equilibrium and full utilization of the reducing potential of the gas is not being made. As a result, the blast furnace operates at a coke rate per ton of iron that is higher than is theoretically necessary.

Another reaction that is of prime importance in the blast furnace is the thermal decomposition of the fluxstone, such as

(6) $$CaCO_3 \rightarrow CaO + CO_2.$$

This reaction occurs mostly in the temperature range of 800 to 1000°C. The decomposition of $CaCO_3$ and $MgCO_3$ is highly endothermic, using up large amounts of heat in the course of decomposition. Also, the liberation of large quantities of CO_2 gas due to the fluxstone decomposition reduces the CO/CO_2 ratio existing in that region of the furnace lowering the reducing power of the hot gas stream. As a result of these two drawbacks associated with limestone and dolomite, attempts are made to keep the amount of uncalcined fluxes entering the furnace to a minimum by the increased use of self-fluxing burdens, such as sinter.

The last reaction of importance in the stack region is the Boudouard or "solution-loss" reaction of

(7) $$C + CO_2 \rightarrow 2CO.$$

For the direction shown this reaction goes to an appreciable extent

in the high temperature regions of the stack, at temperatures of approximately 1000° C and higher. Although this reaction helps replenish the reducing power of the gas stream by production of additional CO, it is a highly endothermic reaction, using up considerable quantities of heat.

In the high temperature regions of the furnace, the lower portions of the stack and the bosh, the slag forming materials will begin to melt in the 1200-1300°C region and this sticky slag running over the remaining solid particles tends to eliminate further gas-solid oxide reduction and the "solution-loss" reaction. As a result, the remaining FeO melts and is then reduced by solid carbon,

(8) $FeO + C \rightarrow Fe + CO.$

This reaction is highly endothermic and tends to have a cooling effect on the high temperature regions of the furnace. Because of this large heat requirement, it is desirable to reduce as much of the ore by gaseous reduction as is possible, lowering the heat requirement in the bosh region of the furnace.

The major source of heat in the blast furnace is the reaction of the oxygen in the hot blast with the hot coke particles in front of the tuyeres,

(9) $2\ C + O_2 \rightarrow 2\ CO.$

This reaction is extremely exothermic, liberating large quantities of heat and at the same time producing the prime reducing agent of the blast furnace-CO.

The molten materials collect in the hearth of the furnace with the slag material, being lighter, floating on top of the liquid pig iron. In this region of the furnace SiO_2, MnO, and P_2O_5 are reduced by solid carbon,

(10) $SiO_2 + 2C \rightarrow Si + 2CO$

(11) $MnO + C \rightarrow Mn + CO$

(12) $P_2O_5 + 5C \rightarrow 2P + 5CO$

producing Si, Mn, and P which dissolve in the hot metal. All of these reactions are very endothermic.

The lack of equilibrium between the gases exiting the blast furnace and the charge of iron oxide or carbon is largely due to the extreme velocities of the ascending gas stream. These gases have a retention time in the entire furnace of somewhere between 5 and 10 seconds, and the rapid flow of gas allows little time for reaction with the solid materials in the charge column.

PROCESS SIMULATION AND COMPUTER APPLICATION

The development of high-speed electronic computers has had a tremendous impact on the modern way of life. Computers now handle, almost exclusively, banking and credit records, billing, payrolls, inventories, and all other forms of business for our fast moving economy. However, perhaps the most important contribution of computers has been to the scientific and engineering communities. The speed with which the modern computer can perform complex and/or repetitive, tedious mathematical operations has enabled scientists to solve and analyze an extremely complex problem, the scope of which

was prohibitive before the advent of the computer. From this expanded problem solving ability has come attempts to simulate or model mathematically very intricate industrial machinery and processes.

The ultimate goal of process simulation is direct control of the process itself. In on-line computer control the computer monitors the various inputs and outputs of the process and makes decisions and required corrections automatically. Before a process can be controlled a model describing the process must be constructed which will simulate the actual process very closely. To achieve this the process under consideration must be very well understood and the various aspects of it very well defined.

While much is known about the operation and intricacies of the blast furnace, it is not yet so thoroughly understood that accurate simulation models for the entire process have not been developed at this time. As a result, with no precise simulation models, on-line computer control of the iron blast furnace is still in the distant future.

In spite of the problems associated with blast-furnace simulation the complexities of the operation have stimulated numerous attempts to devise methods to assist the furnace operators with their difficult task of controlling the blast furnace. Nearly all of these approaches have incorporated assumptions, many or few, about some very basic aspects of the furnace operation, especially in areas where knowledge is very

scant. Most often the worth of the approach depends on the soundness of the basic assumptions.

PREVIOUS MODELS

The problem of modeling the blast furnace has been approached from many points of view with varying degrees of complexity. One of the most wide-spread approaches to assessing furnace operations has been the use of simple thermal or combination thermal and material balances for the entire furnace. Thermal balances for the blast furnace were developed and used long before the invention of electronic computers. Investigators such as Bell, Gruner, and Vatere employed heat balances as a method of blast furnace analysis as early as 1866. The thermal balance approaches have become increasingly complex as shown by the Poos and Decker[5,6] thermal balance which was designed to be easily adaptable to the computer for extremely quick calculation. These workers went beyond the classical heat balances and attempted to predict coke rates per ton of iron from their balance by estimating the amounts of ore reduction due to CO, C, and H_2. Although the technique of overall heat and mass balances helps in the understanding of the relationship between certain operating variables, the allocation of the various percentages of the total heat input into the furnace, and the fundamental thermochemical characteristics of the process, it has very little applicability in the prediction of the behavior or control of the process.

Statistical correlation of existing blast furnace data has

been carried out extensively by many investigators. One of the earliest approaches to the problem of relating the blast-furnace operating variables to production and coke rates was that developed by Marshall[7] who derived three equations consisting of rudimentary carbon balances, heat balances, and the relations between production rate, wind rate, and the carbon burned at the tuyeres. This appears to be one of the earliest attempts to achieve any success in relating prior furnace data to the prediction of furnace behavior under new blast conditions.

R.V. Flint,[8,9] using an approach based on multiple-correlation of blast furnace variables, has developed expressions which may be used to predict the changes in coke rate that will result from some changes in operating conditions-thus offering some usefulness for production planning. More recently, regression analysis by Pokvisnev[10] and Rebeko[11] enabled the relationships between the thermal state of the furnace and the composition of the pig iron to be made. Statistical approaches may have some usefulness in production planning and in anticipating furnace results under certain operating conditions.

The modeling approaches became more complex with the staged heat and mass balances or thermochemical approaches. Ridgion[12] developed a stagewise heat balance, designed for the computer, in which he assigned various furnace reactions to certain temperature regions and considered the heat requirement of the solid phase which he calculated in 50°C steps from 0° to 1500°C. The rate of

chemical reaction and hence the heat of reaction for each individual reaction are divided up equally over the temperature range in which the reaction is assumed to proceed. A further assumption made by Ridgion is that for each level in the furnace the gas temperature is higher than that of the solid. This latter assumption by Ridgion that the gas is always at a higher temperature than the solid is not in agreement with actual furnace observations.[13,14] The worth of such a model for predictive purposes, such as coke rate with changing operating variables, is very questionable with operating variables which are even only slightly changed from those of the base period for which the balance was constructed.

Lander, Meyer, and Delve[15] developed a thermochemical model based on a material and thermal balance of the furnace. The model was designed to predict how a given furnace would deviate in operation from a standard or reference state of operation when a change in one or more of the operating variables was effected. The furnace data from a reference operating state are required to determine a "furnace characteristic" which is dependent upon the calculated heat losses of the furnace. With this characteristic the furnace behavior can be predicted for operating variables which depart from the reference state.

Hodge and Wyczalek[16] also developed a thermochemical model for the furnace using a stagewise heat and mass balance to predict changes in furnace behavior with changes in operating parameters. Operating data from a "standard case" are required to determine

(a) the amount of heat transfer between the gas and solids in the shaft, (b) the amount of carbon consumed in direct reduction of iron oxide, and (c) the amount of hydrogen gas taking part in the reduction of iron oxide. With these values and the staged heat and mass balance, predictions of the furnace performance with new operating variables can be made. This type of thermochemical model which requires a "standard operating state" from which characteristic furnace constants are obtained has some useful applications when the new operating conditions of interest are only slightly removed from those of the "standard state", but for larger variations from the reference state operating conditions the predictions of the model may very well be on tenuous grounds.

Staib[17,18] and his co-workers at IRSID developed a relatively simple quantitative model of the blast furnace in which they divided the furnace into two portions- the upper portion called the conditioning zone and the lower portion termed the processing zone. In the conditioning zone the solid charge is preheated and the iron oxides reduced to wustite. The reactions involving large amounts of heat, such as the solution loss reaction, occur in the lower portion, or processing zone. The dividing boundary between the zones is assumed to occur within the thermal reserve zone (the zone where the solid and gas temperatures are the same) at the point where the chemical reserve zone (the location at which practically no chemical reaction takes place) exits. The

temperature of the gas leaving the conditioning region is assumed to be at about 1000°C and to be in equilibrium with the wustite phase.

The laws of conservation of mass and energy are applied to the processing zone and predictions on the changes in the performance of the furnace under varying operating conditions are possible. The problems inherent in this model are similar to those of the other thermochemical models mentioned above and, in addition, its application depends on the existence of the chemical reserve zone and the gas temperature associated with that region.

In an attempt to overcome the limitations associated with the above models, investigators have begun to study the process dynamics. Koump[19] and his co-workers devised a model of the furnace stack based on the kinetics of the reduction of iron ore and the solution-loss reaction and the rate of heat transfer between the gas stream and the solid particles of the packed bed. Koump only considered the reduction of iron and the gasification of coke- no consideration being given to decomposition of limestone (the burden was 100% self-fluxing sinter) or to hydrogen reduction of the ore as the gas was assumed to be composed only of N_2, CO, and CO_2. Koump was able to generate temperatures and composition profiles for the gas and solids in the stack, with the curves having the same general shape as those reported experimentally. These investigators concluded that the expected blast-furnace type of behavior occurs with only a very narrow range of operating

conditions. This model is not directly applicable to practical furnace conditions because of its oversimplifications. The model does point out, however, the promise that consideration of the process dynamics holds for the simulation of the blast furnace.

Lahiri and Seshadri[20] made a more detailed study of the stack region, similar to the Koump approach, in an attempt to make a more realistic model for blast furnace simulation. These workers did extensive analysis of the radial gradients of the gas compositions and temperature at each level in the furnace and averaged these quantities at each level to predict temperature and composition profiles for the gas and solids in the stack. As with the Koump model, the decomposition of limestone and reduction of iron oxide by hydrogen were not included in the model. The profiles for temperatures and compositions in the stack have the same general form as those of Koump, however it appears that this model, due to its simplification, is also not directly applicable to the predictions of practical furnace operations.

A more complex and realistic model of the stack portion of the furnace was developed by Muchi[21] and his co-workers in which the kinetics of the limestone decomposition, reduction of ore by hydrogen, and the heat losses to the furnace walls were also taken into consideration. The inputs and outputs of the stack model were derived from and compared with actual furnace operating data. Profiles of gas and solid temperatures, fractions of stone decomposed

and ore reduced, total gas pressure, and density of the charge and gas were generated for the stack region and the general shapes of the profiles agree well with theoretical and experimental results.

A few attempts have been made to predict the change in furnace operation with time due to a change in one or more of the operating variables of the furnace. One such approach was developed by IRSID[22]. However, the model is only good for predicting changes in performance around a specific initial working point or reference state. In addition, experimental data involving changes of the type to be predicted are required for the model. From these data changes in silicon composition of the hot metal were predicted for step-changes in the blast temperature, oil injection in the hot blast, and changes in the blast moisture.

Fielden and Wood[23] also derived a model to predict the transient response of the blast furnace to a change in the furnace inputs. This model is also designed to work around a reference state. The model is tuned to the particular reference state by choosing the proper reaction-rate constants to reproduce the reference-state furnace performance. The furnace is divided into zones based on the temperature of the solid charge with certain chemical reactions being assumed to occur in the various temperature zones. The time response is determined by dividing the furnace further into many thin slices and considering the conservation of mass and energy for each thin furnace slice.

OBJECTIVE OF THE PRESENT WORK

As can be seen from the above descriptions the approaches to the mathematical solution of the blast furnace are indeed numerous and varied. Heat balances have some limited usefulness for the furnace operator in that they can tell him where certain percentages of the available heat come from and how the heat is distributed in the furnace. However the heat balance alone does not enable the furnace operator to make accurate predictions on his furnace behavior under different operating conditions.

The thermochemical models mentioned also have limited applicability to the furnace operator because of the limitations discussed above. These same limitations apply to the models designed to predict transient responses. If the new operating conditions are not close to the original conditions the transient response predictions may be on very tenuous grounds. The objective of this work is to develop a mathematical model of the blast furnace for both the steady-state and dynamic situations, considering the dynamics of the process within the limits that the present knowledge of the furnace operation permits. The model is to be general enough to apply to any blast furnace and not be dependent upon great quantities of prior operating data to serve as a reference point.

The steady-state model of this type would prove invaluable to the furnace operator as an aid to production planning and for studying the various effects of different operating parameters

on the furnace behavior. This model would give many insights into the process and the relationship of the process variables without costly and time-consuming trials on actual operating furnaces.

The dynamic model would indicate the time response of the furnace to a change in operating parameters and perhaps eventually lead to direct control of the blast furnace operation.

MODEL APPROACH

As discussed above, the blast furnace process involves numerous chemical reactions and various modes of heat and mass transfer. Because of the different modes of heat and mass transfer that occur as the descending burden materials undergo melting, and that certain chemical reactions are more important in some regions of the furnace than in others, it is not possible to describe the entire process with one model approach. As done by Hodge, Staib, and other investigators, the furnace is divided into discreet regions, three in this case, with various degrees of difference between the models used to describe each section.

The three regions are (1) the stack, (2) the bosh or intermediate region, and (3) the hearth region. The stack and the bosh regions are handled by a kinetic approach, attempting to describe the dynamic processes involved in these regions as realistically as possible by considering the rates of the various chemical reactions and the rates of heat transfer between the gases and the descending charge materials. A thermodynamic equilibrium argument is applied to the hearth region to predict the final metal and slag chemical compositions and temperature. The three regions are discussed in more detail below.

STACK REGION

The stack region model for the furnace considers the volume of the furnace from the stockline (the height in the stack at which the top of the solids column is maintained) to the plane

lower down in the stack where the temperature of the solids reaches 1673°K (the significance of 1673°K is discussed below).

In this region of the furnace are considered

(1) the rate of heat transfer between the solid charge materials and the ascending gases,

(2) the rate of heat loss from the gases to the furnace walls,

(3) and the reaction rates for six chemical reactions and the heats of chemical reaction associated with them.

Along with the above considerations certain assumptions have been made to facilitate the calculations for the model. Without these assumptions a great deal of additional complexity would be involved in the model. These assumptions are:

(1) All solid particles at a given level of the furnace have the same temperature.

(2) Each particle, regardless of material or size, has a uniform temperature throughout the particle volume. No temperature gradients exist within an individual particle.

(3) The gas stream, at a given level of the furnace, has a uniform temperature and composition. Thus no radial gradients of temperature or composition exist within the gas stream.

(4) At a given furnace level, all particles of a particular type of solid are in the same chemical state. As an

example this means that all ore particles at this level are in the same state of reduction or that all limestone particles have the same fraction decomposed.

The second assumption is quite reasonable for actual furnace operation. The very high rates of heat transfer and the relatively small solid particles that are charged into the furnace would tend to eliminate any temperature gradients within an individual particle. On the other hand, assumptions (1), (3), and (4) are an oversimplification of the actual conditions in the furnace. Large radial gradients have been found to exist in furnace operations for both gas and solid with respect to temperature and composition. These large gradients have been eliminated to an extent by the use of more uniform-sized burden which tends to prevent extensive channeling of the gas and produces a more uniform distribution of solid particles in the furnace.

The chemical reactions that are taken into account in the stack are indirect reduction of iron ore by CO, the solution-loss reaction, the decomposition of limestone, indirect reduction of iron ore by H_2, the reaction of coke with steam, and the reaction of CO with steam. The overall reaction rates that Muchi developed and employed in his stack model are utilized to describe the rate for the various reactions taken into consideration.

STEADY-STATE STACK MODEL

(A listing of variables and additional details concerning Eqs. (13-23) as well as the rate of chemical reaction for the

stack and bosh regions are given in Appendix A.)

On the basis of the above assumptions and the additional assumptions that the furnace is operating in a steady-state condition (there is no fluctuation of the furnace operation or performance with time), and that the volume rate of flow of solid particles and the fractional void in the bed are constant throughout the bed, a mathematical model for the bed between the stockline and the level where 1673°K is reached by the solids was constructed. This model considers heat, mass, and force balances for gas and solid particles around the differential height of the bed dz at any position z below the stockline of the furnace. The result of these balances is nine differential equations and two algebraic equations which must be solved simultaneously.

These equations are

(13) $dx/dz=22.4A_z[(\zeta+\xi x)(R^*_1+R^*_3)+(x-2)R^*_2+xR^*_4+(x-1)R^*_6]/F$

(14) $dy/dz=22.4A_z[(\zeta y-\tau)(R^*_1+R^*_3)+(y+1)R^*_2+(y-1)R^*_4+yR^*_6]/F$

(15) $dw/dz=22.4A_z[\xi w(R^*_1+R^*_3)+wR^*_2+wR^*_4+R^*_5+(w-1)R^*_6]/F$

(16) $d\rho_b/dz=-A_z[(16+12\xi)(R^*_1+R^*_3)+12R^*_2+44R^*_4+16R^*_5+12R^*_6]/F_s$

(17) $df_s/dz=A_z(R^*_1+R^*_3)/3F_sC_{HO}$

(18) $df_1/dz=A_zR^*_4/F_sC_{LO}$

(19) $dp/dz=-f_k(1-\varepsilon)G^2p°T/g_c\varepsilon^3d_p\rho T°p$

(20) $dT/dz=A_z(22.4Cq_2T+q_3)+\pi D_zU(T-T_{we})/\rho F(C+TdC/dT)$

(21) $dt/dz=A_z(q_3+C_stq_5+q_4)/\rho_bF_s[C_s+tdC_s/dt]$

(22) $w=xK_7Con/F(xK_7+y)$

(23) $Con=F(w+v)$

The differential Eqs (13-21) are solved by the Runge-Kutta

numerical method by marching down the furnace column, beginning at the stockline. By using this technique the profiles of x,y,w,v, T,t,ρ_b,p,f_l, and f_s can be generated as a function of the distance down the stack from the stockline. The value of w is modified according to Eq. (22) and the value of v is determined through Eq. (23).

The Runge-Kutta method of solution for such systems of differential equations is a very powerful tool. It permits larger step sizes than the simple Euler method and the local and total truncation errors are of the order of h^5 and h^4 respectively, where h is the increment in z or step-size.

The stack model is terminated at the level at which the charge materials reach a temperature of 1673°K. At 1673°K, it is assumed that any FeO remaining unreduced melts, and that all the charge materials, with the exception of the coke particles, are molten. In actuality, some of the slag forming materials may begin to melt as low as 1400°K, but no melting is assumed to occur above 1673°K. Once the 1673°K level is reached by the charge, the stack model gives way to the model for the intermediate or bosh region.

INTERMEDIATE REGION

The intermediate region of the furnace consists of the furnace volume below the plane at which 1673°K is reached by the charge materials and the plane at the level of the tuyeres.

This region of the furnace is probably the least understood

region of the blast furnace. The physical relationship between the gas and charge materials is not nearly as clearly defined as for the stack region of the furnace. In this region extensive melting of the slag forming, iron, and iron ore materials occurs with the eventual disappearance of all solid particulate material with the exception of the coke which remains solid until it reacts with the air blast at the tuyeres.

The heat and mass transfer in this region becomes quite complex with all combinations of gas-solid, gas-liquid, and liquid-solid reactions and transfer possible. Such a physical situation is extremely difficult to describe and to facilitate the approach to this region it is assumed that no further gas-solid chemical reactions take place. The reasoning is that when melting occurs the molten material will run down over the remaining solid particles (mostly coke) and the liquid, which is probably quite viscous, forms an "insulating" barrier, around the particles thus preventing further gas-solid contact and chemical reaction. As a result the reactions that were considered in the stack region now have zero reaction rates. The one chemical reaction that is considered in this portion of the furnace is the reduction of the remaining liquid FeO by solid carbon. This reaction can be pictured to proceed quite readily because of the intimate liquid-solid coke particle contact that occurs.

The assumptions that were made for the stack model concerning radial gradients of temperature and composition for the gas and

charge materials also hold in this region of the furnace. For the charge materials, the remaining solid particles and the liquid phase which covers the particles are at a uniform temperature at a given furnace level. The differential equations describing the various profiles for the stack region are also considered, except the only chemical reaction rate that is not now zero is the reduction of liquid FeO by solid carbon.

At the initial portion of the intermediate region it is assumed that the charge materials undergo an isothermal hold at 1673°K until all remaining FeO has been reduced. At this temperature level all of the heat that the gas transfers to the charge materials is used to enable the reduction, which is a very endothermic reaction, to proceed. In this manner the rate of reduction is directly dependent on the rate at which heat is supplied by the gas. When all the FeO is melted, the charge materials then resume converting the heat transferred by the gas into an increase in temperature, no heat being consumed or liberated by any further chemical reactions.

The bosh model continues to predict the profiles of the important variables as in the stack region until the tuyere level of the furnace is reached. At the tuyere level the temperature of the charge materials is considerably higher than the temperature at which the slag and metal are tapped from the furnace. This additional heat possessed by the charge materials is consumed by the extensive heat losses through the hearth of the furnace and any

additional heat that is required for the necessary chemical reactions that occur between the slag and metal droplets in the hearth of the furnace.

HEARTH REGION

(For a listing of the symbols and variables used to describe the chemical composition of the metal, as well as an example of the calculations, see Appendix B.)

The end product of the iron blast furnace is not pure iron, but a metal which is completely or almost completely saturated with carbon and contains varying amounts of manganese, phosphorus, silicon, and sulfur which are introduced into the furnace as compounds in the normal furnace burden. If a given blast furnace model is to be worthy of merit it must, of course, be able to predict with a reasonable amount of accuracy the composition of the molten pig iron which collects in the furnace hearth. Although many of the general trends concerning the metal compositions are well known-such as increasing metal temperature promotes silicon recovery in the metal and high slag basicity promotes silicon and sulfur removal into the slag and increases the manganese recovery in the metal-the means of accurate composition predictions do not appear to be available to blast furnace operators.

In order to get a better insight into the problem, consider the physical situation which exists in the hearth of an operating blast furnace (Fig. 2). Between furnace tappings the pool of molten pig iron is collected in the bottom of the hearth on top of which

Figure 2

A schematic diagram of the hearth region of the blast furnace illustrating the physical relationship between the tuyeres, slag and metal bath layers, and the column of coke particles extending through the bath to the hearth bottom. A typical temperature profile is also shown.

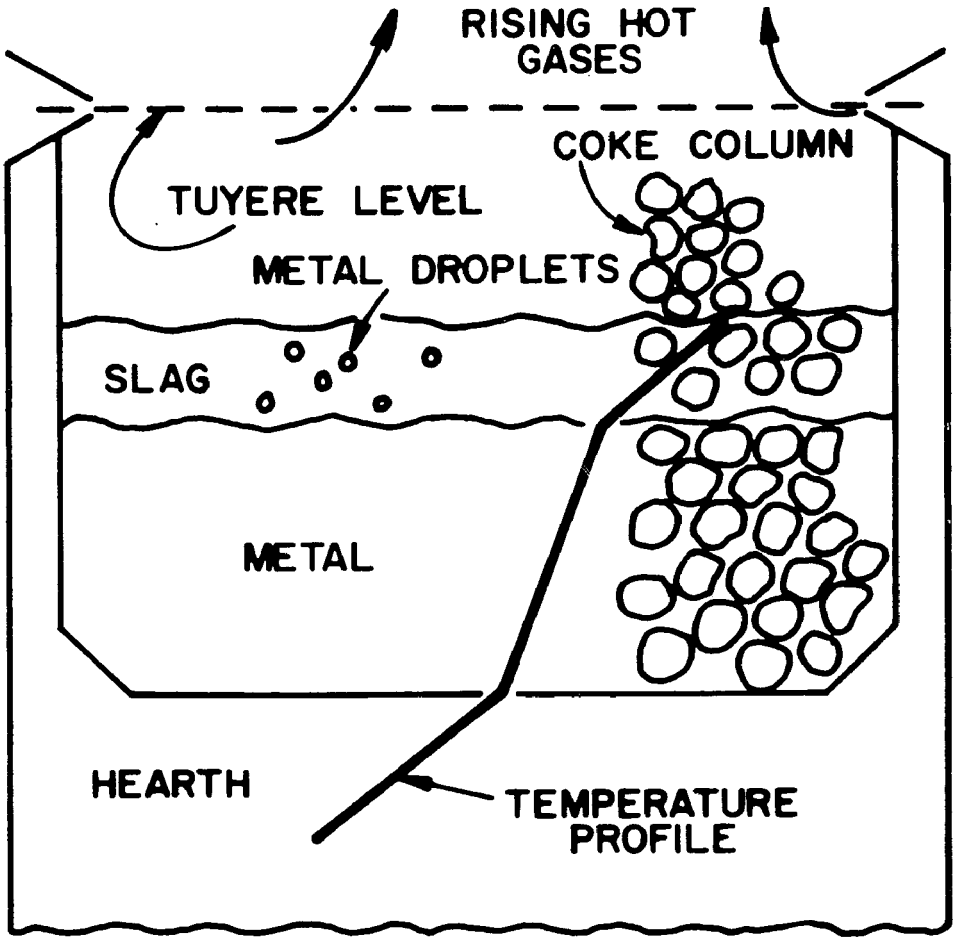
RISING HOT GASES
COKE COLUMN
TUYERE LEVEL
METAL DROPLETS
SLAG
METAL
HEARTH
TEMPERATURE PROFILE

collects and floats the liquid slag, the distinct separation of the layers being due to the difference in the specific gravities of the slag and metal.

The layered bath is relatively quiescent, being disturbed only by the metal droplets falling through the slag layer and entering the metal. Not having the benefit of metal and slag mixing due to violent gas generation, such as in the case of the open-hearth or basic oxygen furnaces, the slag and metal layers in the hearth of the blast furnace are in contact only on a planar interface. Also, as a consequence of the stagnant nature of the bath and the heat losses through the hearth of the furnace, a temperature gradient is established with the temperature decreasing from the top to the bottom of the bath (Fig. 2). As a result of this temperature gradient, circulation of the metal and slag by thermal convection currents is very limited.

It has been generally accepted that the hot metal composition is determined by the kinetics of the transfer of the elements across the slag-metal interface[2], and that the thermodynamic equilibrium for distribution of the various elements between slag and metal is not obtained.

Laboratory studies of blast furnace type slag-metal reactions have almost invariably been carried out at ambient pressure with stagnant metal and slag layers. An example of such work is that of Filer and Darken[24], who remelted actual blast furnace metal and slags in an effort to equilibrate them. Their physical set-up

consisted of very small amounts of slag and metal remelted in a graphite crucible with one atmosphere pressure of CO. The slag and metal were permitted to equilibrate with time at temperature under these conditions. From their work Filer and Darken concluded that by no means was complete equilibrium achieved in the blast furnace, but perhaps equilibrium was achieved by the reaction between manganese and sulfur in the liquid metal and also by the silica reduction reaction if the metal-slag temperature in the furnace (which was unknown) was at 1450°C.

Burgess and Baldwin[25], studying the manganese distribution between the slag and metal, found the actual ratio $(X_{MnO})/[X_{Mn}]$ to be 0.85 at 1505°C with the ratio of CaO/SiO_2 of 1.2 in the slag. Using one atmosphere pressure, their equilibrium calculations produced a ratio of $(X_{MnO})/[X_{Mn}]$ of about 2.7 for equilibrium. These equilibrium calculations are even farther from the actual distribution if it is argued that, although the gas pressure in the hearth of the furnace is greater than one atmosphere, the carbon monoxide partial pressure is less than unity and in the vicinity of 0.7 to 0.9 atmospheres. Work by Hatch and Chipman[26] showed that the sulfur distribution ratio of (%S)/[%S] using equilibrium calculations based on one atmosphere pressure were 2 to 5 times as great as the distributions which are actually obtained with comparable slag basicities in the blast furnace.

As a further argument against the attainment of equilibrium between slag and metal consider a reaction at the slag-metal

interface where it is felt by many that the slag-metal reactions occur. When a reaction involves the transfer of an element across such an interface, a layer on one side of the interface tends to become saturated with the element in question, while the layer on the other side of the interface becomes depleted of the same element. For additional transfer across the interface there must occur replenishment of the depleted layer from the bulk material on that side of the interface and/or depletion of the saturated layer on the other side of the interface. Due to the lack of bath agitation in the blast furnace hearth this needed replenishment and/or depletion in the boundary layer must be brought about by diffusion of the species in the slag and metal layers. However, even at the high temperatures encountered in the hearth region the rate of transport is relatively slow. The diffusion coefficients for solutes in liquid carbon-saturated iron melts are in the range of 10^{-4} to 10^{-5} cm^2/sec, while the corresponding rates in typical blast furnace slags are even an order or two of magnitude lower.

Because of the experimental results cited above as well as the indicated slowness of species movement in the slag and metal layers, it is easy to see why it is assumed that equilibrium is not achieved and that the compositions of the slag and metal are indeed the result of the kinetics of the mass transfer in the boundary layers of the slag and metal.

Returning to the physical situation occurring in the hearth

of the blast furnace (Fig. 2), it can be seen that any metal droplets entering the hearth region must pass through the slag layer covering the molten metal pool. Due to the smallness of these metal droplets a very large surface area to droplet volume ratio is created and it is reasonable to expect that a considerable amount of chemical reaction would occur between the slag and the finely divided droplets. Also, the droplets would provide their own "stirring", in that by their very movement through the slag regions of saturation or depletion of a given species are left behind and do not hinder additional reaction. Also, the droplet size is small enough so that the length of diffusion path in the droplet is quite short. Once the droplet has passed through the slag layer and entered the metal bath it is reasonable to assume that no significant amount of chemical reaction can continue due to the quiescent nature the bath.

Although the experimental results indicate that equilibrium is not reached between the slag and metal, it is the thinking of Philbrook and Manning[27] that equilibrium between slag and metal is approached if the correct factors relevant to the various reactions are considered. All of the chemical reactions that will be subsequently considered involve the formation of CO gas and it is the contention of Philbrook and Manning that the effective pressure opposing the reactions is that pressure against which the bubbles of CO have to grow-the absolute pressure existing at the slag-metal interface which is the absolute pressure in the furnace

above the slag layer plus the static pressure produced by the slag layer above the location where the chemical reaction occurs. Because the blast furnace is an open, dynamic system, rather than a static system in which all phases would ultimately come to equilibrium, the actual partial pressure of CO existing in the bosh gas above the slag layer is not relevant to the chemical reactions under consideration.

In this region of the furnace there is no shortage of surfaces on which the resulting CO bubbles can nucleate due to the column of coke extending through the slag and metal to the bottom of the hearth. Philbrook and Manning estimated the absolute pressure on the droplets by allowing for a few psi drop in the tuyeres, connections, and bustle pipe, plus an increment for the head of slag in the furnace, and arrived at an approximate value of 2.5 atmospheres as a reasonable figure for a furnace operating with normal top pressure.

In summary of this argument, it is felt that due to the large surface area to volume ratio between the metal droplets, and the slag, and the abundance of pores available for gas bubble nucleation, equilibrium slag-metal distribution is attained or closely approached in the hearth of the blast furnace. The pressure against which the gas bubbles must form is the absolute pressure existing at the slag-droplet interface-in the neighborhood of 2.5 atmospheres, not 1.0 atmosphere as used in the laboratory work discussed earlier. Thus, the slag and metal compositions can be

predicted for given temperatures and burden, if the necessary thermodynamic data are available.

THE IMPORTANT HEARTH CHEMICAL REACTIONS

Carbon Solubility

It has been found that the basic irons (made with basic slags) become saturated, or very nearly so, with carbon in the hearth of the blast furnace. This can reasonably be expected due to the column of coke which has been found to extend through the liquid slag and metal layers to the bottom of the hearth.

Numerous detailed studies of the effects of the various elements normally encountered in pig iron on the solubility of carbon in the iron have been carried out by Elliott, Gleiser, and Ramakrishna,[28] Newman and Schenck,[29] Schenck, Frohberg and Steinmetz,[30] Feldman,[31,32] and Skiredj and Elliott.[33] From these, Philbrook and Manning[27] selected the following temperature and compositional dependence of carbon solubility in iron as being a good representation within the composition ranges typical of most North American hot-metal practice:

(24) $[\%C]_{SAT}=1.28+0.00142(T°F)+0.024[\%Mn]-0.304[\%Si]-0.31[\%P]-0.37[\%S]$

Silicon Distribution

The reaction of interest concerning silicon in the blast furnace is

(10) $SiO_2+2C=Si+2CO$

A number of investigations and interpretations concerning

the activity of silicon in liquid iron and Fe-C-Si melts were published in a short period of time.[34-38] There now appears to be agreement on the values of γ_{Si} within a factor of 2 or 3 at the low silicon compositions where unfortunately, direct experimental measurements are meager. The work of Turkdogan, Grieveson, and Beisler[35] lends itself well for application to the low silicon range of carbon-saturated iron melts and their work is in relatively good agreement with that of Bowles, Ramstad and Richardson.[36]

Activities of silica in blast furnace type $CaO-MgO-SiO_2-Al_2O_3$ slags can be derived from experimental values arrived at by equilibrating silicon in iron with SiO_2 in the slag. The resulting activity of the SiO_2 depends on the activity coefficients selected for silicon in iron melts, and as a result there still are large differences in the reported activities of SiO_2 in blast-furnace type slags.

The work of Rein and Chipman,[39] along with the determination of Kay and Taylor,[40] serves as a comprehensive study on the equilibrium of silicon in carbon-saturated iron with various slag compositions at one atmosphere pressure of CO and given temperatures.

Sulfur Distribution

Fincham and Richardson[41] established the thermodynamics of the desulfurization reaction and their treatment agrees nicely with the ionic theory of slags. The addition of a sulfide ion to the slag is accompanied by removal of an oxide ion from the slag,

however, the sulfur can not replace oxygen that is linked singly or doubly with silicon atoms. The ability of a slag to remove sulfur from the metal and hold it in the slag is dependent on the supply of O^{-2} ions present in the slag and the activity coefficient of the sulfur in the metal. The quantity C_s, called the sulfur capacity, was introduced by Fincham and Richardson to describe the ability of a slag to retain sulfur. C_s, an experimental quantity, depends on the slag composition and the temperature and is defined as

$$(25) \qquad C_s=(\%S)(p_{O_2}/p_{S_2})^{1/2}$$

from work on gas-slag equilibria.

The sulfur distribution depends on the two reactions

$$(26) \qquad C_g+1/2O_2 \rightleftarrows CO, \qquad K_4=p_{CO}/p_{O_2}^{1/2}$$

$$(27) \qquad 1/2S_2 \rightleftarrows \underline{S}, \qquad K_5=f_s[\%S]/p_{s_2}^{1/2}$$

C_s can be related to slag-metal equilibrium by simple algebra as

$$(28) \qquad (\%S)/f_s[\%S]=C_sK_4/p_{CO}K_5$$

The quantities f_s, K_4, and K_5 can be determined from thermodynamic data given in references 41-48. Values for C_s, determined experimentally by several investigators, are available in references 48 and 49.

Phosphorus Distribution

It has been found in practice that virtually 100% of the phosphorus that enters the blast furnace with the burden leaves the furnace in the hot metal. The conditions in the hearth are

very reducing and the temperatures sufficiently high such that virtually all the P_2O_5 is reduced, the phosphorus content of the slag being negligible.

Manganese Distribution

Regarding the distribution of manganese between hot metal and slag, Philbrook[50] concluded that an entirely satisfactory basis for predicting the manganese content of hot metal as a function of slag composition is not yet available. He attempted to use the data of Neumann and Schenck[51] to predict the manganese distribution and concluded that manganese distribution could be predicted from these data within $\pm$ 50% and that the pressure corrections for the absolute pressure in the furnace was on a sound basis. However, he later felt that the values for log $\gamma_{Mn}^{(Si)}$ and log γ_{MnO} should not be accepted as correct measures of these properties but only as mathematical devices for correlating the data. The Neumann-Schenck[51] data were collected from manganese distribution studies between metal and slags composed of $CaO-SiO_2-MgO-Al_2O_3$.

Filer and Darken,[24] through their remelting experiments, found the ratio (MnO)(S)/[Mn][S] to be constant for a given temperature and slag composition. From the determined sulfur distribution the manganese distribution could then be determined using the appropriate constant for the temperature and slag composition of interest.

Bodsworth has collected data for the value of γ_{MnO} as a

function of CaO/SiO_2 (wt.%) from various manganese distribution investigations.[52-54] The MgO and Al_2O_3 contents of the slags have been neglected in this collection because it had been reported that the effect of MgO, as well as that of Al_2O_3, on the manganese distribution is very small. Bodsworth regards the values of γ_{MnO} as minimum values. These values were calculated assuming a constant γ_{Mn} value in the metal, thus neglecting the metal compositions that accompanied the various slags.

Once the value of γ_{MnO} has been determined, the value of γ_{Mn} can be determined from the metal composition and interaction coefficients and the manganese distribution can be predicted.

PREDICTION OF SLAG AND METAL COMPOSITION AND TEMPERATURE

After the charge materials have passed the tuyere level of the furnace and enter the hearth region, they are assumed to receive no additional heat from the gases due to radiation or convection. Thus all hearth heat losses are supplied by these "super-heated" materials as they cool down. All required heats of chemical reaction are also supplied by these materials. The reductions of SiO_2, P_2O_5, and MnO require considerable heat as do the formation of carbides in the metal and sulfides in the slag. This heat requirement is off-set somewhat by the slag formation which liberates large quantities of heat.

The final slag and metal chemistry and temperature result from a balance between the heat required for the chemical reactions

to produce the metal composition predicted by the thermodynamic equilibrium and the heat available due to the slag formation and the further cooling of the charge materials. The slag temperature is the controlling temperature for the chemical reactions since the reactions are assumed to occur at the interface between the metal droplets and the slag as the droplets fall through the slag layer. The metal is assumed to be tapped from the furnace at 30°K lower than the slag due to the temperature profile shown in Fig. 2.

The hearth model predicts the carbon, manganese, silicon, sulfur, and phosphorus contents of the metal as well as the SiO_2, MnO, CaO, Al_2O_3, S, and MgO composition of the slag.

OVERALL FURNACE MODEL

Steady-State

Now that the three regions of the furnace have been described in detail it is possible to examine how they work together when assembled.

It is assumed that the furnace dimensions are known along with the flow rate, temperature, and amounts of injection in the blast, as well as the flow rates of the various solids and their chemical compositions and particle sizes.

The information that is not known and which the steady-state model predicts concerns the furnace outputs. These outputs are the temperature and composition of the metal tapped from the hearth and the temperature and chemical make-up of the gas exiting at the top of the furnace.

The first step is to calculate the adiabatic flame temperature that the blast conditions produce at the tuyeres. This serves as an aim temperature for the gas as the temperature profile is predicted down the furnace.

Since the top gas conditions are unknown, values are initially chosen for these conditions and the model is run to the tuyere level using the stack and bosh models. The validity of the values chosen for the top gas as well as for the heat losses is checked by comparing the gas temperature predicted at the tuyere level with the flame temperature calculated initially and through an overall heat balance and carbon and oxygen balances for the entire furnace.

The hearth model acts upon the superheated charge materials and determines the final chemistry and temperature of the liquid phases.

If the gas temperatures do not agree well at the tuyeres, and/or if the overall heat and mass balances do not agree well, new conditions are chosen for the top gas until all the balances are satisfied.

DYNAMIC MODEL

The prediction of the response of the blast furnace with time to a change in one or more of the furnace operating parameters has proven to be quite a task as witnessed by the scarcity of reported attempts in the literature. Such predictions are necessary before the direct control of the blast furnace process can be implemented.

The problem arises due to the physical situation that exists in the furnace volume between the tuyere level and the stockline. The gas phase moves through this large volume of packed bed in a matter of mere seconds (in the furnace under consideration the gas travels the distance from the tuyeres to the stockline in under 10 seconds) while the charge materials pass through the same volume in a matter of hours (approximately 7 hours for the furnaces under consideration). On a smaller scale, if a volume element of the stack 0.5 meters high is considered, the gas residence time is of the order of 0.2 to 0.3 seconds while that of the solid materials is approximately 7 to 8 minutes.

In order to achieve a good reading on the gas phase response within such a relatively small volume element, time intervals of 0.1 to 0.2 seconds are necessary. In the same small time interval the solid materials within this small volume element show no appreciable change in the chemical or thermal state. The few reports available[22-23] concerning the blast furnace time response indicate the furnace approaches a new steady-state in the order of hours (or even days) and to march along in time from the existing steady-state to a new one by time jumps of 0.1 to 0.2 seconds requires a tremendous number of calculations to achieve a few hours time of furnace simulation. Even with the speed of today's electronic computers this number of calculations would tie up the fastest computers for a prohibitive amount of time. (Using a finite difference approach to the problem, only a few seconds of furnace

time could be simulated in one minute of computer time with time intervals of 0.05 to 0.1 seconds.) In order to avoid this problem, a number of assumptions were made and these are discussed below.

Method of Solution

The overall method of solution involves division of the furnace into two regions (as opposed to three in the steady-state model)-(1) a lower region or hearth and (2) an upper region encompassing the volume between the tuyere level and the stockline (the sum of the stack and bosh regions of the steady-state model). The upper region is sub-divided into numerous horizontal slabs or slices 0.5 meters in thickness.

It was found by writing heat and materials balances around such a slab that at any level in the furnace the gas temperature and composition responded so rapidly to an impulse that if the thermal and chemical conditions of the charge materials are held constant the gas temperature and composition achieve a new "steady-state" within an extremely small period of time-in less than 1 second. Within this same period, less than 1 second, the thermal and chemical conditions of the charge materials show no detectable change, so that in essence while the gas is reaching a new "steady-state" the conditions of the charge materials are constant.

Based on these findings, it is assumed that the conditions of the charge materials remain constant at any level of the furnace for a period considerably longer than 1 second, while in this same period the gas conditions reach their new "steady-states" at all

furnace levels. The period of time selected for the charge materials to remain constant is 1 minute. Thus, the furnace conditions are updated at each level at time intervals of 1 minute and with the selection of such a time period the charge materials exhibit detectable responses.

With the above assumptions concerning time an hour of furnace time can be simulated by only 60 cycles or time steps of the computer program as opposed to 36,000 cycles required by moving along in time with 0.1 second intervals.

For the parameters of interest-CO, CO_2, H_2, and H_2O composition of the gas stream, temperatures of the gas and charge materials, fraction of iron ore and limestone decomposed, and density of the charge materials-the appropriate balances were written around each of the subdivisions of the upper region of the furnace. As an example, a typical balance is that for the energy of the charge materials which balances the flow of heat into the volume element due to movement of materials into the top of the element and heat transfer from the gas to the charge materials against the flow of heat out due to movement of materials from the bottom of the element and chemical reactions that occur within the volume element.

The chemical reactions that are considered are the same as those considered in the steady-state model with the exception of the reaction between $CO + H_2O \rightleftharpoons H_2 + CO_2$ which is not taken into consideration. Also, the assumption concerning reactions above

1673°K holds with only the reduction of liquid FeO by solid C occurring above 1673°K. The reaction rates for all of the reactions considered are determined by the same expressions exployed in the steady-state and discussed in more detail in Appendix A. The method for calculating the rate of heat transfer and the values used for the properties of the gas and charge materials and also the same as those of the steady-state (see Appendix A).

Two additional assumptions made for the dynamic model are that the rate of heat loss by the gases to the furnace walls is the same as that existing at the same level in steady-state and the total pressure is the same at each level as that of the steady-state.

Hearth Region

The function of the hearth region is the same as that of the steady-state model. The hearth model calculates the final temperature of the slag and metal as well as the compositions of the slag and metal phases. The one difference in the dynamic model is that successive droplets of metal enter the hearth region at different temperatures and as a result the temperatures of the slag and metal pools change with time.

The temperatures of the slag and metal pools are determined by keeping a running average of the droplet temperatures at each 1 minute interval. The heat losses in the hearth region are assumed to be the same as those that occurred in the steady-state.

The slag and metal compositions are determined by the equilibrium considerations discussed in Appendix B with the instantaneous temperature of the slag controlling the equilibrium. The pressure that obtained in the hearth region in the steady-state is assumed to hold in the dynamic model also.

MODEL RESULTS

SLAG AND METAL CHEMISTRY

The hearth model for predicting the chemical compositions of the slag and metal was tested on some actual blast furnace data for which reasonably good chemical analyses of the charge materials was available.

The first of these trials shows the variation in the composition of the metal in Si, Mn, and S as the absolute pressure governing the reactions is varied between 1.0 and 5.0 atmospheres at a constant temperature. (Figs. 3-5) indicate the effect of the pressure change for the charge data reported in Table I for a slag temperature of 1800°K. The silicon and manganese contents of the metal decrease appreciably with increased pressure, the silicon showing a greater sensitivity. The sulfur composition, on the other hand, shows an increase with increasing pressure in the furnace hearth. All of these trends are in agreement with the reported experimental work discussed earlier and the examples carried out in Appendix B.

The reported compositions of the slag and metal for the data of Table I are indicated in Table I. The hearth model predictions for 2.7 atmospheres are 1.06%Si, 0.91%Mn, 0.102%P, 0.0282%S, 4.80%C. Thus, for a hearth pressure very close to the pressure roughly approximated by Philbrook and Manning (2.7 atmospheres versus 2.5 atmospheres) the composition of the metal predicted by the model shows very good agreement with the reported compositions (the reported compositions are an average over a lengthy period of

operation).

The data of Tables II and III were also treated as the data for Table I with the results shown in Figs. (6-8) for Table II and Figs. (9-11) for Table II. Again, as with the data of Table I, the silicon and manganese compositions decrease with increasing pressure and the sulfur content increases with increasing pressure.

Using a hearth pressure of 2.8 atmospheres, the predictions for the composition data of Tables II and III are also in quite good agreement with the reported metal compositions. The carbon content of the tapped metal was not reported for either of these data sets. The discrepancy between the reported and calculated S compositions for these data results from the lack of reported S composition for the ore, coke, and stone charged to these furnaces. As a result assumed S compositions for ore and coke were used in these predictions.

The hearth model was also tested for its composition response to changes in the slag temperature with the pressure in the hearth being constant. The data from Table I were used with the pressure held at 2.7 atmospheres and the slag temperature varied from 1700°K to 1850°K. The resulting predictions for Si, Mn, and S compositions of the hot metal are shown in Figs. (12-14). The trends that are observed in actual practice are reflected by the model predictions. Si and Mn recovery in the hot metal increase with increasing temperature and the hot metal S decreases with increasing temperature-all three being quite

sensitive to temperature changes.

The results obtained from these trials with actual furnace data lend great support to the thinking of Philbrook and Manning. At reasonable pressures, the model predictions are in very good agreement with the reported compositions and the model reflects all the trends concerning metal composition that is encountered in actual practice.

An interesting observation from these results is that as the absolute pressure increases the sulfur composition of the hot metal also increases, thus desulfurization problems may be encountered if increased top pressure practice is employed unless the temperature of the slag is considerably higher to counteract the pressure effects. A silicon content lower than desired by the BOF shop may also result from the use of elevated top pressure.

Although the results of the model predictions are in quite good agreement with actual reported analyses, there are many limitations inherent with the hearth model. The available thermodynamic data is skimpy at best for the various activity coefficients needed, and where the data are sufficient for a given temperature they are not available over a range of temperatures. The accuracy of the free energy data for the various reactions is also extremely critical for the correct predictions of the metal compositions.

There are also real practical problems that exist in normal furnace operations. The compositions of the charge materials are

not often known with sufficient accuracy to enable a meaningful metal composition determination to be made. The compositions of the charge materials may also fluctuate a great deal as the stock pile is consumed. Of extreme importance is the slag temperature in the furnace. It is in the slag that the metal composition is determined and if the slag temperature is not accurately known the resulting metal composition may not represent the true picture. Figs. (12-14) show just how sensitive the Si, S, and Mn distributions are to the slag temperature.

It is realized that the depth of the slag layer will vary between furnace tappings, thus changing the pressure contribution of the slag to the total pressure and also the slag composition may vary with time between tappings. The metal compositions resulting from the slag-metal droplet equilibrium are assumed to be an "average" of the slag conditions existing between the furnace taps with no consideration given to changing slag depth, composition, or temperature with time.

Taylor[55] applied a similar argument for the total pressure of CO to the problem of the silicon distribution for a number of furnace tapping data. Although admitting great amounts of scatter and unreliability in the data, Taylor concluded that equilibrium is approached in the slag between the slag and metal droplets. He felt the most important controlling variable was slag temperature.

TABLE I

Blast furnace data from Hodge and Wyczalek[16]

Production rate (basic iron) tons/day	2100
Weight of ore (lbs/ton)	3300
Weight of coke (lbs/ton)	1416
Weight of limestone (lbs/ton)	627
Temperature of iron (°K)	1780-1800
Temperature of slag (°K)	1800-1835
Slag volume (lbs/ton)	905

COMPOSITION OF RAW MATERIALS (wt%)

	Ore	Coke	Limestone
Fe (total)	55.238%	0.86%	-%
MnO	0.908	-	-
P_2O_5	0.125	0.03	-
S	0.009	0.86	-
SiO_2	9.203	4.59	0.67
Al_2O_3	2.764	2.89	-
$CaCO_3$	0.844	-	96.91
$MgCO_3$	0.489	-	1.99
CaO	2.014	0.28	-
MgO	0.841	0.08	-
C	-	87.11	-
H_2O	4.428	3.00	0.43

TABLE I (Continued)

REPORTED CHEMICAL COMPOSITION

Hot Metal (Wt %)	1.11% Si	0.88% Mn	0.110% P
	0.032% S	4.0% C	
Slag (Wt %)	47.2% CaO	5.8% MgO	37.5% SiO_2
	5.9% Al_2O_3	1.2% S	

PREDICTED CHEMICAL COMPOSITIONS

(CO pressure = 2.7 atmospheres, slag temperature = 1800°K)

Hot Metal (Wt %)	1.06% Si	0.91% Mn	0.102% P
	0.0282% S	4.8% C	
Slag (Wt %)	43.4% CaO	3.7% MgO	35.5% SiO_2
	14.3% Al_2O_3	1.26% S	

TABLE II

Blast furnace data from Muchi.[21]

Production (kg/hr)	124,800
Weight of ore (kg/hr)	195,500
Weight of coke (kg/hr)	69,400
Weight of limestone (kg/hr)	13,100
Weight of manganese ore (kg/hr)	4,376
Temperature of iron (°K)	1,750
Temperature of slag (°K)	1,780
Slag volume (kg/hr)	42,900

COMPOSITION OF RAW MATERIALS (wt%)

	Ore	Coke	Limestone	Mn Ore
Fe (total)	59.01%	-%	-%	14.93%
C	-	87.3	-	-
SiO_2	6.43	5.25	2.82	27.02
CaO	5.54	0.35	53.18	0.83
MgO	1.55	0.19	-	0.497
MnO	0.29	0.10	-	30.04
Al_2O_3	4.96	-	-	4.31

No sulfur analyses available.

No phosphorus analyses available.

TABLE II (Continued)

REPORTED CHEMICAL COMPOSITION

Hot Metal (Wt %)	0.76% Si	1.00% Mn	0.122% P
	0.028% S	No C composition reported.	
Slag (Wt %)	43.4% CaO	6.29% MgO	34.8% SiO_2
	14.4% Al_2O_3	0.77% S	

PREDICTED CHEMICAL COMPOSITIONS

(CO pressure = 2.8 atmospheres, slag temperature = 1780°K)

Hot Metal (Wt %)	0.73% Si	0.96% Mn	0.122% P
	0.021% S	4.94% C	
Slag (Wt %)	43.6% CaO	7.75% MgO	35.6% SiO_2
	9.42% Al_2O_3	1.46% S	

TABLE III

Blast furnace data from Muchi.[21]

Production (kg/hr)	145,600
Weight of ore (kg/hr)	230,600
Weight of coke (kg/hr)	68,000
Weight of limestone (kg/hr)	11,500
Weight of manganese ore (kg/hr)	2,927
Temperature of iron (°K)	1,723
Temperature of slag (°K)	1,753
Slag volume (kg/hr)	41,700

COMPOSITION OF RAW MATERIALS (wt%)

	Ore	Coke	Limestone	Mn Ore
Fe (total)	59.11%	-%	-%	17.01%
C	-	89.42	-	-
SiO_2	5.42	3.99	1.43	10.40
CaO	4.54	0.66	54.57	0.81
MgO	0.88	0.25	-	0.29
MnO	0.36	0.065	-	39.44
Al_2O_3	2.17	-	-	6.54

No sulfur analyses available.

No phosphorus analyses available.

TABLE III (Continued)

REPORTED CHEMICAL COMPOSITION

Hot Metal (Wt %)	0.58% Si	0.76% Mn	0.184% P
	0.038% S	No C composition reported.	
Slag (Wt %)	39.54% CaO	4.24% MgO	39.50% SiO_2
	15.90% Al_2O_3	0.98% S	

PREDICTED CHEMICAL COMPOSITIONS

(CO pressure = 2.8 atmospheres, slag temperature = 1753°K)

Hot Metal (Wt %)	0.48% Si	0.89% Mn	0.182% P
	0.028% S	4.90% C	
Slag (Wt %)	43.4% CaO	5.52% MgO	35.0% SiO_2
	12.5% Al_2O_3	1.46% S	

Figure 3

Weight per cent silicon in the hot metal for the charge data of Table I as a function of absolute pressure for a slag temperature of 1800°K based on equilibrium calculations.

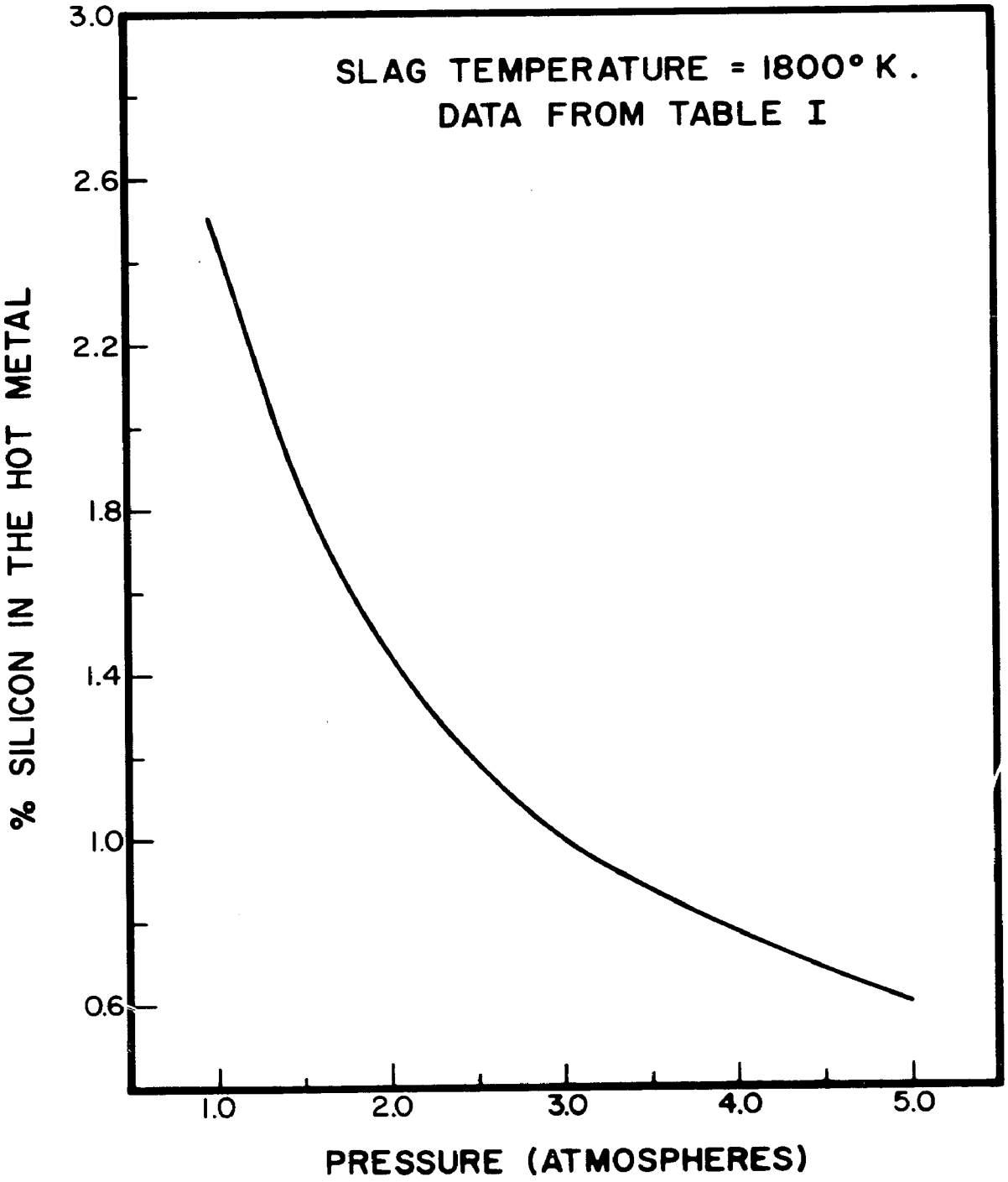
SLAG TEMPERATURE = 1800° K.
DATA FROM TABLE I
% SILICON IN THE HOT METAL
3.0
2.6
2.2
1.8
1.4
1.0
0.6
1.0
2.0
3.0
4.0
5.0
PRESSURE (ATMOSPHERES)

Figure 4

Equilibrium predictions of the weight per cent manganese in the hot metal for the charge data of Table I as a function of absolute pressure for a slag temperature of 1800°K.

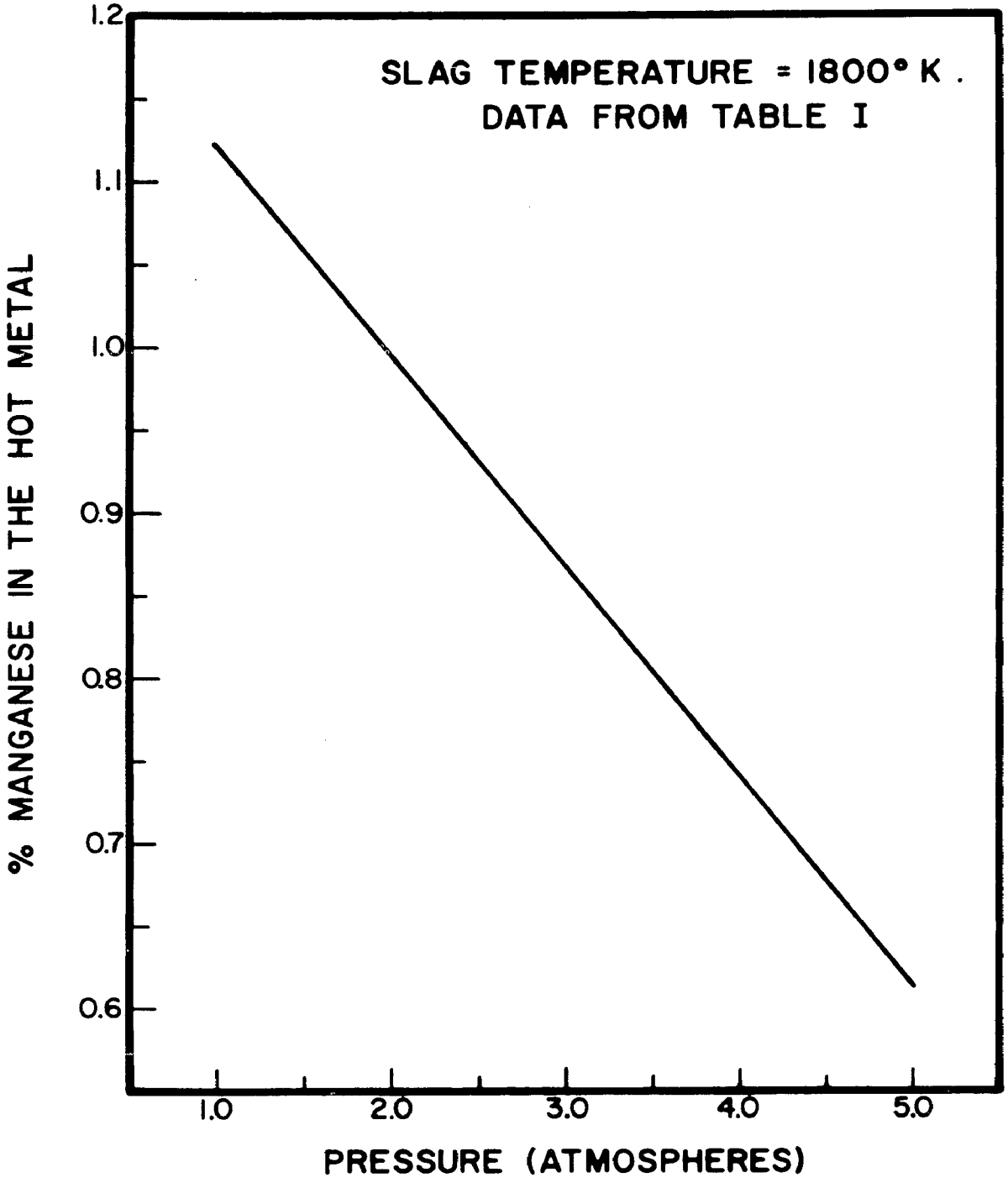
SLAG TEMPERATURE = 1800° K.
DATA FROM TABLE I
% MANGANESE IN THE HOT METAL
1.2
1.1
1.0
0.9
0.8
0.7
0.6
1.0
2.0
3.0
4.0
5.0
PRESSURE (ATMOSPHERES)

Figure 5

The effect of absolute pressure on the equilibrium predictions for the weight per cent sulfur in the hot metal for a slag temperature of 1800°K. The charge data are taken from Table I.

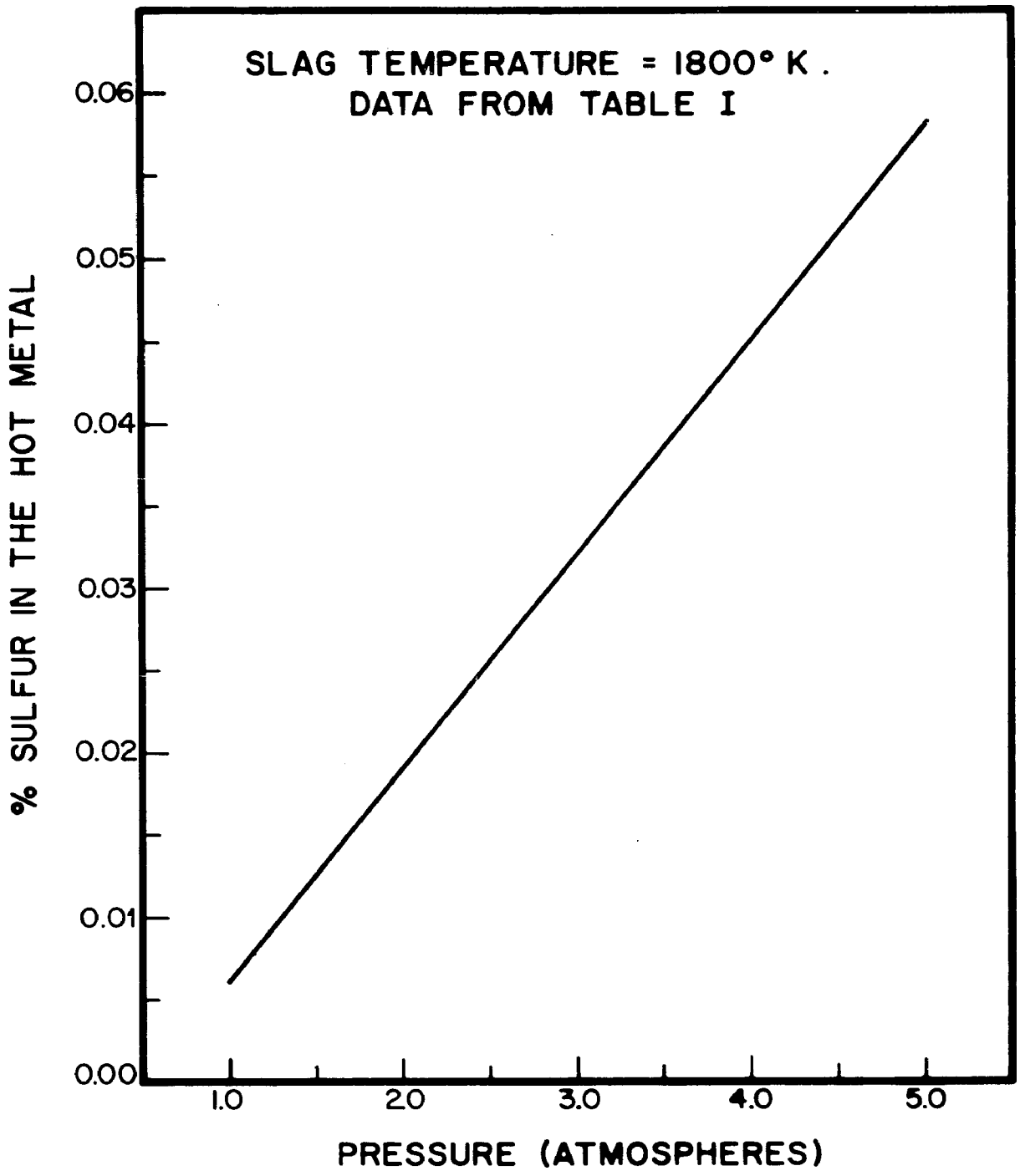
SLAG TEMPERATURE = 1800° K.
DATA FROM TABLE I
% SULFUR IN THE HOT METAL
0.06
0.05
0.04
0.03
0.02
0.01
0.00
1.0
2.0
3.0
4.0
5.0
PRESSURE (ATMOSPHERES)

Figure 6

Equilibrium predictions of the weight per cent silicon in the hot metal as a function of the absolute pressure in the hearth for a slag temperature of 1780°K. The charge data are reported in Table II.

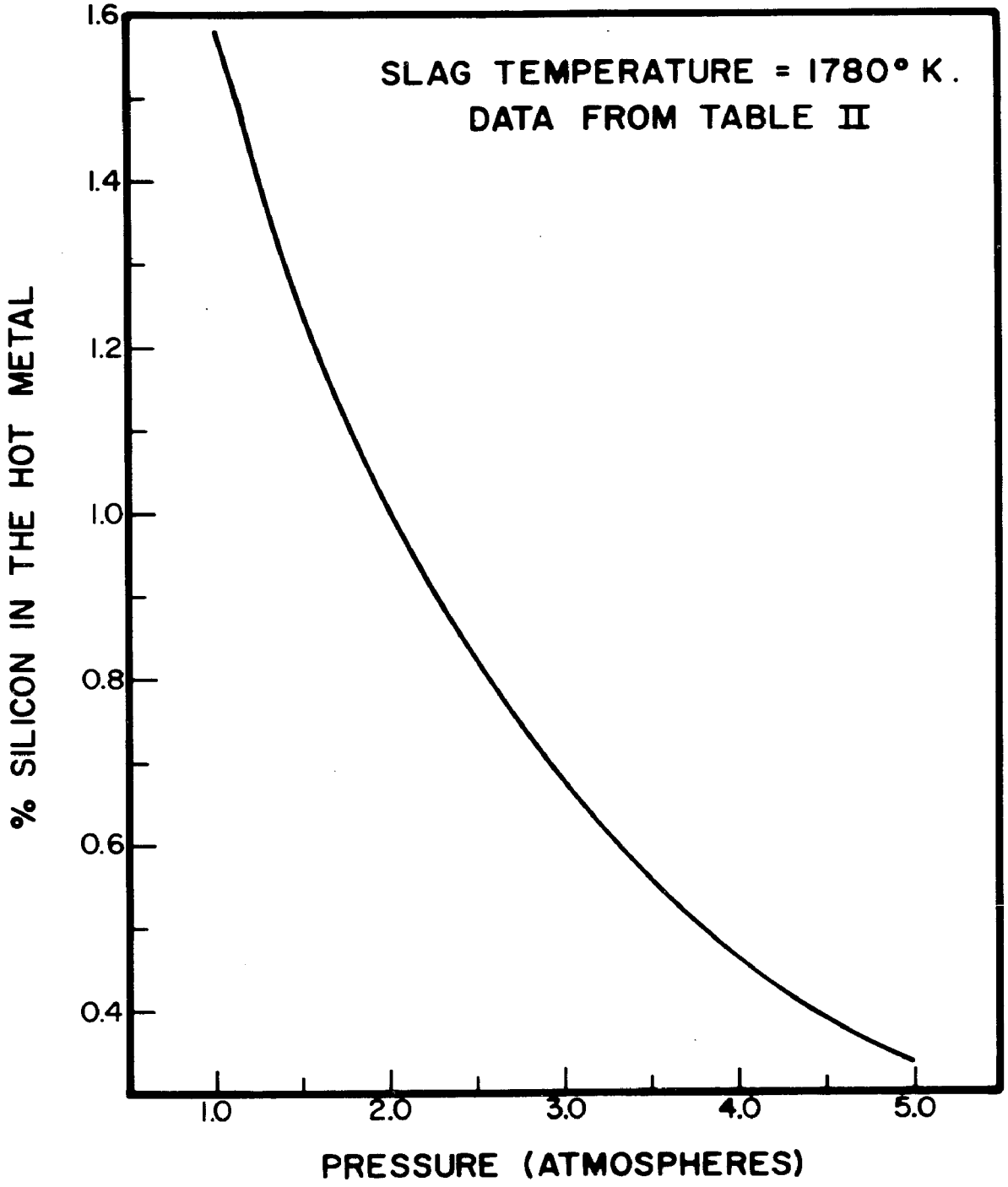
SLAG TEMPERATURE = 1780° K.
DATA FROM TABLE II
% SILICON IN THE HOT METAL
1.6
1.4
1.2
1.0
0.8
0.6
0.4
1.0
2.0
3.0
4.0
5.0
PRESSURE (ATMOSPHERES)

Figure 7

Weight per cent manganese in the hot metal for the charge data of Table II as a function of absolute pressure. A slag temperature of 1780°K is used in the equilibrium calculations.

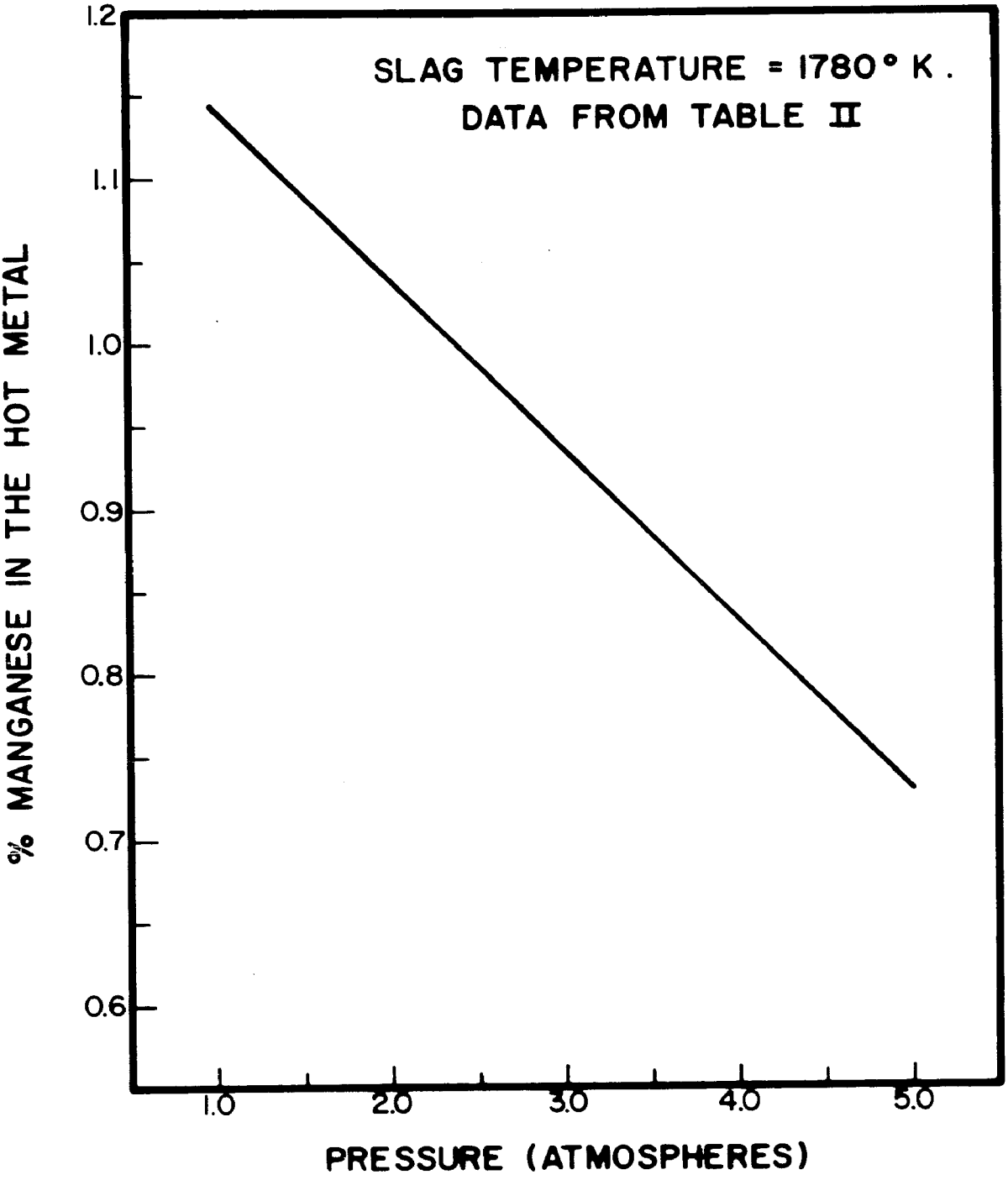
SLAG TEMPERATURE = 1780° K.
DATA FROM TABLE II
% MANGANESE IN THE HOT METAL
1.2
1.1
1.0
0.9
0.8
0.7
0.6
1.0
2.0
3.0
4.0
5.0
PRESSURE (ATMOSPHERES)

Figure 8

Weight per cent sulfur in the hot metal as a function of absolute pressure for a slag temperature of 1780°K. The charge data are reported in Table II.

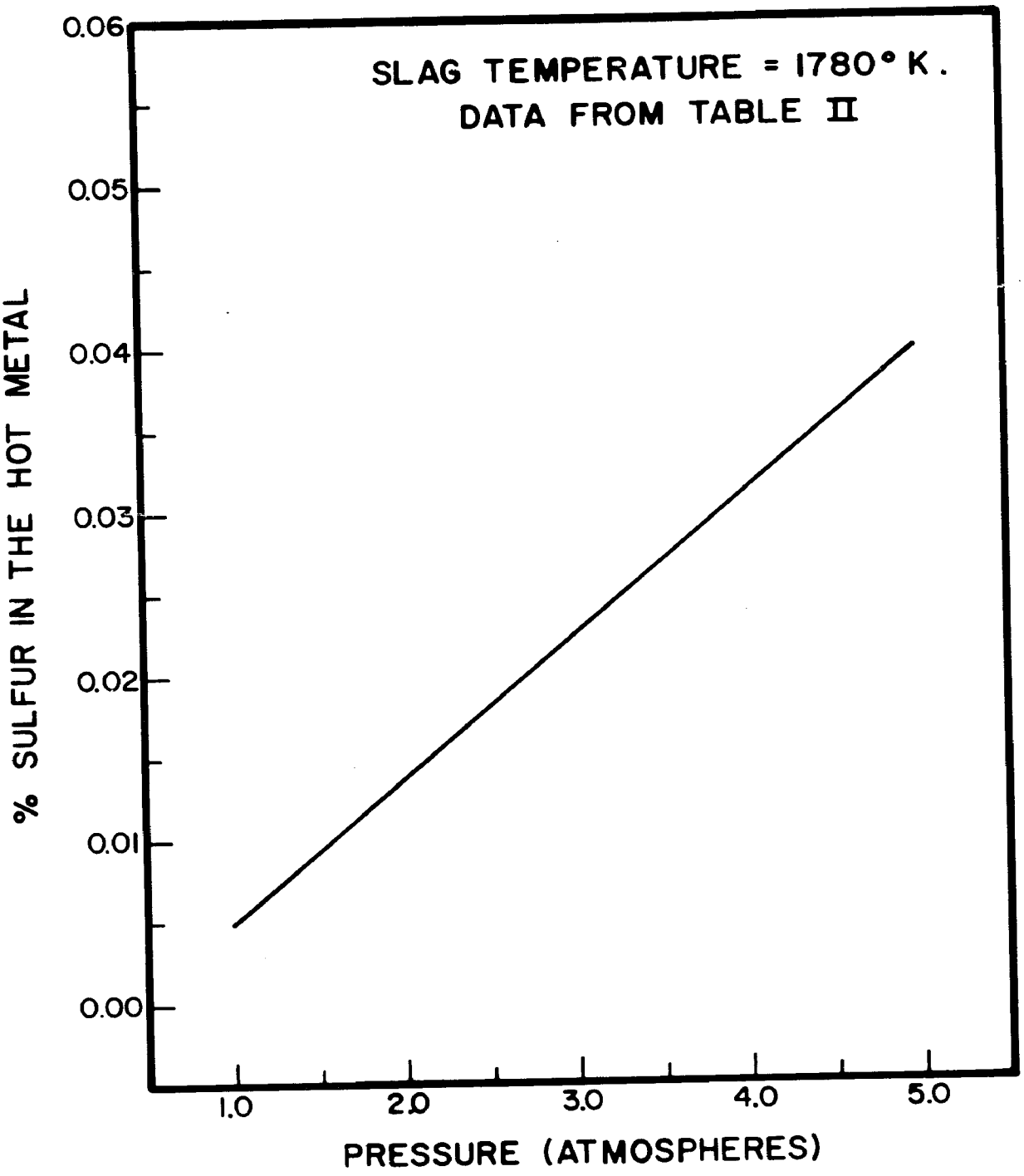
SLAG TEMPERATURE = 1780° K.
DATA FROM TABLE II
% SULFUR IN THE HOT METAL
0.06
0.05
0.04
0.03
0.02
0.01
0.00
1.0
2.0
3.0
4.0
5.0
PRESSURE (ATMOSPHERES)

Figure 9

The effect of absolute pressure in the hearth on the equilibrium predictions for the weight per cent silicon in the hot metal. The slag temperature controlling the equilibrium is 1753°K and the charge data are reported in Table III.

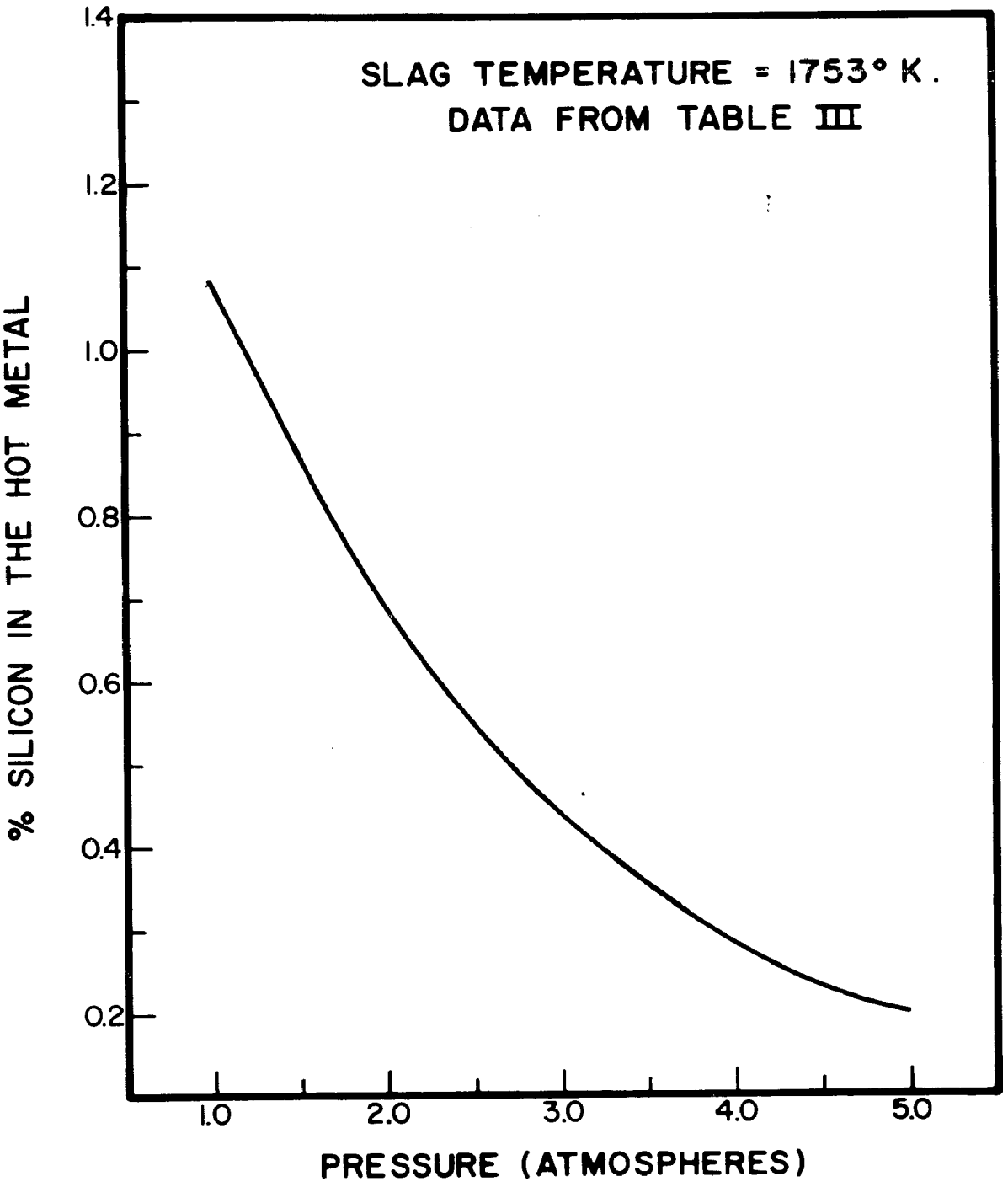
SLAG TEMPERATURE = 1753° K.
DATA FROM TABLE III
% SILICON IN THE HOT METAL
1.4
1.2
1.0
0.8
0.6
0.4
0.2
1.0
2.0
3.0
4.0
5.0
PRESSURE (ATMOSPHERES)

Figure 10

Weight per cent manganese in the hot metal as a function of absolute pressure for a slag temperature of 1753°K. The charge data are taken from Table III.

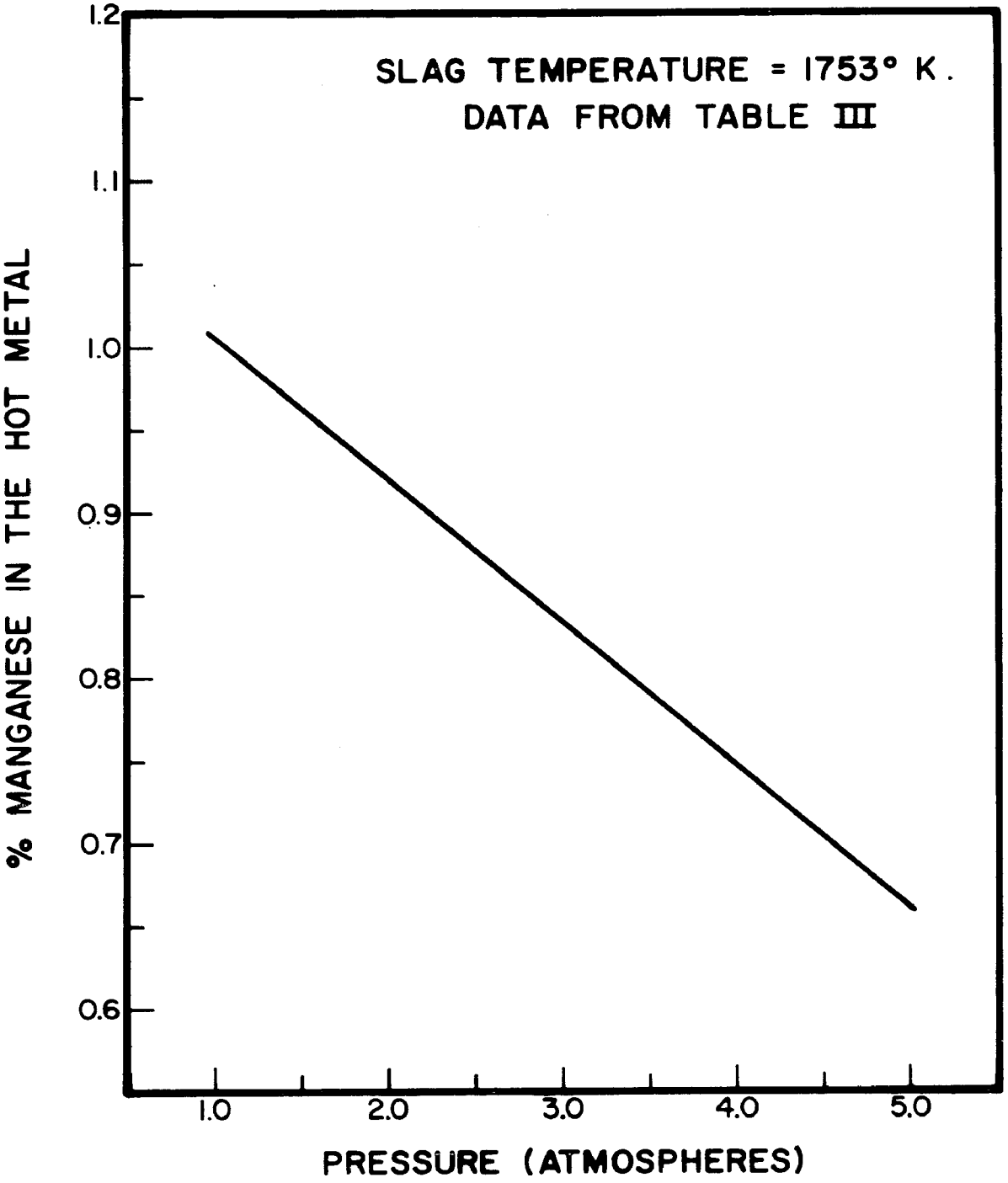
SLAG TEMPERATURE = 1753° K.
DATA FROM TABLE III
% MANGANESE IN THE HOT METAL
1.2
1.1
1.0
0.9
0.8
0.7
0.6
1.0
2.0
3.0
4.0
5.0
PRESSURE (ATMOSPHERES)

Figure 11

The effect of absolute pressure on the weight per cent sulfur in the hot metal. The slag temperature controlling the equilibrium is 1753°K. The charge data are taken from Table III.

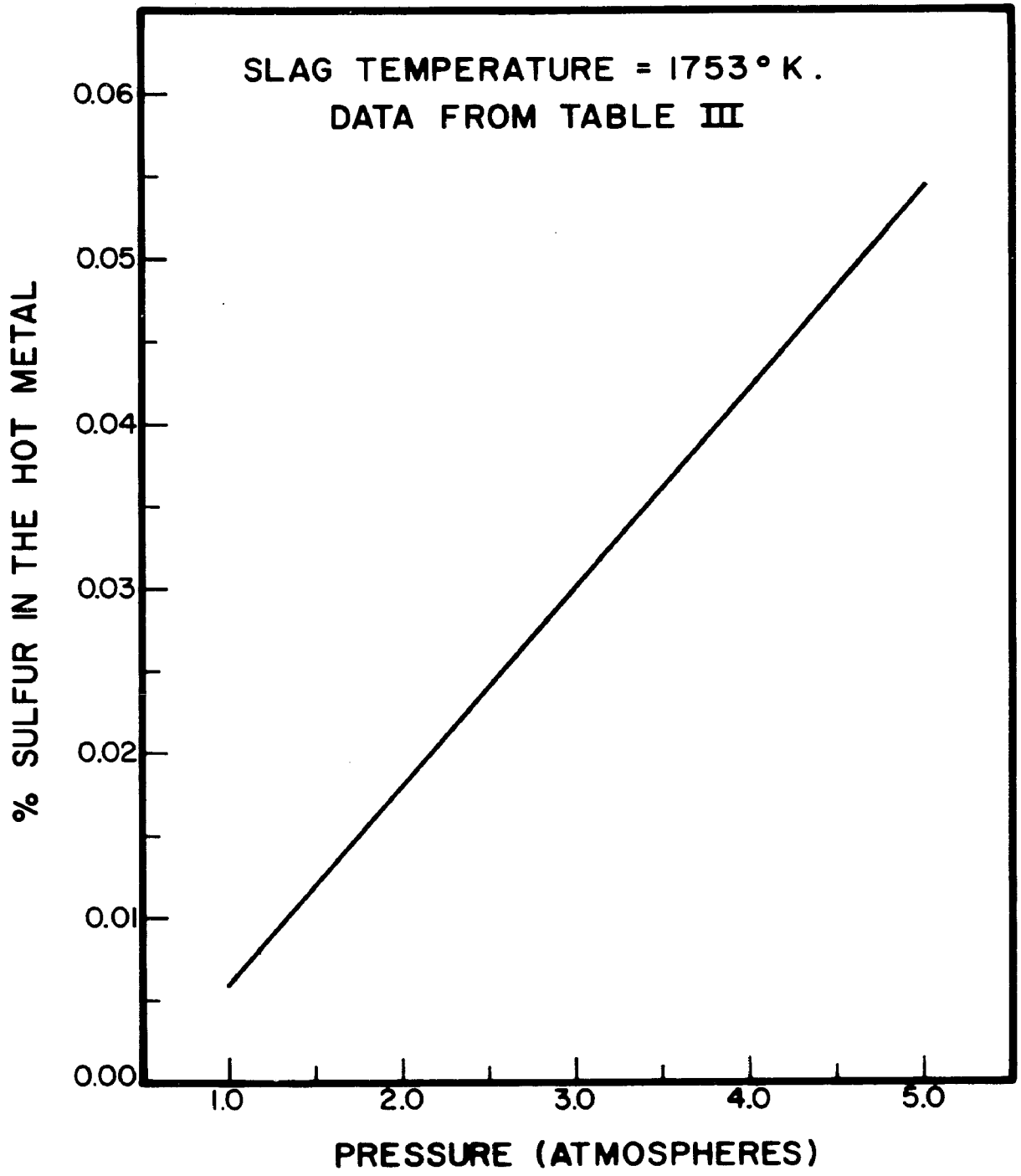
SLAG TEMPERATURE = 1753° K.
DATA FROM TABLE III
% SULFUR IN THE HOT METAL
0.06
0.05
0.04
0.03
0.02
0.01
0.00
1.0
2.0
3.0
4.0
5.0
PRESSURE (ATMOSPHERES)

Figure 12

Weight per cent silicon in the hot metal as a function of the slag temperature controlling the equilibrium. The absolute pressure in the hearth is 2.7 atmospheres. The charge data are reported in Table I.

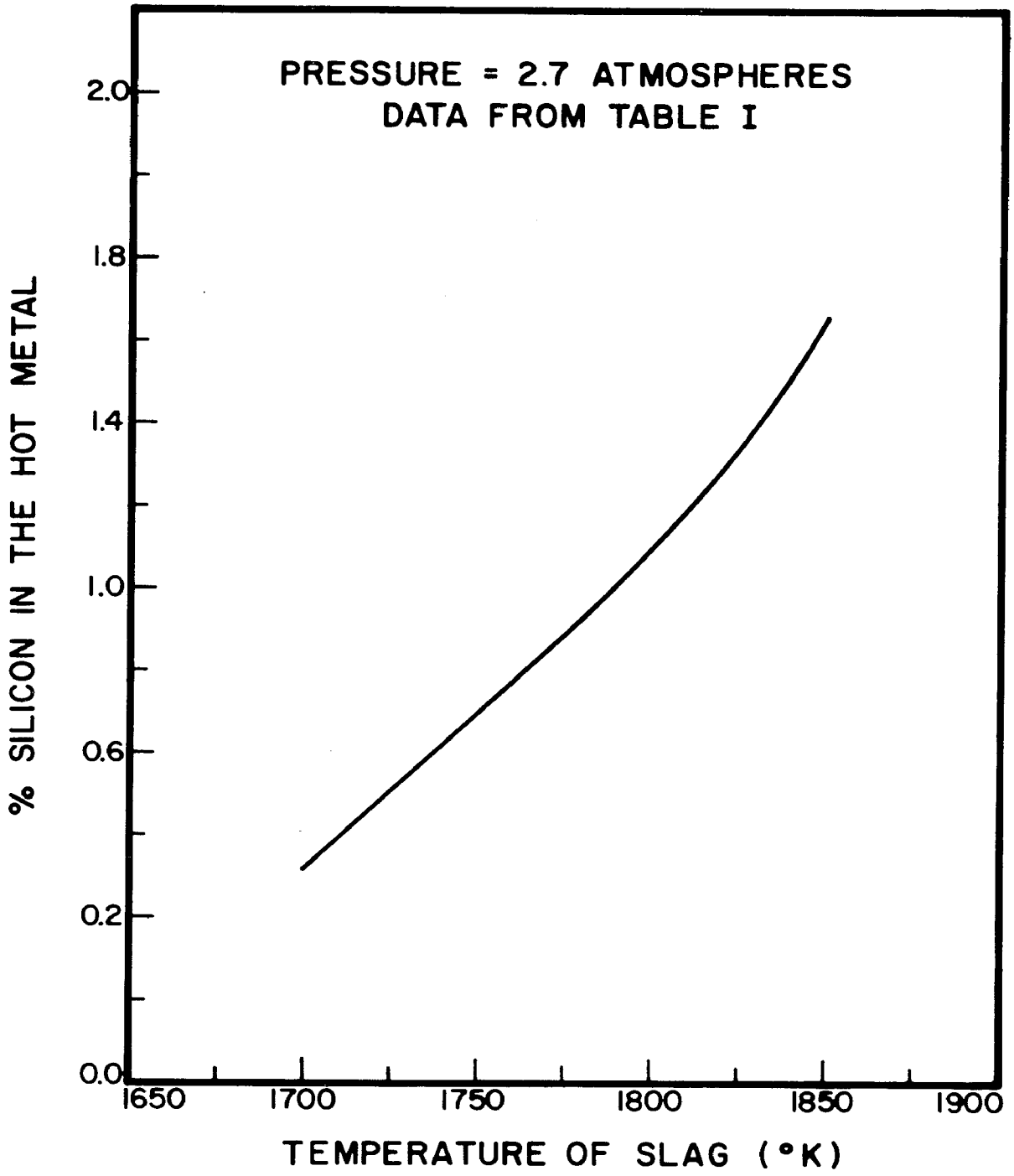
PRESSURE = 2.7 ATMOSPHERES
DATA FROM TABLE I
% SILICON IN THE HOT METAL
2.0
1.8
1.4
1.0
0.6
0.2
0.0
1650
1700
1750
1800
1850
1900
TEMPERATURE OF SLAG (°K)

Figure 13

The effect of slag temperature on the weight per cent manganese in the hot metal. The absolute pressure controlling the equilibrium is 2.7 atmospheres. The charge data are taken from Table I.

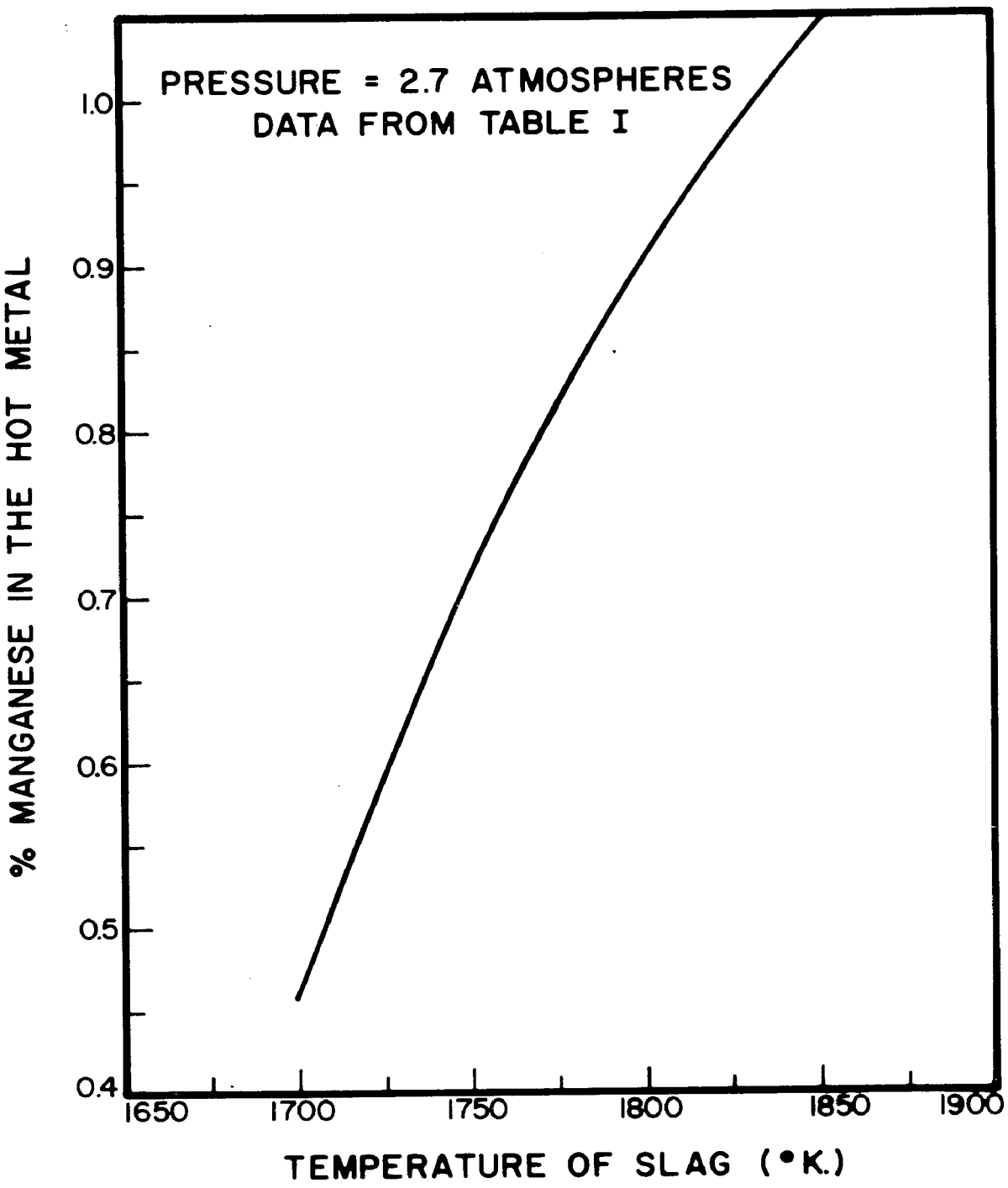
PRESSURE = 2.7 ATMOSPHERES
DATA FROM TABLE I
% MANGANESE IN THE HOT METAL
1.0
0.9
0.8
0.7
0.6
0.5
0.4
1650
1700
1750
1800
1850
1900
TEMPERATURE OF SLAG (°K.)

Figure 14

Equilibrium predictions of the weight per cent sulfur in the hot metal as a function of the slag temperature for a pressure of 2.7 atmospheres. The charge data are taken from Table I.

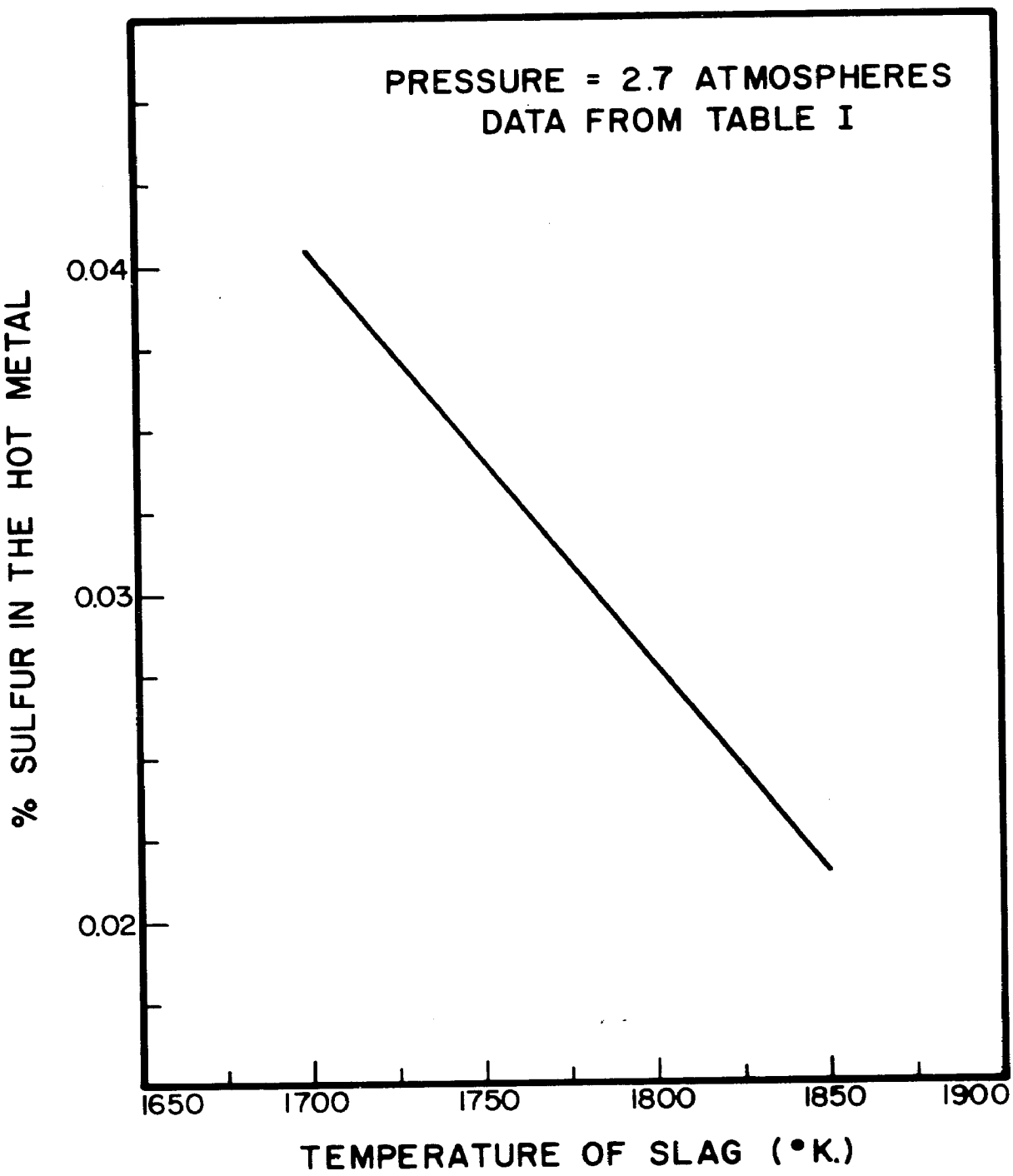
PRESSURE = 2.7 ATMOSPHERES
DATA FROM TABLE I
% SULFUR IN THE HOT METAL
0.04
0.03
0.02
1650
1700
1750
1800
1850
1900
TEMPERATURE OF SLAG (°K.)

STACK AND BOSH MODELS

STEADY STATE

The general shape of the profiles for the CO, CO_2, and H_2 contents of the blast furnace gas and the temperatures of the solid and gas phases are fairly well known from experimental probe studies done on actual operating blast furnaces.[13,14] Fig. 15, taken from the work of Schurmann and his co-workers, illustrates quite well the trends of these profiles with distance above the tuyeres. The CO_2 gas composition decreases steadily and eventually quite rapidly until the CO_2 composition of the gas finally becomes 0.0 a short distance above the tuyeres. The CO composition increases steadily, peaks, and then begins to decrease just above the tuyere line. The H_2 composition, which is quite small remains relatively constant the entire length of the furnace. No attempt is made to distinguish between the solid and gas temperature in Fig. 15 and for a great portion of the stack length it has been found that the temperature of the gas and solid are extremely close, sometimes being identical.

The stack and bosh models were tested on two sets of actual blast furnace operating data. The data are tabulated in Tables IV and V for furnaces 1 and 2 respectively. From these data, the profiles of $x,y,w,v,t,T,f_s,f_l,\rho_b$, and p were generated from the stockline to the tuyere level with the combined stack and bosh models. The resulting profiles for the ten variables mentioned are shown in Figs. 16-20 for furnace 1 and Figs. 21-25

for furnace 2. As can be seen from Figs. 16,17, and 18 for furnace 1 and Figs. 21,22, and 23 for furnace 2 the profiles of CO, CO_2, and H_2 content of the gas and the gas and solid temperature profiles parallel the respective profiles determined experimentally.

For both furnaces the gas and solid temperatures rise rapidly near the stockline where the initial large temperature difference between the solids and the gas results in a very high rate of heat transfer. However, the solid temperature quickly approaches that of the gas and the temperatures remain very close to each other down to only a very few meters above the tuyeres. The large temperature difference near the tuyeres results from the solution-loss reaction and the direct reduction of FeO, both reactions being very endothermic.

The peak in the CO curve for both furnaces results from the solution-loss reaction which goes very rapidly below the peak, but is very sluggish higher up in the furnace. The CO peak corresponds to the location in the furnace where the CO_2 composition of the gas stream becomes zero.

The H_2 composition of the gas stream for both furnaces varies over only a fairly narrow composition range showing a decrease followed by an increase with distance down the stack, reflecting the measured behavior as shown by Schurmann's probe work. The H_2O content of the gas stream for both cases goes to zero at the same level as the CO_2 content.

The fraction of iron ore reduced indicates that the ore is

reduced by CO and H_2 throughout the entire length of the stack, but it is not until just above the tuyeres that the reduction of the ore is completed by the rapid reduction of the liquid FeO by solid carbon. For both furnaces, Figs. 19 and 24, the profiles for the fraction of ore reduced show slight humps or peaks in the vicinity of 6 meters from the stockline. These slight peaks indicate a peak in the rate of reduction of ore in these regions which corresponds with the findings of Michard and his co-workers on operating furnaces.

The limestone decomposition for both cases is seen to be completed quite rapidly within a narrow temperature range of 1000-1400°K.

Differences between Furnaces 1 and 2

Although the respective curves for both furnaces clearly show the same trends and patterns, there are some noticeable differences between the performances of the furnaces. These differences can be explained by elementary heat-transfer and kinetic considerations. The average particle size for furnace 2 is larger than that for furnace 1 and as a result of the slightly less inefficient heat-transfer the top gas temperature for furnace 2 is higher than that for furnace 1. Also, a considerably higher blast temperature was employed with furnace 2 to enable the required temperatures to be achieved.

The ore particles of the charge for furnace 2 were also larger than those for furnace 1, and as a result the available surface

area for reaction was smaller and the diffusion distance within the particles was greater for these particles. Thus the amount of reduction in the stack was considerably less and much more liquid FeO had to be reduced by solid C for furnace 2, resulting in a lower slag and metal temperature.

PREDICTIONS FOR THE ENTIRE FURNACE

STEADY-STATE

The stack, bosh, and hearth models were combined to predict the steady state operating conditions for the data listed in Tables IV and V. The chemical composition of the charge materials for furnaces 1 and 2 were previously listed in Tables II and III respectively. The profiles for the stack and bosh regions of the furnaces are as shown in Figs. 16-25. The resulting chemical compositions of the slag and metal for furnace 1 along with the results of the heat, oxygen, and carbon balances are given in Table IV. Similar results for furnace 2 are listed in Table V.

The results from both furnaces show good agreement with the reported temperatures and compositions of the slag and metal. The reported data are averaged over a number of furnace taps and as a result incorporate the numerous fluctuations that occur with normal furnace operations even in furnaces that are being operated under constant blast and charge conditions for considerable lengths of time.

Both furnaces show differences between the predicted and reported S compositions of the hot metal, attributed to the lack

of S compositions for the charge materials. No reported carbon compositions of the hot metal were available, but the predicted value of 4.93% for both furnaces is very reasonable for the temperatures encountered in these furnaces.

The heat balances for both furnaces show very good agreement between the total heat in and the total heat out of the furnaces with the differences being less than 2% of the total heat in for both furnaces. The carbon balances are also in excellent agreement for both furnaces with the differences being less than 3%.

The oxygen balances do not show quite the excellent agreement as found with the heat and carbon balances. The differences in this case are 5.5% and 5.8% for furnaces 1 and 2 respectively. This larger difference is attributed to the reliance on the reported oxygen contents of the actual charge materials which are usually not as well known as one desires. Even with the errors inherent in reported chemical compositions of the charge materials it is felt that the oxygen agreement is still quite good.

The pressures in the hearth that determined the final chemical compositions of the hot metal were 2.8 atmospheres for furnace 1 and 3.1 atmospheres for furnace 2.

Heat Losses

The magnitude of the heat losses to both the cooling water and to the hearth walls play a significant role in the results of the steady-state model. The cooling water heat losses greatly influence the gas temperature profile in the stack and bosh regions

of the furnace and the hearth losses supplied by the cooling of the slag and metal directly influences the resulting temperature and hence the chemical compositions for the slag and metal.

As a result of these strong influences a knowledge of the heat losses to the cooling water and to the hearth for a particular furnace is a considerable aid in applying the steady-state model to this furnace. If this knowledge is not available reasonable estimates based on the construction of the furnace and past experiences with similar furnaces must be used. The magnitude of both types of losses is dependent on the type of cooling employed in the stack region and the construction of the hearth and methods of cooling the hearth region. Heat losses have often been estimated by the method of difference (the difference in the heat that can be accounted for and the total heat input is the heat loss), but for this model unless all sources and sinks of heat are considered carefully, the estimate by difference may be in error to a very large degree.

The total heat losses that are employed for furnaces 1 and 2 are in good agreement with the losses estimated by the Bethlehem Steel Corporation for furnaces of similar size. This value is taken as 25,000,000 kcal/hr with well over half of the heat loss occurring in the hearth and high temperature regions of the furnace. On a percentage basis of the total heat out the values of 13.8 and 13.5% for furnaces 1 and 2 are in excellent agreement with the values of 13.2 and 11.4% which were calculated by Hodge and

Wyczalek for actual operating data.

Runge-Kutta Technique-Step Size

The convergence of the solution of the Runge-Kutta method employed to solve the system of differential equations was tested by repeated calculations using progressively smaller intervals of z. The step-sizes tested ranged from 1.0 meters down to 0.125 meters with the value of 0.5 meters finally selected and used in subsequent runs. Intervals smaller than 0.5 meters did not produce any appreciable change in the results.

Selection of Conditions at the Stockline

As discussed earlier in the Model Approach section the conditions at the stockline must be chosen initially to enable the stack and bosh models to predict the profiles for the important variables between the stockline and the tuyeres. The temperature of the charge materials at the stockline was taken to be 450°K for both furnaces. Although the charge materials are placed on the bell at approximately 300°K they remain on the bell for a period of time before being dropped into the furnace and during this period of time they are heated. The solids also are in contact with the exiting gases when they fall from the bell to the stockline, thus heating up further. Using the geometry of the furnace bells for furnaces 1 and 2, and the usual periods of time for which the solids remained on the bell, Muchi estimated the temperature of the solids to be between 450 and 460°K.

The composition of the top gas can be checked through the

oxygen and carbon balances combined with a comparison of the predicted and calculated gas compositions at the tuyeres. The temperature of the top gas can be checked through the heat balance and also by comparing the resulting temperature at the tuyeres predicted by the bosh model with the flame temperature computed with the blast variables.

For furnaces 1 and 2 the top gas temperature was varied until the predicted and calculated gas temperatures at the tuyeres agreed to within 20°K or less. It was possible to get the agreement to less than 10°K for both cases.

The pressure of the top gas must also be selected. This selection is more difficult than the others and experience with blast furnace operation is probably of great benefit. The selection of the pressure can be checked through a rough estimation of the pressure existing at the tuyere level from the known blast conditions.

Flame Temperature Calculations

The flame temperature calculations were performed by the same method employed by Muchi and his co-workers[21]. The flame temperature determines the resulting aim temperature for the gas as predicted by the stack and bosh models, and is thus quite important.

It has been found that a variation of 10°K or 20°K in the flame temperature does not have a great effect on the model results, and indeed the blast temperature of the incoming hot gases is

probably not known to within 10°K or 20°K. As the blast variables become known or controlled more accurately, it will be possible to determine the flame temperature more accurately.

TABLE IV

Operating Data for Furnace 1

Blast Factors

Volume (Nm^3/min)	2,962
Temperature (°K)	1,195
Humidity (g/Nm^3)	35.5
Oil injected (g/Nm^3)	0.0

Charge Factors

	Particle diameter (cm)	Flow rate (kg/hr)	No. of particles ($1/m^3$)	Concentration ($kgmol/m^3$)
Ore	1.78	195,500	82,750	4.852
Limestone	1.85	12,700	5,300	0.5846
Coke	5.63	69,400	2,470	-
Mn Ore	2.19	4,376	-	-

Volume flow rate of solids (m^3/hr)	223.8
Density of solids at stock line (kg/m^3)	1297
Average particle diameter (cm)	2.59
Cooling water losses (kcal/hr)	8,400,000

TABLE IV (Continued)

Metal and Slag Output

Pig iron			
Production (kg/hr)		124,800	
Temperature (°K)		1,750	
Composition (Wt %)	0.76% Si	1.00% Mn	0.122% P
	0.028% S		
Slag			
Production (kg/hr)		42,900	
Temperature (°K)		1,780	
Composition (Wt %)	43.4% CaO	6.29% MgO	34.8% SiO_2
	14.4% Al_2O_3	0.77% S	

Results for Furnace 1 Predicted from the Steady-State Model

Pig Iron			
Production (kg/hr)		124,300	
Temperature (°K)		1,757	
Composition (Wt %)	0.80% Si	1.02% Mn	0.122% P
	0.018% S	4.93% C	
Slag			
Production (kg/hr)		40,900	
Temperature (°K)		1,787	
Composition (Wt %)	43.5% CaO	7.73% MgO	35.4% SiO_2
	9.39% Al_2O_3	1.47% S	1.01% MnO

TABLE IV (Continued)

Heat Balance and Distribution

Heat In (kcal/hr)		% of Total
Heat of slag	5,490,000	3.6
Sensible heat in the blast	52,388,000	34.6
Sensible heat in the charge materials	10,472,000	6.9
Heat liberated by the combustion of coke and fuel oil at the tuyeres	83,301,000	54.9
Total	151,651,000	100.0

Heat Out (kcal/hr)		% of Total
Heat consumed by chemical reactions in the hearth and stack	48,851,000	31.6
Sensible heat in the top gas	24,643,000	16.0
Sensible heat in the liquid pig iron and slag	56,597,000	36.6
Heat losses-cooling water plus hearth losses	21,400,000	13.8
Heat lost in compound formation	1,895,000	1.2
Heat lost in sulfide formation	1,205,000	0.8
Total	154,591,000	100.0

TABLE V

Operating Data for Furnace 2

Blast Factors

Volume (Nm^3/min)	3,027
Temperature (°K)	1,366
Humidity (g/Nm^3)	22.5
Oil injected (g/Nm^3)	41.93

Charge Factors

	Particle diameter (cm)	Flow rate (kg/hr)	No. of particles ($1/m^3$)	Concentration ($kgmol/m^3$)
Ore	1.95	230,630	55,800	4.505
Limestone	3.31	11,226	695	0.4281
Coke	5.30	68,000	3,410	-
Mn Ore	-	2,927	-	-

Volume flow rate of solids (m^3/hr)	271.7
Density of solids at stock line (kg/m^3)	1156
Average particle diameter (cm)	2.97
Cooling water losses (kcal/hr)	12,600,000

TABLE V (Continued)

Metal and Slag Output

Pig Iron			
Production (kg/hr)		145,600	
Temperature (°K)		1,723	
Composition (Wt %)	0.58% Si	0.76% Mn	0.184% P
	0.038% S		
Slag			
Production (kg/hr)		41,700	
Temperature (°K)		1,753	
Composition (Wt %)	39.54% CaO	4.24% MgO	33.5% SiO_2
	15.9% Al_2O_3	0.98% S	

Results for Furnace 2 Predicted from the Steady-State Model

Pig Iron			
Production (kg/hr)		143,000	
Temperature (°K)		1,728	
Composition (Wt %)	0.46% Si	0.87% Mn	0.186% P
	0.030% S	4.93% C	
Slag			
Production (kg/hr)		39,500	
Temperature (°K)		1,758	
Composition (Wt %)	42.3% CaO	5.47% MgO	34.9% SiO_2
	12.4% Al_2O_3	1.45% S	1.28% MnO

TABLE V (Continued)

Heat Balance and Distribution

Heat In (kcal/hr)		% of Total
Heat of Slag	5,333,000	3.2
Sensible heat in the blast	64,456,000	39.2
Sensible heat in the solid charge materials	11,178,000	6.8
Heat liberated by the combustion of coke and fuel oil at the tuyeres	83,765,000	50.8
Total	164,732,000	100.0

Heat Out (kcal/hr)		% of Total
Heat consumed by the chemical reactions in the hearth and stack	51,602,000	30.7
Sensible heat in the top gas	29,350,000	17.5
Sensible heat in the liquid pig iron and slag	60,737,000	36.2
Heat losses-cooling water plus hearth losses	22,600,000	13.5
Heat lost in compound formation	2,395,000	1.4
Heat lost in sulfide formation	1,152,000	0.7
Total	167,836,000	100.0

Figure 15

Profiles for temperature and percentage of CO, CO_2 and H_2 in the blast furnace as determined through experimental probe work on an operating furnace by Schurmann and his co-workers. (See reference 14)

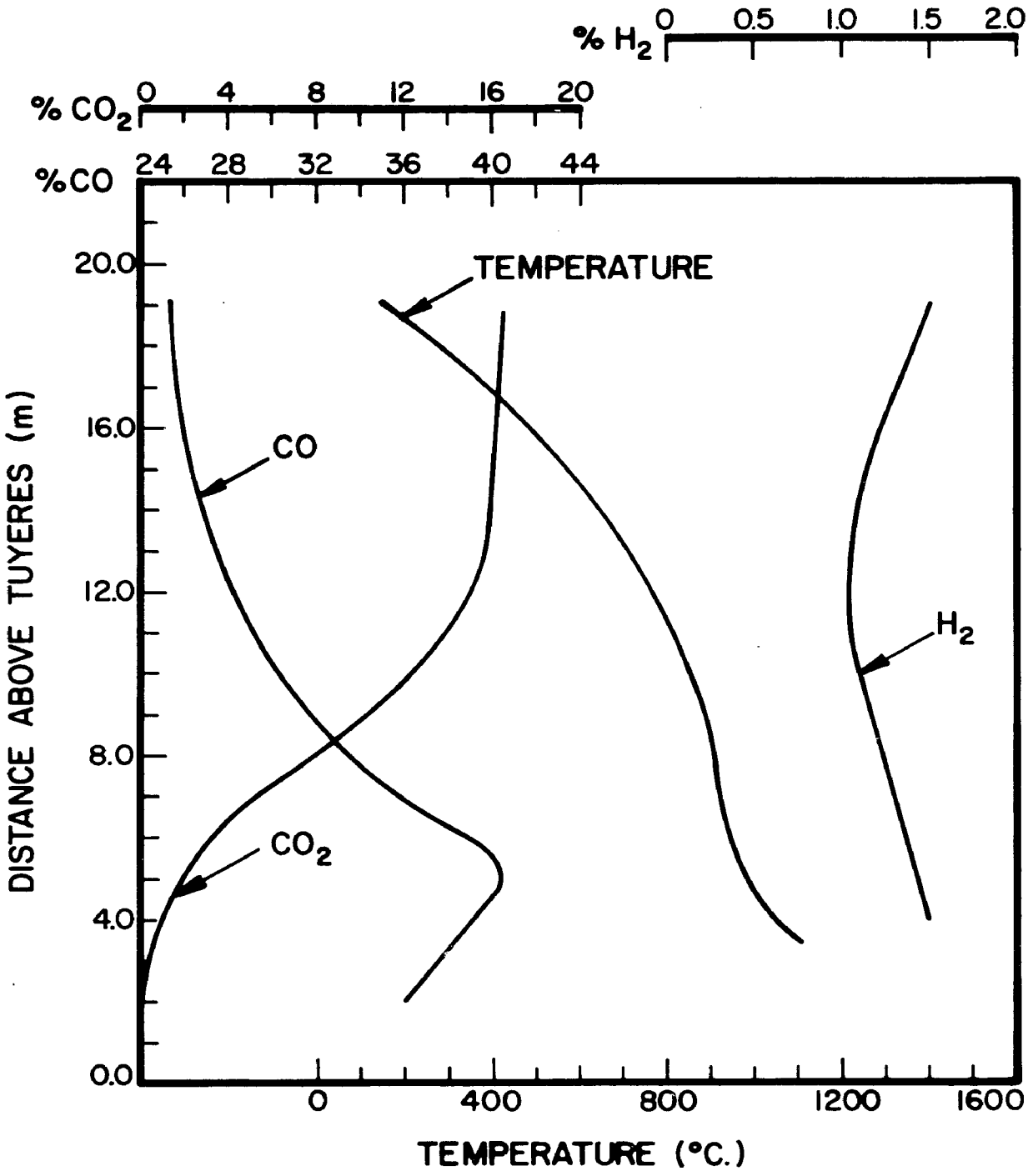
% H2
0
0.5
1.0
1.5
2.0
% CO2
0
4
8
12
16
20
%CO
24
28
32
36
40
44
TEMPERATURE
CO
CO2
H2
DISTANCE ABOVE TUYERES (m)
20.0
16.0
12.0
8.0
4.0
0.0
0
400
800
1200
1600
TEMPERATURE (°C.)

Figure 16

Profiles for the gas and solid temperatures as predicted by the steady-state model for Furnace 1.

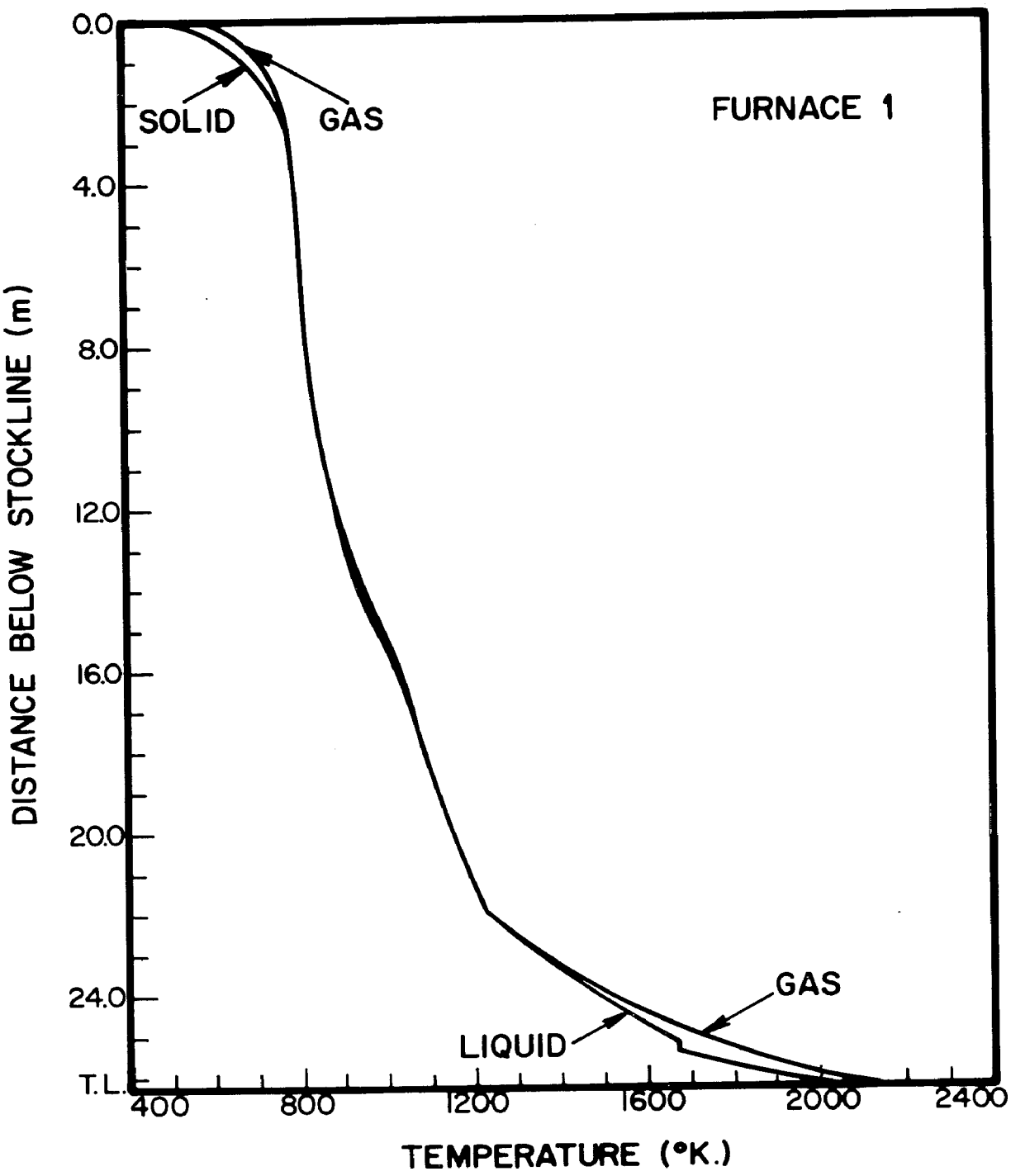
FURNACE 1
SOLID
GAS
GAS
LIQUID
DISTANCE BELOW STOCKLINE (m)
0.0
4.0
8.0
12.0
16.0
20.0
24.0
T.L.
400
800
1200
1600
2000
2400
TEMPERATURE (°K.)

Figure 17

Steady-state profiles for the mole fractions of CO and CO_2 in the blast furnace gas phase for Furnace 1.

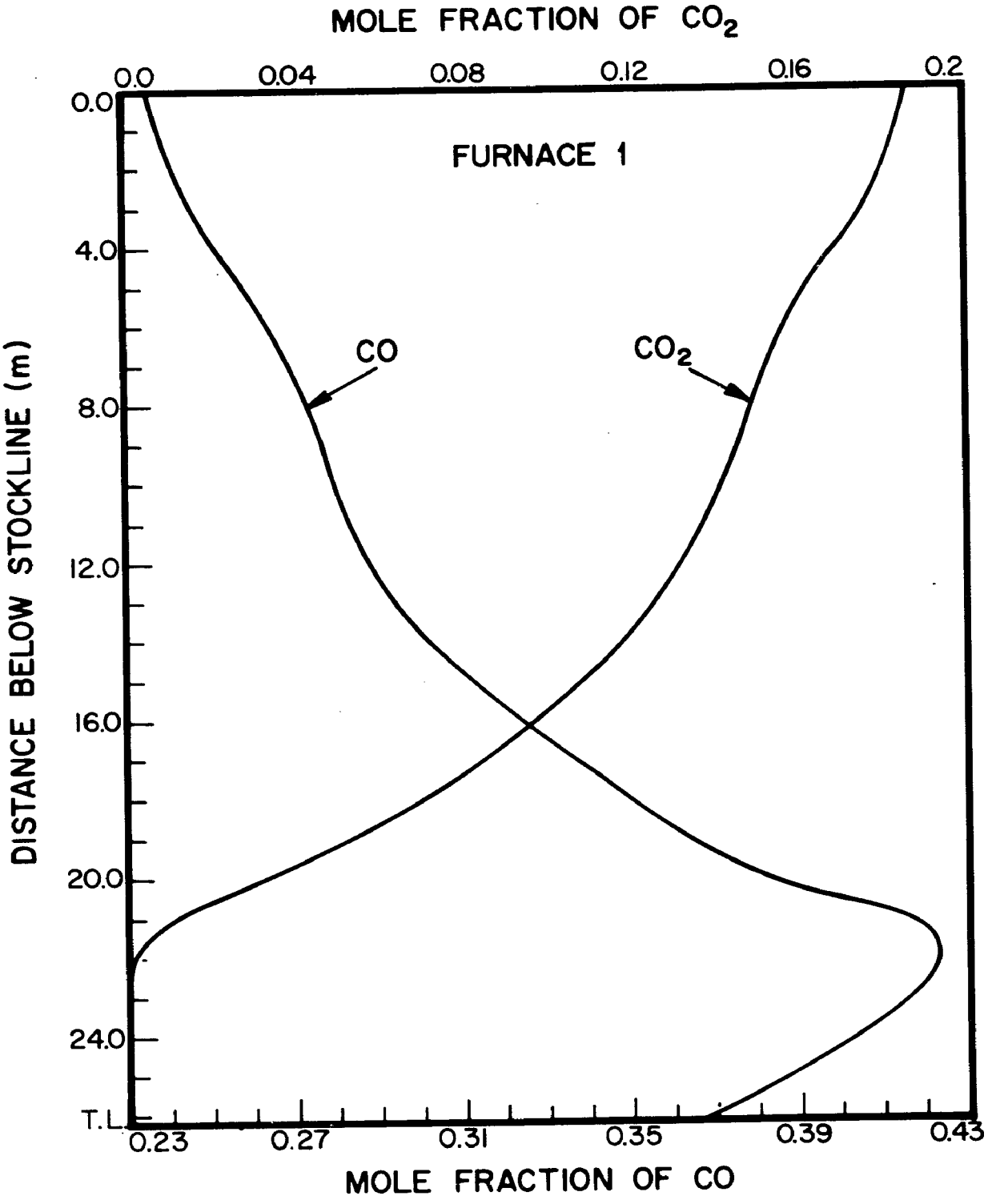
MOLE FRACTION OF CO_2
0.0
0.04
0.08
0.12
0.16
0.2
FURNACE 1
CO
CO_2
DISTANCE BELOW STOCKLINE (m)
0.0
4.0
8.0
12.0
16.0
20.0
24.0
T.L.
0.23
0.27
0.31
0.35
0.39
0.43
MOLE FRACTION OF CO

Figure 18

Profiles of the mole fraction of H_2 and H_2O in the gas phase for the steady state as predicted for Furnace 1.

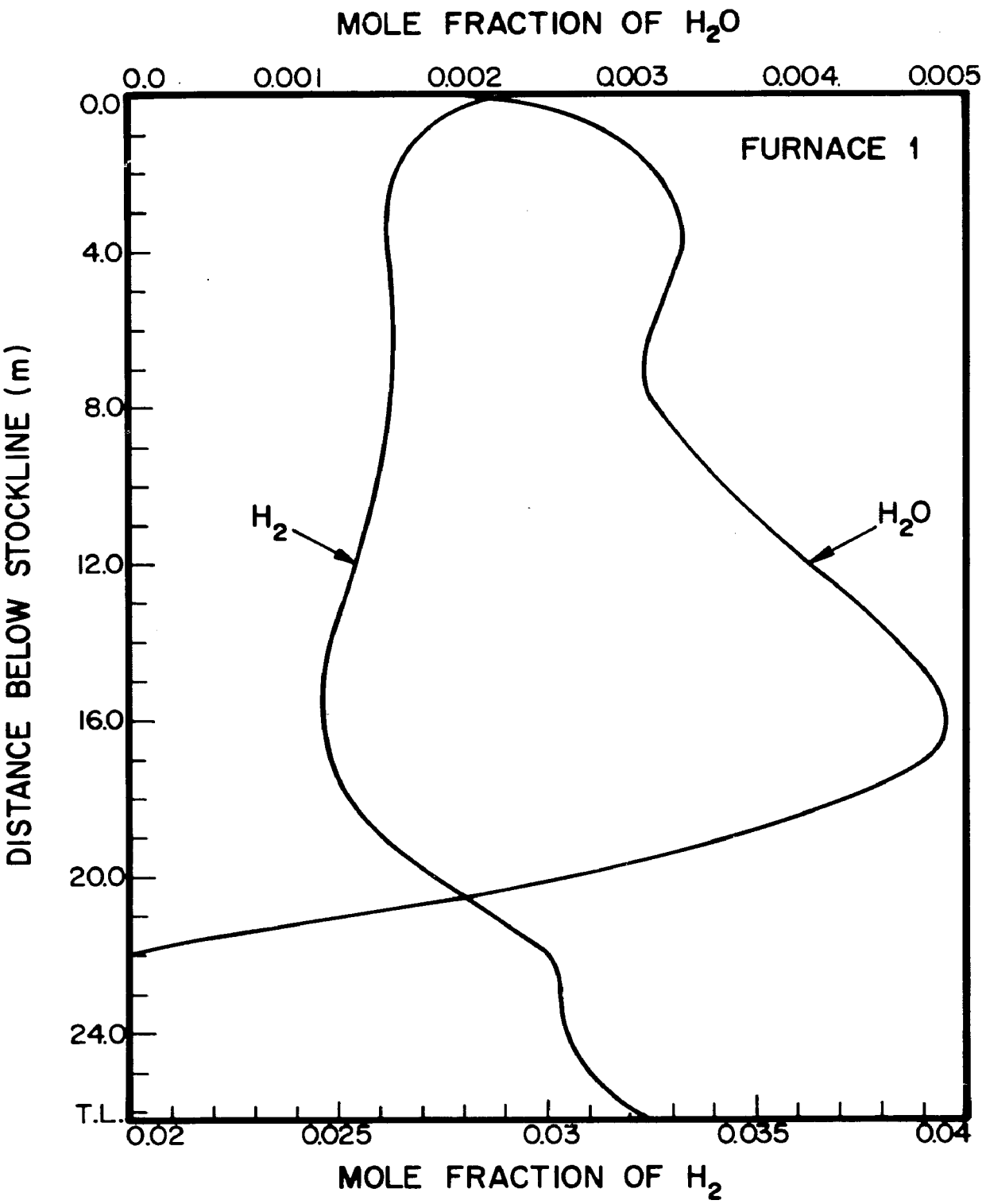
MOLE FRACTION OF H_2O
0.0
0.001
0.002
0.003
0.004
0.005
FURNACE 1
H_2
H_2O
DISTANCE BELOW STOCKLINE (m)
0.0
4.0
8.0
12.0
16.0
20.0
24.0
T.L.
0.02
0.025
0.03
0.035
0.04
MOLE FRACTION OF H_2

Figure 19

The fraction reacted for the iron ore and limestone as a function of distance below the stockline predicted by the steady-state model for Furnace 1.

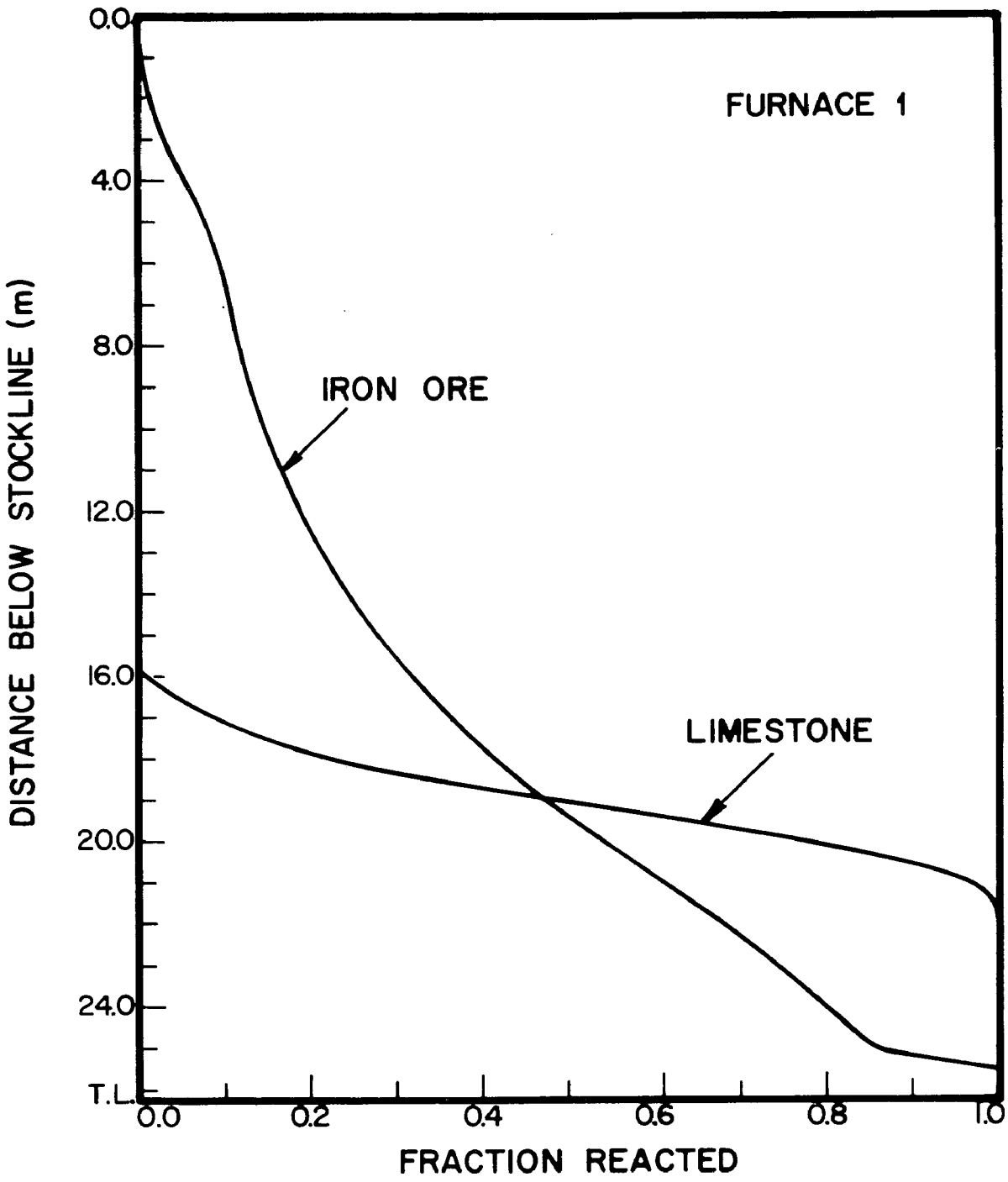
FURNACE 1
IRON ORE
LIMESTONE
DISTANCE BELOW STOCKLINE (m)
0.0
4.0
8.0
12.0
16.0
20.0
24.0
T.L.
0.0
0.2
0.4
0.6
0.8
1.0
FRACTION REACTED

Figure 20

Steady-state profiles of gas pressure and solid bulk density predicted for Furnace 1.

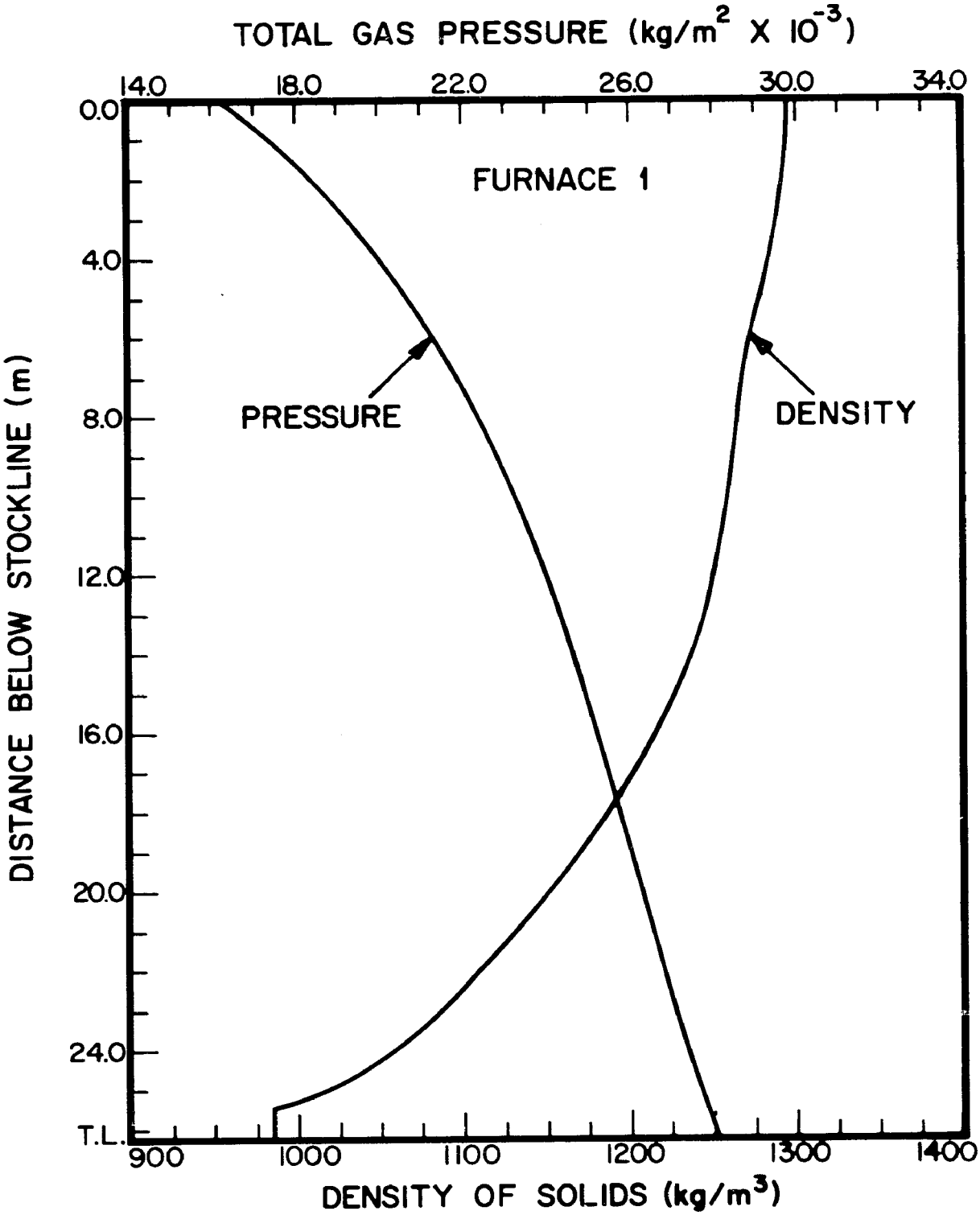
TOTAL GAS PRESSURE (kg/m^2 X 10^{-3})
14.0
18.0
22.0
26.0
30.0
34.0
FURNACE 1
PRESSURE
DENSITY
DISTANCE BELOW STOCKLINE (m)
0.0
4.0
8.0
12.0
16.0
20.0
24.0
T.L.
900
1000
1100
1200
1300
1400
DENSITY OF SOLIDS (kg/m^3)

Figure 21

Profiles of the gas and solid temperatures as predicted by the steady-state model for Furnace 2.

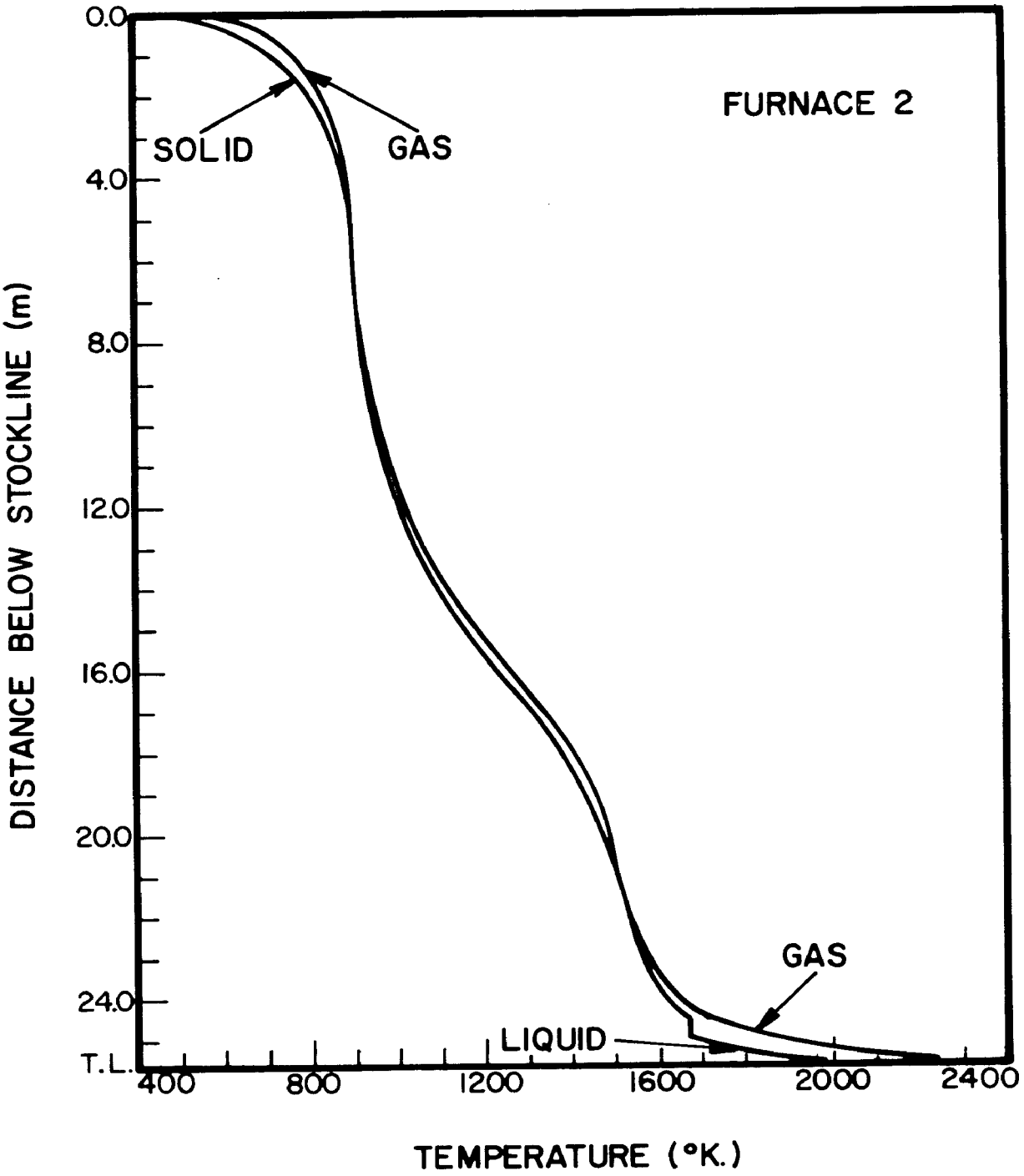
FURNACE 2
SOLID
GAS
GAS
LIQUID
0.0
4.0
8.0
12.0
16.0
20.0
24.0
T.L.
400
800
1200
1600
2000
2400
DISTANCE BELOW STOCKLINE (m)
TEMPERATURE (°K.)

Figure 22

Steady-state profiles for the mole fractions of CO and CO_2 in the blast furnace gas phase for Furnace 2.

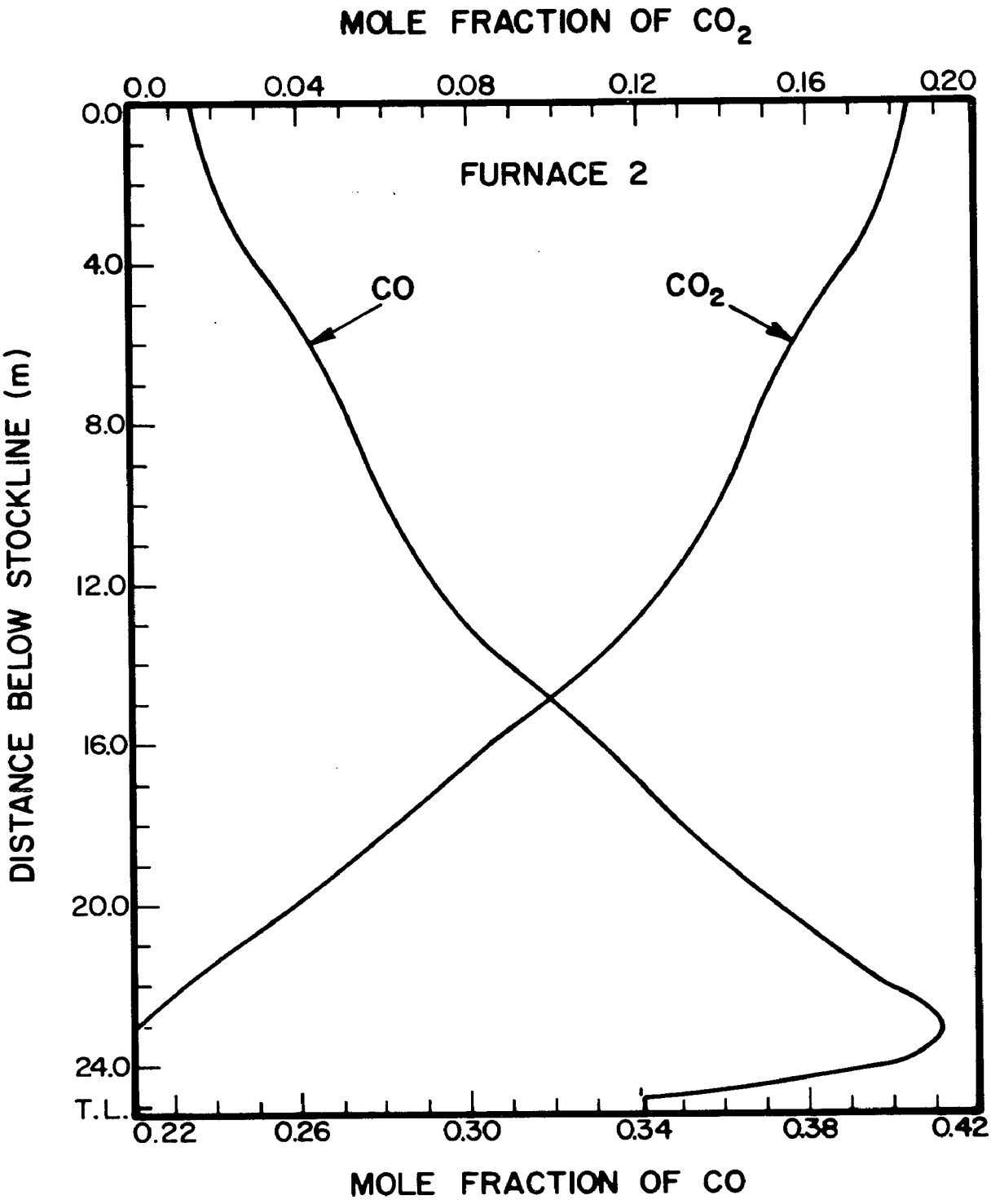
MOLE FRACTION OF CO_2
0.0
0.04
0.08
0.12
0.16
0.20
FURNACE 2
CO
CO_2
DISTANCE BELOW STOCKLINE (m)
0.0
4.0
8.0
12.0
16.0
20.0
24.0
T.L.
0.22
0.26
0.30
0.34
0.38
0.42
MOLE FRACTION OF CO

Figure 23

Profiles of the mole fraction of H_2 and H_2O in the gas phase for the steady-state as predicted for Furnace 2.

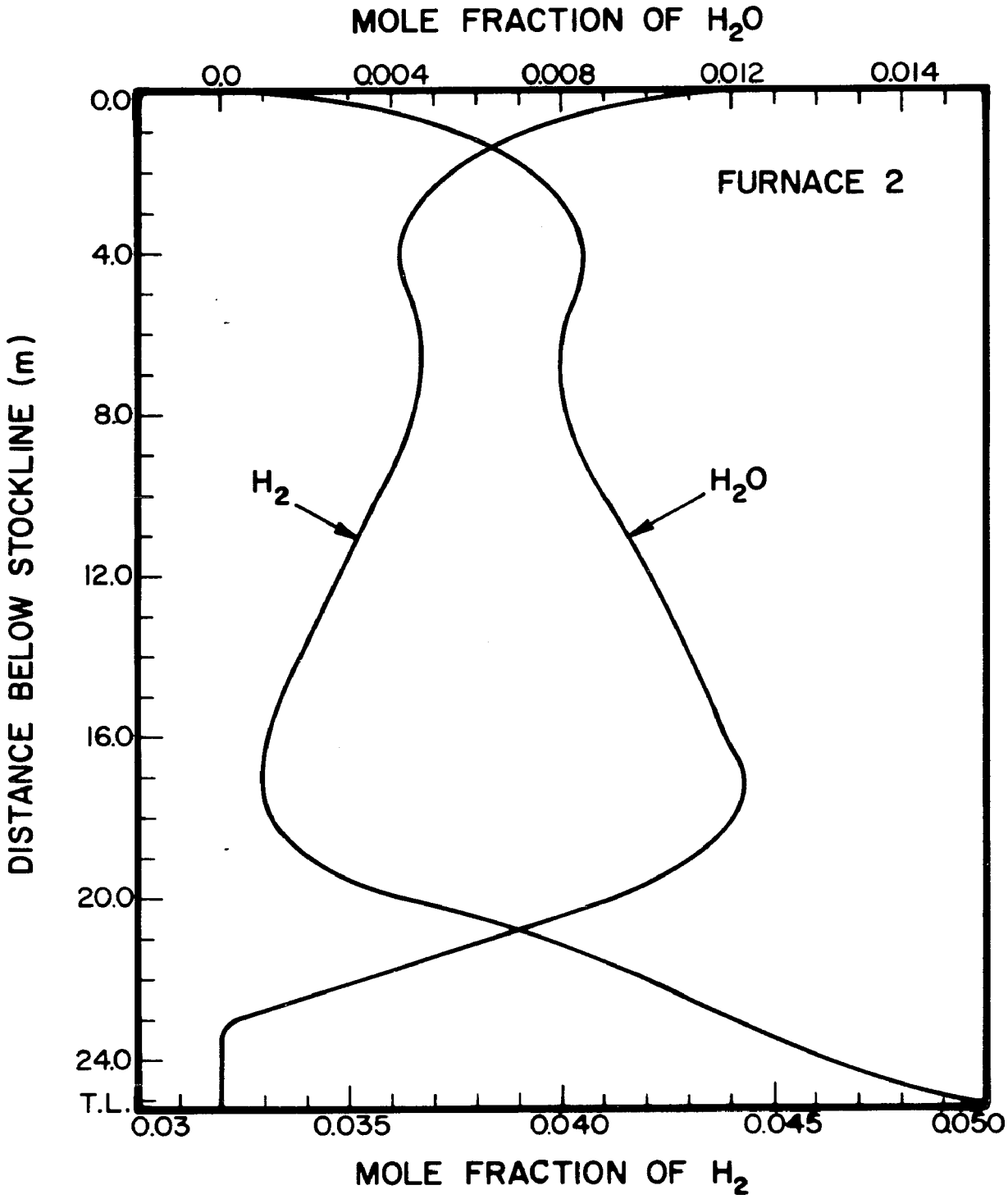
MOLE FRACTION OF H_2O
0.0
0.004
0.008
0.012
0.014
FURNACE 2
H_2
H_2O
DISTANCE BELOW STOCKLINE (m)
0.0
4.0
8.0
12.0
16.0
20.0
24.0
T.L.
0.03
0.035
0.040
0.045
0.050
MOLE FRACTION OF H_2

Figure 24

The fraction reacted for the iron ore and limestone as a function of distance below the stockline predicted by the steady-state model for Furnace 2.

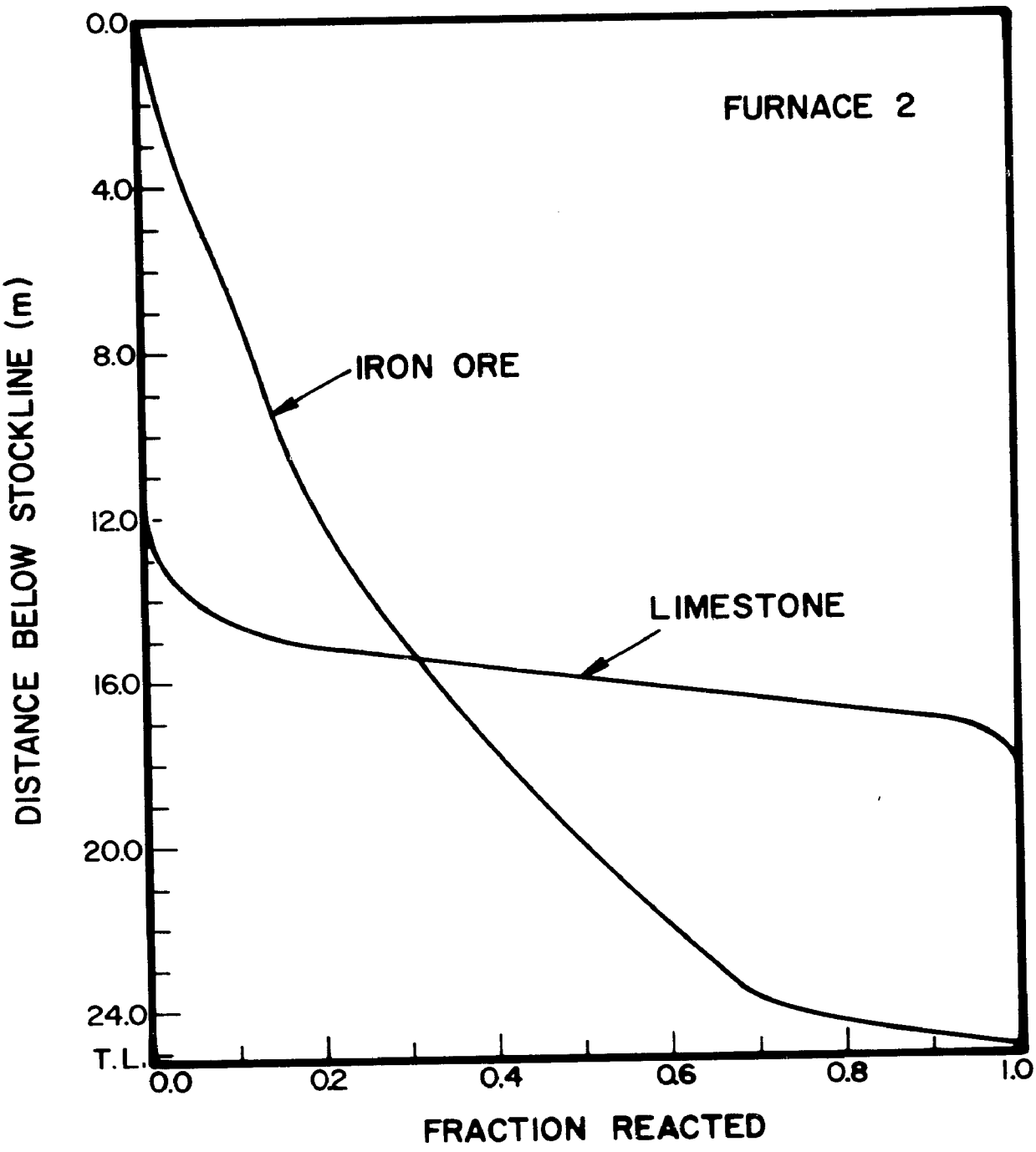
FURNACE 2
IRON ORE
LIMESTONE
DISTANCE BELOW STOCKLINE (m)
0.0
4.0
8.0
12.0
16.0
20.0
24.0
T.L.
0.0
0.2
0.4
0.6
0.8
1.0
FRACTION REACTED

Figure 25

Steady-state profiles of gas pressure and solid bulk density predicted for Furnace 2.

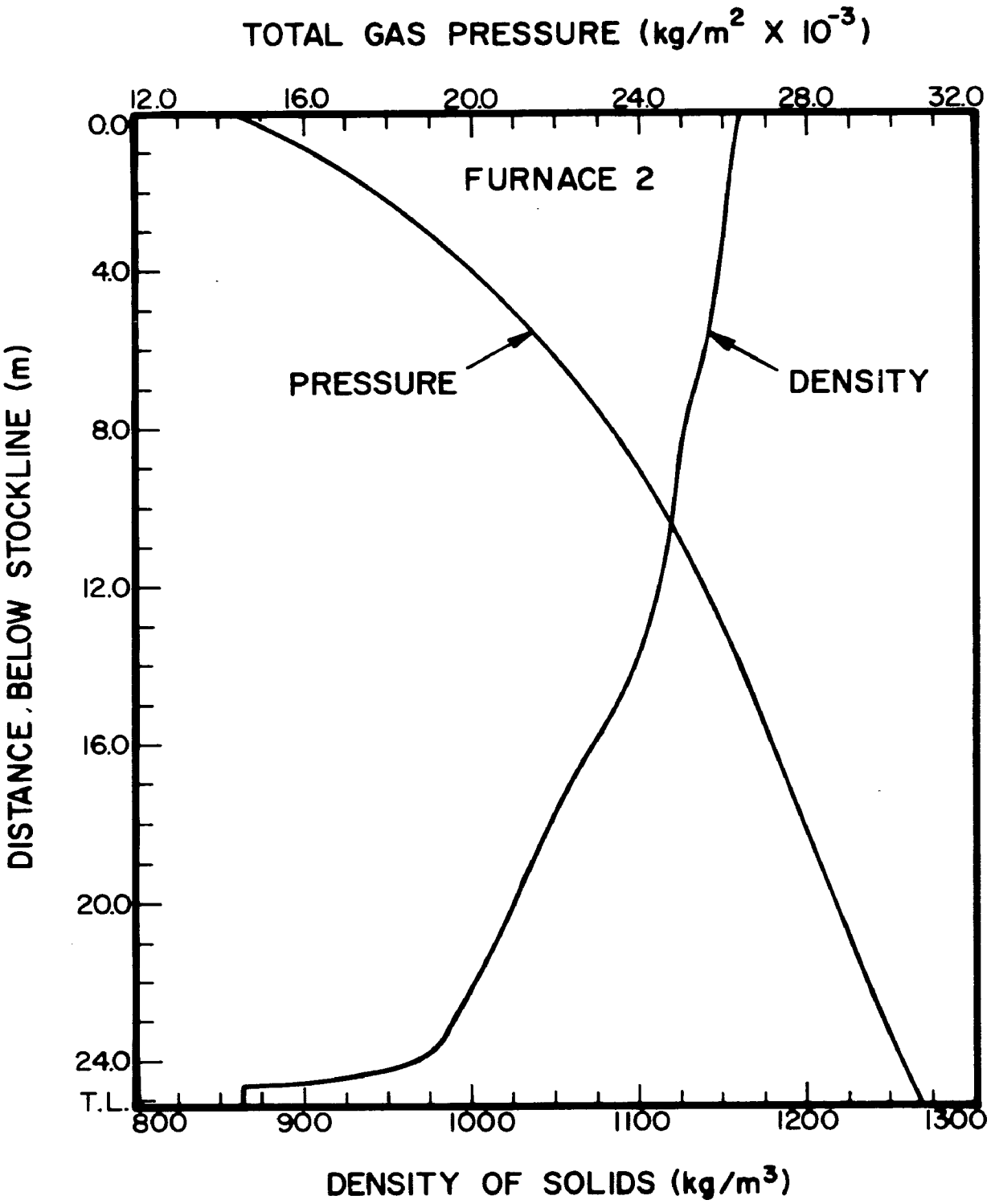
TOTAL GAS PRESSURE (kg/m² X 10⁻³)
12.0
16.0
20.0
24.0
28.0
32.0
0.0
4.0
8.0
12.0
16.0
20.0
24.0
T.L.
FURNACE 2
PRESSURE
DENSITY
DISTANCE, BELOW STOCKLINE (m)
800
900
1000
1100
1200
1300
DENSITY OF SOLIDS (kg/m³)

DYNAMIC MODEL

The dynamic model for the furnace was tested on two cases-changing the flame temperature and changing the blast moisture of the hot blast. The operating parameters of furnace 1 were chosen as the initial operating conditions for the furnace and the profiles in the stack and bosh regions of furnace 1 as predicted by the static model were read into the model to serve as the initial conditions at each 0.5 meter level of the stack and bosh.

The changes introduced into the operating conditions of furnace 1 were (1) an increase in the flame temperature of 50°K, holding all other operating parameters constant, and (2) a decrease in the blast moisture content of approximately 10 g/Nm^3 such that the resulting flame temperature was also increased by 50°K. The responses of the liquid temperature at the tuyere level and the temperature of the slag bath for both conditions are shown in Fig. 26. The response of the metal silicon composition for both conditions is given in Fig. 27, and the responses of the metal manganese and sulfur compositions are given in Fig. 28.

From Fig. 26 it can be seen that the temperature of the liquid materials at the tuyere level rises quite rapidly and then levels out at a new value for both cases tested, the overall increase for the change in flame temperature being 51°K while that for the decrease in blast moisture is 46°K. The temperature of the slag bath shows a more gradual increase and a smaller overall increase as compared with the behavior of the liquid at the tuyeres. The

more gradual behavior is due to the averaging of the temperatures of the liquid droplets as they enter the bath and the smaller overall increase is due to the increased silicon and manganese content of the metal which require large additional amounts of heat as well as the averaging of the liquid droplets. The slag temperature shows a final rise of 24°K, 2°K higher than that produced by the decrease in the blast moisture.

The hot metal silicon content as well as the manganese and sulfur of the hot metal follow the behavior of the slag bath temperature response very closely for both cases. The final silicon and manganese contents are lower and the final sulfur is higher for the decrease in blast moisture, due to the lower temperature of the slag bath. The overall changes in the hot metal compositions (after 2 1/2 hours) are +0.20 and +0.18 wt %Si, +0.058 and +0.054 wt %Mn, and -0.0028 and -0.0026 wt %S for the increase in flame temperature and decrease in the blast moisture, respectively.

It is extremely difficult to compare two such different cases and to be able to draw meaningful conclusions as to what causes the magnitude and the difference in the responses. The blast furnace is such a complex operation, both thermally and chemically, with all the chemical reactions and heat transfers being interrelated, that once a change in an operating variable is introduced all of the initial conditions in the stack and bosh may be changed within a very short time. For the cases considered, the change in flame temperature left all the other operating variables unchanged initially, but the gas composition and the

fraction of iron ore reduced were changed in the lower levels of the furnace quite quickly. The decrease in blast moisture resulted in a 50°K increase in the flame temperature, increased the mole fraction of CO in the gas phase at the tuyeres, decreased the H_2 mole fraction of the gas at the tuyeres, decreased slightly the overall flow of gas from the tuyere region, and also decreased slightly the driving rate of the furnace. With this large number of changes being introduced at one time it is impossible to predict, without use of a complex model, the final overall effect these changes will have on the furnace. As an example, it appears from the results obtained that the increased temperature and CO composition of the gas were able to overcome the decreased H_2 composition such that the fraction of iron ore reduced increased with time-a result not necessarily expected without the model. From these results and the complexity of the process it is very conceivable that the response of the furnace to changes in operating variables would be exactly the opposite as to what would be expected from first principles.

The only method to check the validity of the furnace responses predicted by the model is to compare the predictions with actual operating data. The best data available from production furnaces are cast- to- cast data, since temperatures and compositions at intermediate times are not available. Reports of cast- to- cast data are extremely rare in the literature with the usual reported data being averages of operating periods of a day or longer.

IRSID has, however, published cast- to- cast results observed after step-changes in blast temperature, blast moisture, and oil injections had been introduced into the furnace (see Ref. 22).

These cast- to- cast data were collected from the No. 5 Blast Furnace of the Rombas works which is a furnace considerably smaller in physical dimensions and having wind rates and production rates which are considerably lower than the furnaces under consideration in the model. These data are also susceptible to the normal disturbances and perturbations encountered within the normal furnace operation, and the casting results may not have reflected completely the step-changes in the operating parameter of interest. Normal pertubations arise from slight fluctuations in the wind rate, temperature, and blast additions, as well as slight changes in the composition of the raw materials entering the furnace.

The step-changes in the operating variables for the IRSID furnace were introduced mid-way between casts. Within the limit of the normal fluctuations experienced from cast to cast before the step-change was introduced it appears that the response for both the change in blast moisture and blast-temperature is complete within 2 1/2 casts or approximately 10 hours after the change was introduced.

The predictions made by the model, assuming that the furnace is not between casts when the operating parameter changes are introduced, show that the liquid temperature at the tuyere level

does not change after approximately 1 hour and that the slag bath temperature shows no noticeable change after 1.5 to 1.75 hours. The first cast after the step-change would then show a deviation from the steady-state casting results. However, the second cast, which would occur approximately 8 hours after the introduction of the step-change, would also show a deviation from the previous cast because of the absence of the lower temperature droplets which were averaged into the bath temperature before the first cast.

From the furnace operator's standpoint, a new "steady-state" would be achieved by the furnace in a period of time spanning two casts. From the standpoint of the liquid at the tuyere level the new "steady-state" is achieved in approximately 1 hour.

It is difficult to compare response times and magnitudes of changes between the IRSID results and the dynamic model predictions because of the great differences in operating conditions and furnace geometries considered. The dynamic responses as predicted by the model will have to be checked by comparing them to cast-to-cast data taken from furnaces operating under conditions much closer to those for which the model predictions were made.

The new "steady-state" conditions predicted by the dynamic model for the 50°K increase in flame temperature indicate that the new temperature of the charge materials at the tuyeres to be 2126°K. For a 50°K increase in flame temperature the steady-state model predicted a temperature of 2133°K for the charge materials

at the tuyere level. This indicates that the steady-states arrived at by both models are in good agreement.

Although both cases tested with the model show very similar responses in both length of time and magnitude of change, it is easier for the operator to control the furnace using blast moisture changes as opposed to changes in the blast temperature. Changes in the blast temperature would require changing the stove temperatures and/or changing the sequence of bleeding in the cold air to the hot blast.

Figure 26

The response with time of the liquid temperature at the tuyere level and the temperature of the slag bath due to an increase in the flame temperature and a decrease in the blast moisture.

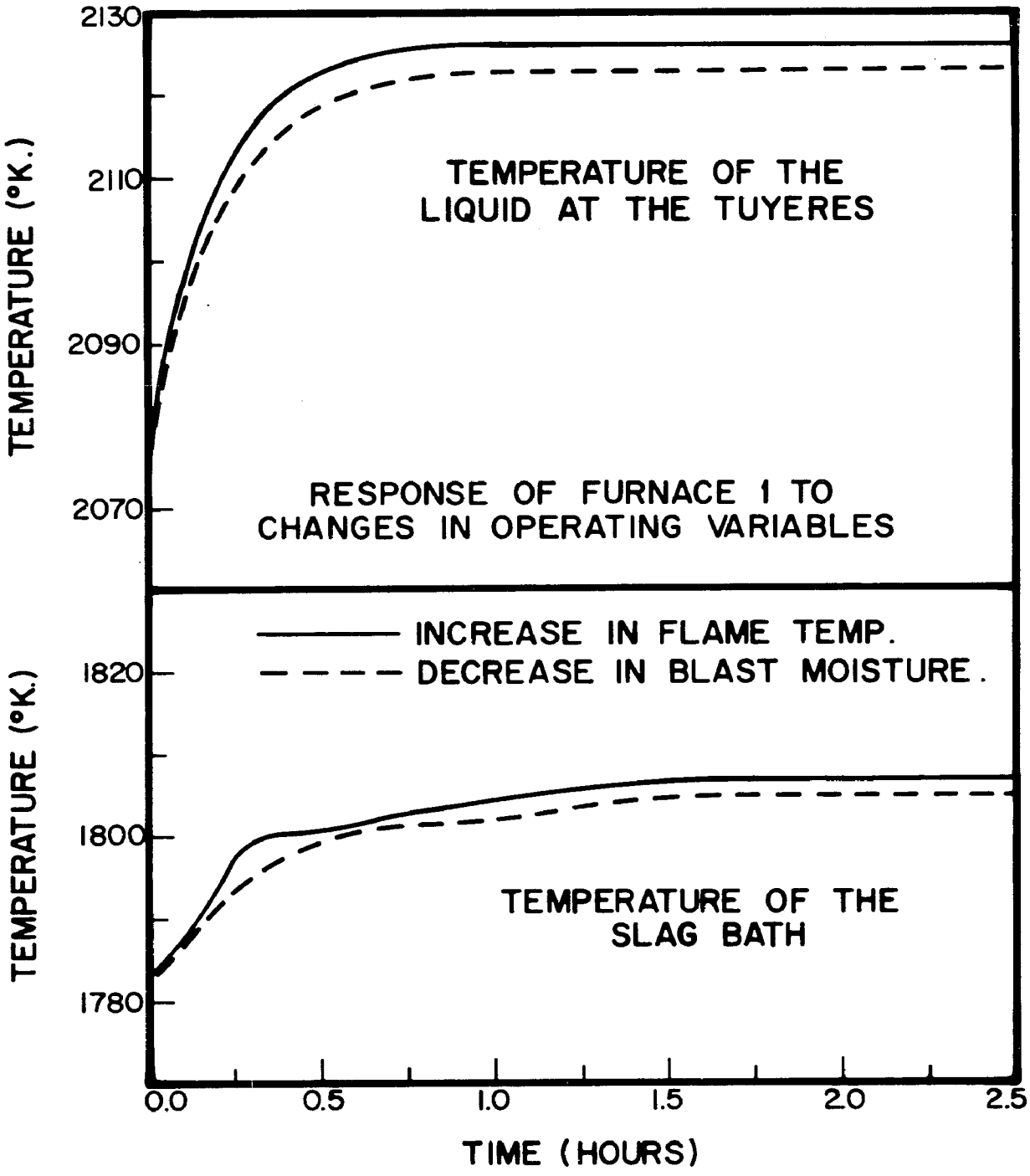
2130
2110
2090
2070
TEMPERATURE (°K.)
TEMPERATURE OF THE
LIQUID AT THE TUYERES
RESPONSE OF FURNACE 1 TO
CHANGES IN OPERATING VARIABLES
INCREASE IN FLAME TEMP.
DECREASE IN BLAST MOISTURE.
1820
1800
1780
TEMPERATURE (°K.)
TEMPERATURE OF THE
SLAG BATH
0.0
0.5
1.0
1.5
2.0
2.5
TIME (HOURS)

Figure 27

The response with time of the hot metal silicon composition corresponding to the slag bath temperatures shown in Figure 26.

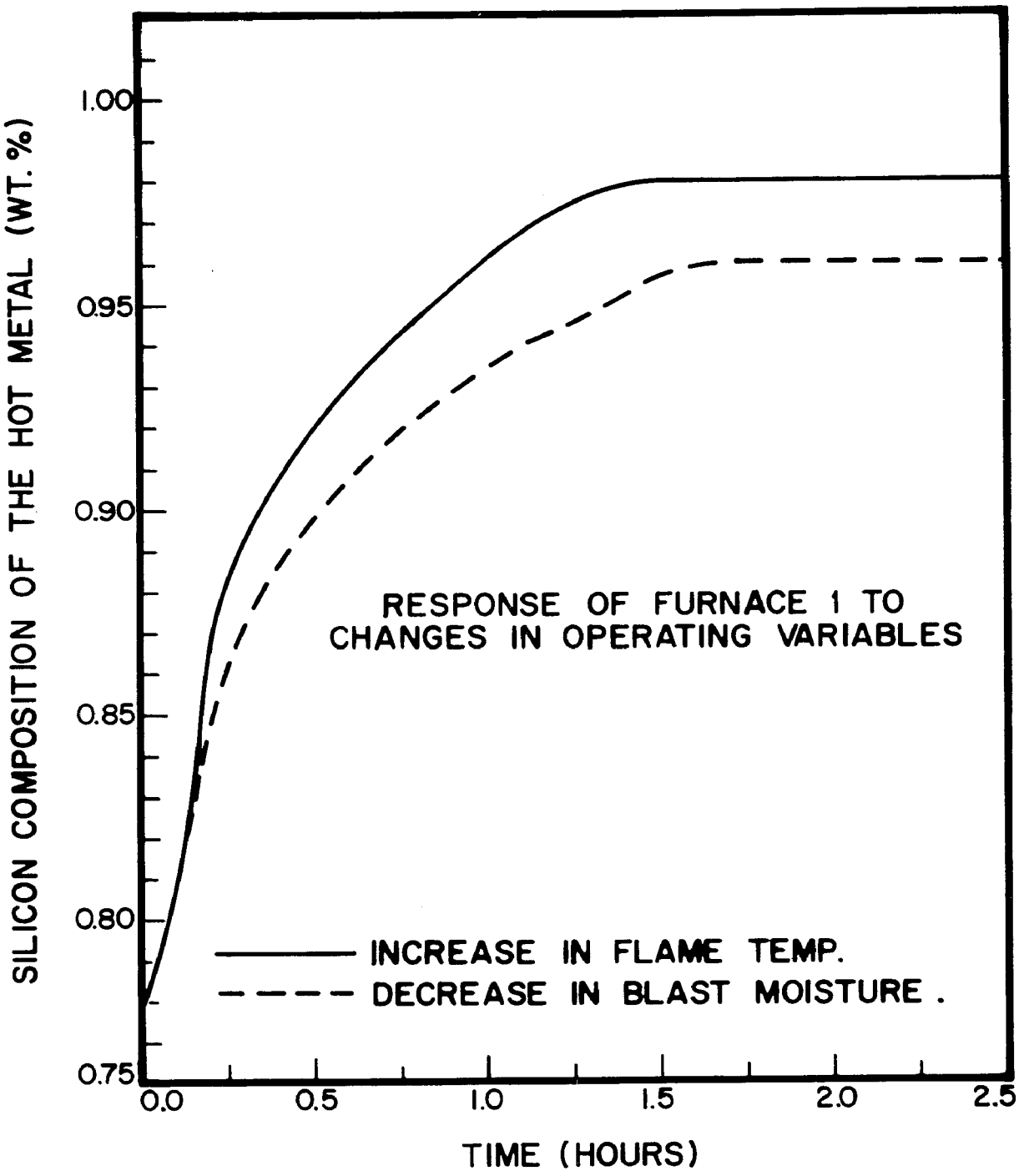
SILICON COMPOSITION OF THE HOT METAL (WT. %)
1.00
0.95
0.90
0.85
0.80
0.75
0.0
0.5
1.0
1.5
2.0
2.5
TIME (HOURS)
RESPONSE OF FURNACE 1 TO
CHANGES IN OPERATING VARIABLES
INCREASE IN FLAME TEMP.
DECREASE IN BLAST MOISTURE .

Figure 28

The time response of the hot metal manganese and sulfur composition corresponding to the slag bath temperatures shown in Figure 26.

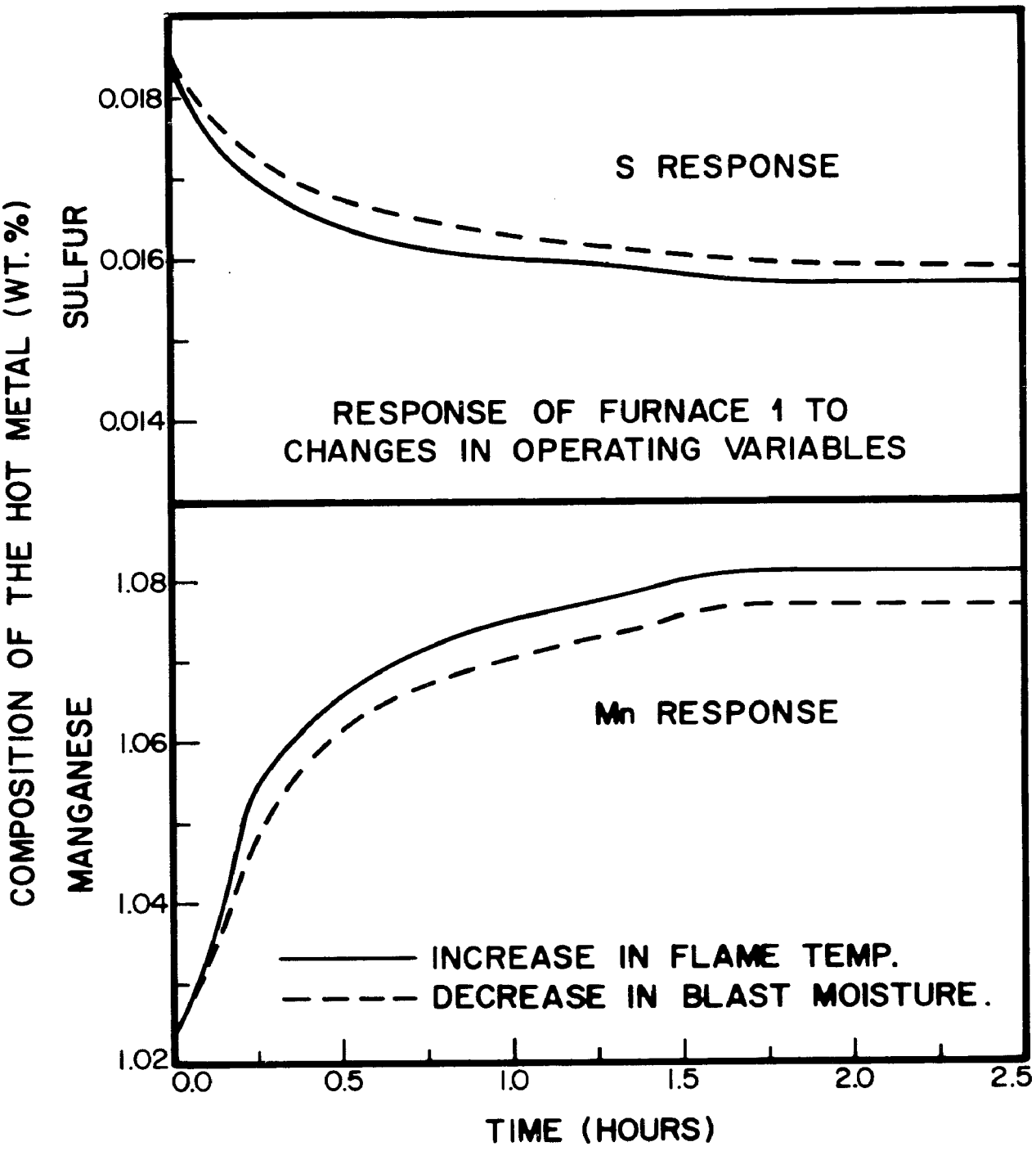
COMPOSITION OF THE HOT METAL (WT. %)
SULFUR
0.018
0.016
0.014
S RESPONSE
RESPONSE OF FURNACE 1 TO
CHANGES IN OPERATING VARIABLES
MANGANESE
1.08
1.06
1.04
1.02
Mn RESPONSE
INCREASE IN FLAME TEMP.
DECREASE IN BLAST MOISTURE.
0.0
0.5
1.0
1.5
2.0
2.5
TIME (HOURS)

SUMMARY AND CONCLUSIONS

In summary of the work presented above it can be stated that a model of the iron blast furnace has been assembled which exhibits excellent agreement with reported operating data and is quite generalized in nature. This model represents a step forward in the state of the art in that previous models of the furnace have been dependent on extensive prior operating data and knowledge of the particular furnace under consideration. Also, until now, no model has been able to predict the metal and slag chemistry and temperature as well as the hearth model presented in this work.

From the results achieved with these models it is concluded that:

Metal Chemistry

1. The liquid metal and slag temperatures and compositions can be determined based on the assumptions of carbon saturation of the hot metal, all phosphorus in the furnace enters the hot metal, and equilibrium distribution of Si, S, and Mn between the slag and metal phases is achieved. To predict the compositions, the proper pressure controlling the formation of CO bubbles in the slag phase must be taken into consideration-this is taken as the absolute pressure obtaining in the hearth region of the furnace.

2. The predictions of the slag and metal compositions and temperatures using actual furnace charge rates and chemical

compositions of the charge materials show excellent agreement with the reported cast results. The model is also able to reflect all expected trends of behavior of the metal composition as a function of temperature, pressure, and slag composition.

3. The excellent results obtained with the hearth model lend considerable weight to the assumptions concerning the physical situation that exists in the hearth between the slag and metal baths, metal droplets, coke particle columns, and absolute pressure.

Steady-State Model

1. The stack and bosh regions of the furnace can be simulated very well considering only the kinetics of the chemical reactions and heat transfer and using the physical properties of the charge materials.

2. The profiles predicted by the stack and bosh models for the gas and solid temperatures and the CO, CO_2, and H_2 mole fractions of the gas phase show excellent agreement with the shapes of the profiles for the same variables obtained with probes on actual operating furnaces.

3. The stack and bosh models do not require any prior knowledge of the furnace behavior or characteristics in order to simulate the furnace. Using only the physical properties and chemical compositions of the charge materials, the physical dimensions of the furnace and the kinetics of the chemical reactions and heat transfer the profiles for a wide range of operating conditions should be able to be simulated. The two cases simulated

in this work had quite different inputs and outputs and were handled quite well by the models.

4. The stack and bosh models can be combined with the hearth model to form a consistent generalized model of the entire blast furnace, capable of making predictions on the outputs of a furnace when the furnace inputs are known. The predicted outputs of the model are in excellent agreement with the reported furnace outputs.

Dynamic Model

1. The dynamic model indicates that the temperature of the liquid phase at the tuyere level achieves a new "steady-state" in approximately 1 hour after the introduction of the step-change for either the increase in flame temperature or decrease in blast moisture.

2. From the furnace operator's viewpoint the furnace achieves a new "steady-state" 2 casts or approximately 8 to 10 hours after the introduction of the step-change for both cases considered.

It must be kept in mind that any results obtained with the simulation are only as good as the knowledge of the process permits (and hence the validity of the assumptions) and the availability and accuracy of the necessary data and parameters.

Further work is required in studying the bosh and hearth regions so that the actual processes occurring in these regions can be more accurately simulated.

Improvements in all measured values are eagerly welcomed. In

particular, complete gas viscosity and thermal conductivity data over a wide range of temperatures are needed. Also, up to date techniques should be brought to bear to determine the specific heats of the charge materials as well as the liquid slag and metal baths. Finally, any improvements in the thermodynamic values of standard free energy changes and heats of reactions for the various reactions considered can only make the simulation better.

COMPUTER PROGRAMMING

The mathematical calculations and models discussed in this thesis were programmed in Fortran IV compiler language and executed on the Control Data Corporation Model 6400 electronic computer. Typical computer times required to execute the steady-state model, including determination of the slag and metal temperatures and compositions, are of the order of 25 seconds as long as the proper values of the parameters that are required at the stockline are known. (60 to 120 seconds of additional computer time are necessary to select the proper initial conditions at the stockline.) The prediction of the time response of the furnace required about 120 seconds of computer time to simulate 2.5 hours of furnace time. Included in the 120 seconds is the determination of the instantaneous temperatures and compositions of the slag and metal baths.

Due to the extensive length of the resulting computer programs required to execute the described simulations, the program listings have not been included in this presentation. However, information pertaining to any aspect of the computer techniques and programming can be obtained by contacting the author or by contacting the Department of Metallurgy and Materials Science of Lehigh University where copies of the computer programs have been left on file with Professors W. C. Hahn and S. K. Tarby.

RECOMMENDATIONS FOR FUTURE WORK

Before any future attempts at modification or refinement of these models, both static and dynamic, are undertaken, they should be tested extensively on additional actual operating blast furnace data in order to determine how widely applicable they are to various operating practices. Once extensive testing has been completed, it will be possible to determine what modifications or parameter adjustments are necessary to meet differing operating conditions. (As an example of such a parameter adjustment, it may be necessary to alter the porosity of the ore particles, consistent with the type of iron oxide being charged to the furnace and its reduction characteristics. Such an alteration can result from laboratory tests on the reducibility of the various ores under consideration.)

The sensitivity of the model can be increased, but it is questionable as to the value of such a change, as the model sensitivity will begin to exceed the accuracy of the available thermodynamic data. It can not be stressed enough that the model predictions are only as good as the data that are fed into the model. As a result, data concerning the raw material particle sizes and chemical compositions must be better than those that result from the normal sampling techniques now employed in practice. The blast variables must also be known with a great deal of accuracy. All improvements in the thermodynamic data are eagerly welcomed, especially with regard to the heat contents and specific heats of

the liquid slag and metal phases.

In the future it may prove worthwhile to investigate the validity of some of the assumptions made for these models, especially those concerning radial gradients in the stack and bosh regions, and the assumptions involving the physical situation existing in the bosh region of the furnace. Valuable information concerning radial gradients may result from actual scaled-down physical models of the particle distribution and gas flow in the shaft and this information may be incorporated into the model. The bosh region is very difficult to study in an operating furnace, and here again scaled-down models of the region may be helpful in describing melting and the relationship of the gas, liquid, and solid phases.

APPENDIX A

Nomenclature for the Stack and Bosh Models

A_w	the area of the stack walls between the stockline and the tuyere level, (m^2)
A_z	cross-sectional area of furnace at z, (m^2)
C, C_S	specific heat of gas and solid particles, (kcal/kg°K)
C_w	specific heat of cooling water, (kcal/kg°K)
c_{HO}, c_L	initial concentration of hematite and limestone in the charge, ($kgmol/m^3$(bed))
c', c'_e, c'_i, c'_o	concentration of CO_2 in the bulk gas, at equilibrium, on the reaction interface, at the outer surface of the solid particles for the decomposition of limestone, ($kgmol(CO_2)/m^3$
D_{CO}, D_{CO_2}, D_{H_2}, D_{H_2O}	diffusion coefficients of CO, CO_2, H_2, and H_2O in the gas phase, (m^2/hr)
D_{S1}, D_{S5}	intraparticle diffusion coefficient of CO and H_2 in the reduced iron phase, (m^2/hr)
D_{S4}, D_{S2}, D_{S6}	intraparticle diffusion coefficient of CO_2 in the decomposed CaO, of CO_2 and H_2 in coke particles, (m^2/hr)
D_z	inner diameter of furnace at z, (m)
d_{pa}	average diameter of all solid particles, (m)
d_c, d_l, d_p	average diameter of particles of coke, limestone, and iron ore, (m)
F, F_S	volume rate of flow of gas and solid particles, (Nm^3/hr, m^3(bed)/hr)
F_b, F_{bw}	volume rate of dry blast and wet blast, (Nm^3/hr)
f_l	fraction of limestone decomposed
f_s	fraction of iron ore reduced

G, G_S	mass flux of gas and solid particles, (kg/m^2hr)
g	acceleration due to gravity, (m/hr^2)
g_c	conversion factor, ($kg\ m/Kg\ hr^2$)
K'	constant equal to F (w + v)
K_1, K_4, K_5 K_7	equilibrium constants for reactions (1a), (33a), (43a), and (60a)
k	thermal conductivity of gases, (kcal/m hr °K)
k_{f1}, k_{f2}, k_{f4}, k_{f5}, k_{f6}	gas-film mass-transfer coefficient for reactions (1a), (23a), (33a), (43a), and (54a), (m/hr)
k_1, k_2, k_4, k_5, k_6	rate constants for reactions (1a), (23a), (33a), (43a), and (54a), (m/hr, m^3kg hr, kgmol (CO_2)/ m^2 hr, m/hr, m^3/kg hr)
m_c	mass of a coke particle, (kg)
N, N_c, N_L	number of particles of iron ore, coke, and limestone per unit volume of bed, ($1/m^3$(bed))
Nu	Nusselt number
p, $p°$	pressure of gas and pressure at standard states, (Kg/m^2)
Pr	Prandtl number
R, R'	Gas constants, (kcal/kgmol °K, atm-m^3/kgmol °K)
Re	Reynolds number
R_3^*	overall reaction rate for direct reduction of ore by carbon, (kgmol CO/m^3 hr)
R_1^*, R_2^*, R_4^*, R_5^*, R_6^*, R_7^*	overall reaction rate per unit volume of bed for reactions (1a), (23a), (33a), (43a), (54a), and (60a), (kgmol (CO)/m^3 hr, kgmol (CO_2)/m^3 hr, kgmol (CO_2)/m^3 hr, kgmol (H_2)/m^3 hr, kgmol (H_2O)/ m^3 hr, and kgmol H_2/m^3 hr)
r_i, r_o	radius of reaction interface and outer surface of particle, (m)
Sc	Schmidt number

Sh	Sherwood number
T, t	temperature of gas and solid particles, (°K)
T°	temperature of gas at standard states, (°K)
T_b	blast temperature, (°K)
T_{we}, T_{wi}	exit and inlet temperature of the cooling water, (°K)
U	overall heat transfer coefficient based on inner surface area of furnace wall, ($kcal/m^2$ hr °C)
u	velocity of the gas, (m/hr)
v, v_o	mole fraction of H_2O in gas stream and in the top gas
w, w_o, w_e	mole fraction of H_2 in the gas stream, in the top gas and at equilibrium
W_w	flow rate of cooling water (kg/hr)
X_i	volume fraction of solid particles having diameter d_i
x, x_o, x_i, x_e	mole fraction of CO in the bulk gas stream, at the outer particle surface, at the reaction interface, and at equilibrium
y, y_s	mole fraction of CO_2 in the bulk gas stream and at the outer surface of solid particle
ε	void fraction in the bed
ε_c, ε_p, ε_{pl}	porosity of coke, iron ore, and limestone particles
ε_v, ε_{vl}	porosity in the reduced Fe and the outer layer of CaO
μ	viscosity of the gas stream, (kg/m hr)
ξ_p, ξ_c, ξ_l	labyrinth factor of iron ore, coke, and limestone
ρ_g	density of the gas stream, (kg/Nm^3)
ρ_b	density of solid particles, (kg/m^3(bed))

ρ_c	density of coke (kg/m^3)
ϕ, ϕ_c, ϕ_l	shape factor for iron ore, coke, and limestone particles

DETAILS FOR THE CHEMICAL REACTIONS, THERMAL PROPERTIES, AND DERIVATION OF DIFFERENTIAL EQUATIONS FOR THE STACK AND BOSH MODELS

Chemical Reactions

(The expressions for the rates of the chemical reactions and the data required to compute these rates are taken from the derivations and compilations of Muchi[21]).

1. Indirect Reduction of Iron Ore by CO.

The overall reaction involved with the indirect reduction of iron ore by CO is

(1a) $1/3\ Fe_2O_3 + CO \rightleftarrows 2/3\ Fe + CO_2$

The overall reaction rate for Eq. (1a) is dependent upon three distinct reaction steps which are (1) diffusion of product and reactant species through the gas film surrounding the particle, (2) intraparticle diffusion of the gaseous species through the reacted particle layer, and (3) chemical reaction at the reaction interface. These three steps occur continuously and simultaneously and expressions can be written for each of them.

The rate of diffusion through the gas film:

(2a) $$R_1^* = \pi d_p^2 \phi^{-1} N k_{f1} 273(x-x_o)/22.4t$$

The rate of diffusion through the solid product layer:

(3a) $$R_1^* = \pi d_p^2 \phi^{-1} N D_{S_1} 273(x_o-x_i) r_i / 22.4t (r_o-r_i) r_o$$

The rate of chemical reaction at the reaction interface:

(4a) $$R_1^* = \pi d_p^2 \phi^{-1} N k_1 (1+1/K_1)(r_i/r_o)^2 273(x_i-x_e)/22.4t$$

Since the slowest process limits the overall reaction rate, the overall rate can be found by combining Eqs. (2a-4a) and

solving for R_1^* which yields:

$$(5a)\quad R_1^* = \frac{\pi d_p^2 \phi^{-1} N273(x-x_e)/22.4t}{(1/k_{f1})+(d_p/2)\{(1-f_s)^{-1/3}-1\}/D_{S1}+\{(1-f_s)^{2/3}k_1(1+1/K_1)\}^{-1}}$$

Each term in the denominator of the right-hand side of Eq. (5a) represents the resistances of the three processes of gas film diffusion, diffusion through the solid product layer, and chemical reaction, respectively.

The value of k_{f1} is evaluated from

(6a) $Sh = 2.0 + 0.55(Re)^{1/2}(Sc)^{1/3}$, where

(7a) $Sh = k_{f1}d_p/D_{CO}$

(8a) $Re = d_p u\rho/\mu$

(9a) $Sc = \mu/\rho D_{CO}$

The diffusion coefficient of CO in the gas phase, D_{CO}, is calculated from

(10a) $D_{CO} = 2.592 \times 10^{-6} T^{1.78}$

for temperatures under 848°K and by

(11a) $D_{CO} = 2.592 \times 10^{-6} T^{2}$

for temperatures greater than 848°K.

The value of D_{S1} for diffusion through the shell of the iron phase surrounding the unreacted core of iron ore is given by

(12a) $D_{S1} = D_{CO}\ \varepsilon_v\ \xi_p$, where

(13a) $\varepsilon_v = 0.53 + 0.47\varepsilon_p$ and

(14a) $\xi_p = 0.238\varepsilon_p + 0.04$ for $0.15 \leq \varepsilon_p \leq 0.5$.

D_{CO} for the D_{S1} calculation is calculated as in Eqs. (10a and

11a) except that t is substituted for T, the temperature of the gas in the particle pores being assumed equal to the particle temperature.

The value of k_1 is given by

(15a) $k_1 = 347 \exp(-3460/t)$

As discussed earlier, reaction (1a) actually goes in three stages

(16a) $3Fe_2O_3 + CO = 2Fe_3O_4 + CO_2$

(17a) $Fe_3O_4 + CO = 3FeO + CO_2$

(18a) $FeO + CO = Fe + CO_2$

As a result of these reactions, K_1 is a function of f_s and t, and the heats of the reactions are dependent on f_s. For the range of temperatures below 848°K

(19a) $f_s < 0.111$, $K_1 = \exp(4.91 + 6235/t)$

(20a) $f_s > 0.111$, $K_1 = \exp(-0.7265 + 543.3/t)$.

For the range of temperatures above 848°K

(21a) $f_s < 0.111$, $K_1 = \exp(4.91 + 6235/t)$

(22a) $0.111 < f_s < 0.333$, $K_1 = \exp(2.13 - 2050.0/t)$

(23a) $f_s > 0.333$, $K_1 = \exp(-2.642 + 2164.0/t)$

The heats of reaction for Eqs. (16a-18a) are -7.88×10^3 kcal/kgmol(CO), 7.12×10^3 kcal/kgmol(CO), and -5.45×10^3 kcal/kgmol(CO), respectively.

2. Solution-Loss Reaction

The solution-loss reaction is

(24a) $C + CO_2 \rightarrow 2CO$.

The solution-loss reaction rate is determined by 2 distinct reaction steps which are (1) diffusion of the product and reactant gases through the gas-film surrounding the particle and (2) diffusion in the pores of the particle and chemical reaction on the interior surface of the coke particle pores. These two reaction steps occur simultaneously and continuously and the rates for each are given by Eqs. (25a and 26a).

Diffusion rate through the gas film:

(25a) $R_2^* = \pi d_c^2 N_c \phi_c^{-1} k_{f_2} 273(y-y_s)/22.4t$

Diffusion rate in the particle pores with chemical reaction:

(26a) $R_2^* = E_f m_c N_c k_2 273 y_s/22.4t$

Combining Eqs. (25a and 26a) produces the overall reaction rate expression

$$(27a)\quad R_2^* = \frac{\pi d_c^2 \phi_c^{-1} N_c 273y/22.4t}{(1/k_{f_2}) + (6/d_c \rho_c E_f k_2)}$$

k_{f_2} is evaluated by using Eqs. (6a-9a) by substituting D_{CO_2} for D_{CO}. D_{CO_2}, defined as the diffusion coefficient of CO_2 in the ternary system of $CO\text{-}CO_2\text{-}N_2$, is expressed as

(28a) $D_{CO_2} = 2.236 \times 10^{-6} T^{1.78}$

The reaction rate coefficient, k_2, is determined from

(29a) $k_2 = 2.99 \times 10^3 \exp(-80000/Rt)$.

E_f, the effectiveness factor, is calculated in terms of the Thiele modulus, m, by

(30a) $E_f = 3(m \coth m - 1)/m^2$, where

(31a) $m = d_c/2(\rho_c k_2/D_{S_2})^{1/2}$

The diffusion coefficient of CO_2 in the pores of the coke particle is given by

(32a) $D_{S_2} = D_{CO_2}\varepsilon_c\xi_c$

with the value of ε_c taken as 0.45 and ξ_c approximated by

(33a) $\xi_c = 0.238\varepsilon_c + 0.04$

D_{CO_2} in Eq. (32a) is calculated by substituting t for T into Eq. (28a).

The heat of reaction for Eq. (24a) is taken as 40.8×10^3 kcal/kgmol(CO_2).

3. Decomposition of Limestone

The decomposition of limestone proceeds by

(34a) $CaCO_3 = CaO + CO_2$

The decomposition of limestone, as with the reduction of ore by CO, proceeds with three distinct reaction steps-(1) the rate of chemical reaction at the interface between CaO and $CaCO_3$, (2) the rate of diffusion through the solid CaO product layer, and (3) the rate of diffusion of CO_2 through the gas film layer surrounding the stone particle. The rates for these three steps are given by Eqs. (35a-37a). The rate of reaction taking place on the reaction interface:

(35a) $R_4^* = 4\pi r_i^2 \phi_1^{-1} N_L k_4 R' t(c_e' - c_i')/K_4$

The rate of diffusion through the decomposed product layer of CaO:

(36a) $R_4^* = \{4\pi r_o r_i/(r_o - r_i)\}\phi_1^{-1} N_L D_{S4}(c_i' - c_o')$

The rate of diffusion through the surrounding gas film-layer:

(37a) $R_4^* = 4\pi r_o^2 \phi_1^{-1} N_L k_{f4} (c_o' - c')$

The overall reaction rate for Eq. (34a) is a combination of Eqs. (35a-37a) and yields

$$(38a)\quad R_4^* = \frac{4\pi r_o^2 \phi_1^{-1} N_L (c_e' - c')}{(1/k_{f_4}) + d_1\{(1-f_1)^{-1/3} - 1\}/2D_{S_4} + \{(1-f_1)^{2/3} k_4 R' t/K_4\}^{-1}}$$

k_{f_4} is determined from Eqs. (6a-9a), substituting D_{CO_2} for D_{CO}. D_{CO_2}, for a temperature below 1173°K, is given by Eq. (28a), but for temperatures greater than 1173°K because of the intense endothermic reaction, (T+t)/2 is substituted for T in Eq. (28a).

D_{S_4}, the diffusion coefficient for CO_2 in the pores of the decomposed outer shell, is determined from

(39a) $D_{S_4} = D_{CO_2} \varepsilon_{v1} \xi_1$

where ε_{v1} is estimated by

(40a) $\varepsilon_{v1} = 0.702\varepsilon_{p1} + 0.298$ with $\varepsilon_{p1} = 0.20$ and

(41a) $\xi_1 = (\varepsilon_{v1})^{0.41}$.

The rate constant for Eq. (34a) is obtained from

(42a) $k_4 = 5.47 \times 10^6 \exp(-40000/RT)$.

The equilibrium constant for the reaction is given by

(43a) $\log K_4 = -8202.5/t + 7.0099$.

The heat of reaction for limestone decomposition is taken as 42.5×10^3 kcal/kgmol(CO_2).

4. Indirect Reduction of Iron Ore by H_2

The reaction expressing the indirect reduction of iron ore

by hydrogen is

(44a) $1/3Fe_2O_3 + H_2 \overset{\rightarrow}{\leftarrow} 2/3Fe + H_2O$

Considering the rates of diffusion in the gas film surrounding the particle, the rate of diffusion in the reduced product layer, and the rate of reaction at the reacting interface, the rate expression for reduction by H_2 parallels the rate expression for reduction by CO as shown in Eq. (45a).

$$(45a)\quad R_5^* = \frac{\pi d_p^2 \phi^{-1} N273(w-w_e)/22.4t}{(1/k_{f_5})+(d_p/2)\{(1-f_s)^{-1/3}-1\}/D_{S_5}+\{(1-f_s)^{2/3}k_5(1+1/K_5)\}^{-1}}$$

k_{f_5} is calculated by substituting D_{H_2} for D_{CO} into Eqs. (6a-9a). The diffusion coefficient of H_2 in the gas surrounding the ore particles, D_{H_2}, is expressed by

(46a) $D_{H_2} = 3.960 \times 10^{-6} T^{1.78}$

and the diffusion coefficient for H_2 through the pores in the product layer is given by

(47a) $D_{S_5} = D_{H_2} \varepsilon_v \xi_p$.

ε_v and ξ_p are calculated by Eqs. (13a and 14a). D_{H_2} for Eq. (47a) is evaluated by substituting t for T in Eq. (46a).

The rate constant, k_5, and the equilibrium constant, K_5, are given by Eqs. (48a and 39a) for temperatures below 848°K.

(48a) $k_5 = 102.78t \exp(-14900.0/Rt)$.

(49a) $K_5 = \exp(8.883-8475.0/t)$.

For temperatures above 848°K,

(50a) $k_5 = 82.05t \exp(-15300/Rt)$

(51a) $K_5 = \exp(1.837-1732.2/t)$.

The reduction of Fe_2O_3 by H_2 also proceeds by 3 processes such that

(52a) $3Fe_2O_3 + H_2 = 2Fe_3O_4 + H_2O$

(53a) $Fe_3O_4 + H_2 = 3FeO + H_2O$

(54a) $FeO + H_2 = Fe + H_2O$

and the heats of reaction are -2.8×10^3kcal/kgmol(H_2), 16.1×10^3kcal/kgmol(H_2), and 6.5×10^3kcal/kgmol(H_2). respectively,

5. Reaction Between Coke and Steam

The reaction between coke and steam can be expressed as

(55a) $C + H_2O = CO + H_2$

Assuming that Eq. (55a) is of the irreversible first-order variety, the reaction rate is expressed as

$$(56a)\quad R_6^* = \frac{\pi d_c^2 \phi_c^{-1} N_c 273v/22.4t}{(1/k_{f6})+(6/d_c\rho_c E_f' k_6)}$$

The value of k_{f6} is found by substituting D_{H_2O} for D_{CO} into Eqs. (6a-9a). The diffusion coefficient in the surrounding gas film, D_{H_2O}, is given by

(57a) $D_{H_2O} = 1.5 \times 10^{-6} T^{1.78}$

The effectiveness factor E_f' is evaluated be Eq. (30a) and substituting m' for m where m' is given by

(58a) $m' = d_c/2\ (\ _ck_6/D_{S_6})^{1/2}$

D_{S_6} is estimated by

(59a) $D_{S_6} = 6.62 \times 10^{-2}(1.5 \times 10^{-6} t^{1.78})$

and the reaction rate coefficient is

(60a) $k_6 = 4.83 \times 10^4 t \exp(-17311/t)$

The heat of reaction for Eq. (55a) is taken as 31.5×10^3 kcal/kgmol(CO).

6. Reaction Between CO and Steam

The CO-steam reaction proceeds according to Eq. (61a).

(61a) $CO + H_2O \rightleftarrows CO_2 + H_2$

It has been reported in the literature that the reaction between CO and steam occurs very rapidly in the presence of iron oxide and coke particles which have catalytic effects on the reaction.

Assuming that the equilibrium for this reaction holds in the gas phase at each position of the furnace from the top of the bed, the reaction rate for Eq. (61a) can be given as

(62a) $R_7^* = \Delta(Fw)/22.4(\pi D_z^2/4)\Delta z$

The equilibrium constant for Eq. (62a) is given as

(63a) $K_7 = \exp(4355/T-3.8297)$

The heat of reaction is taken as -9.84×10^3kcal/kgmol(CO_2).

DERIVATION OF DIFFERENTIAL EQUATIONS

Conservation of Iron Ore

Consider the flux of oxygen in the iron ore through the horizontal plane in the furnace z distance from the stockline.

Flux (kg-moles oxygen/hr m^2)$=F_S c_{HO}[(1-f_s)]/A_z$

Consider the change in the flux with distance down the stack.

d(Flux)/dz= Generation of oxygen in the ore

The generation term in this case is $(-R_1^*-R_5^*-R_3^*)$ since oxygen is removed from the ore by these reactions.

$$F_S c_{HO}(-df_s/dz)/A_z = (-R_1^*-R_3^*-R_5^*) \text{ or}$$

$$\text{(64a)}\quad df_s/dz = A_z(R_1^*+R_3^*+R_5^*)/F_S c_{HO}$$

Conservation of CO_2 in the Fluxstone

Consider the flux of CO_2 contained by the fluxstone similar to the flux of oxygen in the ore considered above.

$$\text{Flux (kg-moles } CO_2/\text{hr m}^2) = F_S c_{LO}(1-f_1)/A_z$$

$$d(\text{Flux})/dz = \text{Generation of } CO_2 \text{ in the fluxstone} = -R_4^*$$

$$F_S c_{LO}(-df_1/dz)/A_z = -R_4^*$$

$$\text{(65a)}\quad df_1/dz = A_z R_4^*/F_S c_{LO}$$

Conservation of the Components in the Gas Phase

The gas phase is composed of CO, CO_2, H_2, H_2O, and N_2. The fluxes for the CO, CO_2, H_2, and H_2O are given as

$$Fx/22.4A_z \text{ - kg-moles CO/hr m}^2, \quad Fy/22.4A_z \text{ - kg-moles } CO_2/\text{hr m}^2$$

$$Fw/22.4A_z \text{ - kg-moles } H_2/\text{hr m}^2, \quad Fv/22.4A_z \text{ - kg-moles } H_2O/\text{hr m}^2$$

where $F = 47.4F_b/(1-x-y-w-v)$.

Equating the change of flux with distance, dz, to the

generation terms for each of these components results in

for CO

$$(66a)\quad \frac{F[(1-x-y-w-v)dx/dz-x(-dx/dz-dy/dz-dw/dz-dv/dz)]}{A_z(22.4)(1-x-y-w-v)} = R_1^*-2R_2^*-R_6^*-R_3^*$$

for CO_2

$$(67a)\quad \frac{F[(1-x-y-w-v)dy/dz-y(-dx/dz-dy/dz-dw/dz-dv/dz)]}{A_z(22.4)(1-x-y-w-v)} = -R_1^* + R_2^* - R_4^*$$

for H_2

$$(68a)\quad \frac{F[(1-x-y-w-v)dw/dz-w(-dx/dz-dy/dz-dw/dz-dv/dz)]}{A_z(22.4)(1-x-y-w-v)} = R_5^* - R_6^*$$

for H_2O

$$(69a)\quad \frac{F[(1-x-y-w-v)dv/dz-v(-dx/dz-dy/dz-dw/dz-dv/dz)]}{A_z(22.4)(1-x-y-w-v)} = -R_5^* + R_6^*$$

Adding Eqs. (66a-69a) produces Eq. (70a)

$$(70a)\quad \frac{(dx/dz+dy/dz+dw/dz+dv/dz) + x(dx/dz+dy/dz+dw/dz+dv/dz) + y(dx/dz+dy/dz+dw/dz+dv/dz)}{(1-x-y-w-v)} + w(dx/dz+dy/dz+dw/dz+dv/dz) + v(dx/dz+dy/dz+dw/dz+dv/dz) = \frac{(-R_3^*-R_2^*-R_4^*-R_6^*)(22.4)A_z}{F}$$

Factor out (dx/dz+dy/dz+dw/dz+dv/dz) in Eq. (70a), producing Eq. (71a).

$$(71a)\quad (dx/dz+dy/dz+dw/dz+dv/dz)[1+(x+y+w+v)/(1-x-y-w-v)] = (-R_2^* - R_3^* - R_4^* - R_6^*)(22.4)A_z/F$$

$$(dx/dz+dy/dz+dw/dz+dv/dz)[1-1+1/(1-x-y-w-v)] = (-R_2^* - R_3^* - R_4^* - R_6^*)(22.4)A_z/F$$

Solving Eq. (71a) for (dx/dz+dy/dz+dw/dz+dv/dz) yields Eq. (72a).

$$(72a)\quad (dx/dz+dy/dz+dw/dz+dv/dz) = (1-x-y-w-v)(-R_2^* - R_3^* - R_4^* - R_6^*)(22.4)A_z/F$$

Substituting (dx/dz+dy/dz+dw/dz+dv/dz) into Eqs. (66a-68a) for CO, CO_2, and H_2 produces

For CO

$$(73a)\quad F[(1-x-y-w-v)dx/dz-x(1-x-y-w-v)(R_3^*+R_2^*+R_4^*+R_6^*)22.4A_z/F]=(1-x-y-w-v)[R_1^*-R_2^*-R_6^*-R_3^*]A_z22.4$$

(74a) $Fdx/dz = [R_1^* + (x-1)R_3^* + (x-2)R_2^* + xR_4^* + (x-1)R_6^*]A_z 22.4$

(75a) $dx/dz = (22.4)A_z[(\delta + \xi x)(R_1^* + R_3^*) + (x-2)R_2^* + xR_4^* + (x-1)R_6^*]/F$

For CO_2

(76a) $F[(1-x-y-w-v)dy/dz - y(1-x-y-w-v)(R_3^*+R_2^*+R_4^*+R_6^*)22.4A_z/F] = (1-x-y-w-v)[-R_1^*+R_2^*-R_4^*]A_z(22.4)$

(77a) $Fdy/dz = [-R_1^* + yR_3^* + (y+1)R_2^* + (y-1)R_4^* + yR_6^*]A_z(22.4)$

(78a) $dy/dz = [(\xi y - \tau)(R_1^* + R_3^*) + (y+1)R_2^* + (y-1)R_4^* + yR_6^*](22.4)A_z/F$

For H_2

(79a) $F[(1-x-y-w-v)dw/dz - w(1-x-y-w-z)(R_3^*+R_2^*+R_4^*+R_6^*)22.4A_z/F] = (1-x-y-w-z)[R_5^*-R_6^*]A_z(22.4)$

(80a) $Fdw/dz = [wR_3^* + wR_2^* + wR_4^* + R_5^* + (w-1)R_6^*]A_z(22.4)$

(81a) $dw/dz = [\xi wR_3^* + wR_2^* + wR_4^* + R_5^* + (w-1)R_6^*]A_z(22.4)/F$

Conservation of Mass of the Charge Materials

Consider the mass flux of the charge materials at a level z distance from the stockline.

$F_S\rho_b/A_z$ - kg/hr m^2

The change of this flux with distance is equal to the generation term and becomes

$$d(F_S\rho_b)/A_z = \text{Generation of mass} = -16R_1^* -12R_2^* -28R_3^* -44R_4^* -16R_5^* - 12R_6^*$$

$$(82a)\quad d\rho_b = -A_z(16R_1^* + 12R_2^* + 28R_3^* + 44R_4^* + 16R_5^* + 12R_6^*)/F_S$$

$$(83a)\quad \text{and } q_5 = 16R_1^* + 12R_2^* + 28R_3^* + 44R_4^* + 16R_5^* + 12R_6^*$$

Conservation of Energy in the Charge Materials

Consider the heat or energy flux of the charge materials

$F_S\rho_b C_S t/A_z$ - units of kcal/hr m^2

The change in flux with distance is equal to the heat generation term which is

$$d(F_S\rho_b C_S t)/A_z dz = \text{Generation} = 6(1-\varepsilon)h_p(T-t)/\phi d_{pa} - [\Delta H_1R_1^* + \Delta H_2R_2^* + \Delta H_3R_3^* + \Delta H_4R_4^* + \Delta H_5R_5^* + \Delta H_6R_6^* + \Delta H_7R_7^*]$$

$$F_S d(\rho_b C_S t)/A_z dz = F_s[\rho_b C_S dt/dz + \rho_b t dC_S/dz + C_S t d\rho_b/dz]/A_z \quad \text{where } dC_S/dz = (dC_S/dt)(dt/dz)$$

$$dt/dz[\rho_b C_S + \rho_b dC_S/dt] = A_z[6(1-\varepsilon)h_p(T-t)/\phi d_{pa} - (\Delta H_1R_1^* + \Delta H_2R_2^* + \Delta H_3R_3^* + \Delta H_4R_4^* + \Delta H_5R_5^* + \Delta H_6R_6^* + \Delta H_7R_7^*) + tC_S q_5]/F_S$$

$$(84a)\quad \frac{dt}{dz} = \frac{A_z[6(1-\varepsilon)h_p(T-t)/\phi d_{pa} + q_4 + tC_S q_5]}{[F_S\rho_b(C_S + tdC_S/dt)]} \qquad \text{where}$$

$$(85a)\quad q_4 = -\Delta H_1 R_1^* - \Delta H_2 R_2^* - \Delta H_3 R_3^* - \Delta H_4 R_4^* - \Delta H_5 R_5^* - \Delta H_6 R_6^* - \Delta H_7 R_7^*$$

Conservation of Energy for the Gas Phase

Consider the energy flux of the gas

$F\rho_g C_g T/A_z$ - kcal/hr m^2

The change in flux is equal to the generation of energy in the gas phase.

$$d(F\rho_g C_g T)/A_z = 6(1-\varepsilon)h_p(T-t)/\phi d_{pa} + \pi D_z U(T-T_{we})/A_z$$

$$(86a)\quad C_g T d(F\rho_g)/dz + F\rho_g T dC_g/dz + F\rho_g C_g dT/dz = [6(1-\varepsilon)h_p(T-t)/\phi d_{pa} + \pi D_z U(T-T_{we})/A_z]A_z$$

This expression simplifies nicely, because due to overall conservation of mass

$$(87a)\quad d(F\rho_g)/dz = d(F_S\rho_b)/dz, \qquad \text{and with } dC_g/dz = (dC_g/dT)(dT/dz)$$

$$dT/dz[F\rho_g C_g + F\rho_g T(dC_g/dT)] = [6(1-\varepsilon)h_p(T-t)/\phi d_{pa} + \pi D_z U(T-T_{we})/A_z - C_g T(dF_S\rho_b/dz)/A_z]A_z$$

$$(88a)\quad \frac{dT}{dz} = \frac{A_z[6(1-\varepsilon)h_p(T-t)/\phi d_{pa} + 22.4C_g T q_2] + \pi D_z U(T-T_{we})}{F\rho_g(C_g + TdC_g/dT)} \qquad \text{where}$$

$$(89a)\quad q_2 = 1.2507R_3^* + 0.7261R_1^* + 0.5246R_2^* + 1.9768R_4^* + 0.7143R_5^* + 0.5364R_6^*$$

The expression for the pressure drop is a slight modification of the equation for pressure drop proposed by Ergun.

$$(90a)\quad dp/dz = (7.25)f_k(1-\varepsilon)G^2 p°T/g_c\varepsilon^3 d_p \rho_g T°p \qquad \text{where}$$

$$(91a)\quad f_k = 1.75 + 150(1-\varepsilon)/Re$$

In the above differential equations for $t < 1673°K$,

$R_3^* = 0$, $\delta = 1$, $\xi = 0$, and $\tau = 1$

while for $t \geq 1673°K$

$R_1^* = 0$, $\delta = -1$, $\xi = 1$, and $\tau = 0$.

The equation

(92a) $w = xK_7K'/F(xK_7 + y)$

which is used to modify the mole fraction of the H_2 in the gas phase arises from the fact that the sum of the molar rate of flow of H_2 and H_2O is constant leading to $F(w + v) \equiv$ constant (K') and the expression for the equilibrium constant of the chemical reaction

$CO + H_2O \rightleftarrows CO_2 + H_2$, which is

$K_7 = yw/xv$.

The value of v is found at each level by the expression

(93a) $v = (K'/F - w)$.

Additional Properties of Gas and Charge Materials

Assuming that the blast furnace gas consists of a gaseous mixture of CO, CO_2, H_2, H_2O, and N_2 and that additivity concerning each of the components holds, the specific heat for the gas phase is expressed as

(94a) $C_g = (S_1 + S_2T - 2.00 \times 10^5 yT^2)/M$ where,

$S_1 = 6.50 + 0.60x + 4.00y + 0.12w + 0.66v$

$S_2 = (1.00 + 0.20x + 1.40y - 0.19w + 1.58v) \times 10^{-3}$ and

$M = 28 + 16y - 26w - 10v$.

The same assumption concerning additivity of the components of the gas phase was applied to the thermal conductivity and the viscosity. The values of the thermal conductivity for each species were taken from the data compiled by the National Bureau of Standards[56].

The specific heat for the charge materials is assumed to be

a linear function of t. Muchi determined such a relationship by considering the compositions of the charge materials at the top, and by using the specific heats of slag, pig iron, and coke at 1600°C and their flow rates at the tuyere level. The resulting expressions were

(95a) For Blast Furnace 1, $C_S = 0.1913 + 3.464 \times 10^{-5} t$

(96a) and for Blast Furnace 2, $C_S = 0.1897 + 3.147 \times 10^{-5} t$.

The particle to fluid heat transfer coefficient, h_p, is determined from the expression

(97a) $Nu = 2.0 + 0.60(Re)^{1/2}(Pr)^{1/3}$, where

(98a) $Nu = h_p d_{pa}/k$

(99a) $Re = d_{pa}G/\mu$

(100a) $Pr = C_g \mu/k$, and

(101a) $G = \rho_g F/A_z$

The mean diameter of the solid particles, d_{pa}, of the burden materials is determined by

(102a) $d_{pa} = \Sigma X_i / \Sigma(X_i d_i)$

The overall heat transfer coefficient for the heat loss by the gas to the furnace walls is described by

(103a)
$$U = \frac{W_w C_w (T_{we} - T_{wi})}{A_w (T_m - T_o)/\ln[(T_m - T_{we})/(T_o - T_{we})]}$$

APPENDIX B

Nomenclature and Symbols for the Hearth Model

[ ]	indicates the enclosed component is in the liquid metal phase
( )	indicates the enclosed component is in the liquid slag phase
a_i	activity of species i
C_s	sulfur capacity, (ability of a slag to retain sulfur as described by Fincham and Richardson)
f_s	Henrian activity coefficient for S in liquid metal phase
K	equilibrium constant for the chemical reaction under consideration
p_i	partial pressure of the species i
R	universal gas constant (kcal/kgmol°K)
R_n	basicity ratio of the slag (moles CaO + moles MgO/ moles SiO_2 + moles Al_2O_3)
T	temperature at which the reaction under consideration preceeds, in most cases the temperature of the slag phase (°K unless otherwise specified)
X_i	mole fraction of component i
$\Delta G°$	standard free energy change for the chemical reaction under consideration, (kcal/kgmol)
γ_i	the Raoultian activity coefficient for species i
ε_i^X	the interaction parameter for the effect element X has on the Raoultian activity coefficient of species i

COMPUTATIONS AND EXAMPLES FOR DETERMINING THE CHEMICAL COMPOSITION OF THE SLAG AND METAL

As an example of the equilibrium distribution discussed earlier, consider the following predictions of silicon, sulfur, and manganese contents of the hot metal using equilibrium constants and selected activity data from the literature.

A representative slag composition of 45.0 wt% CaO, 36.3 wt% SiO_2, 14.8 wt% Al_2O_3, and 3.9 wt% MgO was selected and a slag temperature of 1800°K was arbitrarily chosen. For this slag

45.0 wt% CaO+3.9 wt% MgO/36.3 wt% SiO_2+14.8 wt% Al_2O_3=0.957

45.0 wt% CaO/36.3 wt% SiO_2=1.24

Since the reactions are assumed to come to equilibrium as the metal droplets fall through the slag, the temperature at which the reactions should be considered is that of the slag and not that of the hot metal as cast.

Silicon Composition

Although the silica activity data of Rein and Chipman[39] and Kay and Taylor[40] are reported for the ternary system Al_2O_3-SiO_2-CaO and a quaternary slag-Al_2O_3-SiO_2-CaO-MgO-is under consideration, Chipman[49] reported that MgO can be considered as equivalent to CaO on a weight percentage basis and therefore the ternary data are reasonably sufficient. The slag can now be considered as one of 48.9% CaO, 36.3% SiO_2, and 14.8% Al_2O_3, equating MgO to CaO by weight. On a mole fraction basis the slag composition becomes

Component	Moles/100lbs.	Mole Fraction	Mole Fraction
SiO_2	36.3/60.1=0.604	0.372	0.342
Al_2O_3	14.8/102.0=0.145	0.090	-
$AlO_{1.5}$	14.8/51.0=0.290	-	0.164
CaO+MgO	48.9/56.1=0.873	0.538	0.494
		1.000	1.000

For this slag composition, Fig. 4 of reference 39 shown the value of a_{SiO_2} to be approximately 0.06 at 1550°C. From Figs. 4 and 5 of Rein and Chipman it is seen that the a_{SiO_2} increases slightly with falling temperature and is taken as approximately 0.064 for 1527°C (1800°K).

The standard free energy change and the equilibrium constant are calculated from the expression

$$1/2\ SiO_2+C=1/2\ Si(l)+CO, \quad K=a_{Si}^{1/2}\ P_{CO}/a_{SiO_2}^{1/2}\ a_C$$

$$\Delta G°=-RT\ln K=85{,}050-43.91T(°K)$$

and at 1800°K

$$\Delta G°=85{,}050-43.91(1800)=5{,}950$$

$$\ln K=-\ G°/RT=-5{,}950/(1.987)(1800)=-1.663$$

$$K=0.188$$

Because of carbon saturation of the iron, $a_C=1$, and with a_{SiO_2} approximately 0.064, the a_{Si} is

$$a_{Si}=K^2 a_{SiO_2} a_C^{\ 2}/P_{CO}^{\ 2}$$

$$a_{Si}=(0.188)(0.188)(0.064)(1)/P_{CO}^{\ 2}=0.00226/P_{CO}^{\ 2}$$

Comparing the variations in the a_{Si} with 1 atmosphere pressure of CO and 2.5 atmospheres pressure of CO it is seen for 1 atmosphere

$$a_{Si}=0.00226/1^2=0.00226$$

and for 2.5 atmospheres

$$a_{Si}=0.00226/2.5^2=0.00226/6.25=0.000362$$

Once the a_{Si} is known for the metal droplets the concentration of silicon corresponding to this activity value must be determined. The data from Figure 10 of reference 35 expresses log γ_{Si} as a function of the mole fraction of silicon for carbon-saturated melts and for the composition range of interest. A linear approximation may be used.

At 1800°K,

$$\ln \gamma_{SI}=2.3(-1.85+3.5X_{Si}) \qquad (X_{Si}\leq 0.10)$$

Also, the relationship of $a_{Si}=\gamma_{Si}X_{Si}$ must be satisfied.

For one atmosphere pressure of CO, with $a_{Si}=0.00226$ it is easily found by a few simple calculations the $X_{Si}=0.083$ and this value satisfies both relationships.

$$\gamma_{Si}=0.00226/0.083=0.0273$$

$$\ln\gamma_{Si}=2.3(-1.85+3.5(0.083))=-3.59$$

$$\gamma_{Si}=0.0273$$

To convert the mole fraction of silicon to weight per cent silicon it is necessary to estimate the amount of carbon in the melt as well. Considering only iron-carbon-silicon melts, the solubility of carbon can be determined by

$[\%C]_{Sat}=1.28+0.00142(2780°F)-0.304[\%Si]$

$=5.23-0.304[\%Si]$

A mole fraction of 0.083 silicon results in a carbon composition of 3.74% and a silicon content of 4.90%.

Repeating the same procedure for 2.5 atmospheres of CO and $a_{Si}=0.000362$, it is found that $X_{Si}=0.021$.

$\gamma_{Si}=0.000362/0.021=0.0172$

$\ln\gamma_{Si}=2.3(-1.85+3.5(0.021))$

$\ln\gamma_{Si}=-4.07$

$\gamma_{Si}=0.017$

For 2.5 atmospheres of pressure a 0.021 mole fraction of silicon results in 4.85% carbon and a silicon composition of 1.25% (see Table Ib).

TABLE Ib

Pressure	%Si	%C	%Fe	X_{Si}	X_C	$\ln\gamma_{Si}$	γ_{Si}	a_{Si}
1.0	4.90	3.74	91.36	0.083	0.146	-3.59	0.0273	0.00226
2.5	1.25	4.85	93.90	0.021	0.190	-4.07	0.0172	0.000362

Sulfur Distribution

As an example of the prediction for sulfur distribution consider the slag mentioned in the above silicon example-48.9% CaO (this includes MgO as equivalent to CaO by weight), 36.3% SiO_2, and 14.8% Al_2O_3-and a slag temperature of 1800°K. Further, assume the additional data of

%S in the ore	0.009 wt %
%Fe in the ore	55.238 wt %

%S in the coke 0.86 wt %

Coke rate 1416 lbs coke/ton hot metal

First, the carbon content of the hot metal is calculated by Eq. (24), considering only manganese and silicon (assuming 1 wt % Mn in the hot metal).

$$[\%C]_{SAT}=5.23+0.024[\%Mn]-0.304[\%Si]$$

$$[\%C]_{SAT}=5.23+0.024(1\%)-0.304(1.25\%)$$

$$[\%C]_{SAT}=5.23+0.024-0.38=4.87$$

f_s is estimated from the method of Sherman and Chipman[54] (see Figs. 16-19 of reference 37) for 4.87% C, 1% Mn, and 1.25% Si.

$\ln f_s=1.7$ $\quad f_s=5.5$ (1873°K)

C_s is estimated from page 601 of reference 28 and is a function of the basicity ratio of the slag.

$$\ln C_s=2.3[1.215(R_n-1.0)-4.031]$$

where the basicity ratio R_n is defined as

R_n=moles CaO+moles MgO/moles SiO_2+moles Al_2O_3 per 100 lbs of slag

For the slag under consideration,

$$R_n=(45.0/56.1)+(3.9/40.3)/(36.3/60.1)+(14.8/102.0)$$

$$=0.899/0.749=1.19$$

and

$$\ln C_s=2.3[1.215(1.19-1.0)-4.031]$$

$$\ln C_s=-8.74$$

$$C_s=1.6X10^{-4}\ (1773°K)$$

Although f_s is calculated for 1873°K and C_s for 1773°K the

temperature corrections for these values to 1800°K are not known exactly, and it is assumed that the errors are not very large.

The equilibrium constants, K_4 and K_5, are calculated from the data in Tables 16-5 and 16-6 of reference 37.

$\ln K_4 = 28200/[(1.987)(°K)] + 20.16/1.987$

at 1800°K, $\ln K_4 = 7.87 + 10.1 = 17.97$

$K_4 = 7.0 \times 10^7$

$\ln K_5 = 31520/[(1.987)(°K)] - 5.27/1.987$

at 1800°K, $\ln K_5 = 8.80 - 2.65 = 6.15$

$K_5 = 4.75 \times 10^2$

Using the relationship developed by Fincham and Richardson, Eq. (28),

$$(\%S)/[\%S] = f_s C_s K_4 / P_{CO} K_5 = (5.5)(1.6 \times 10^{-4})(7.0 \times 10^7)/P_{CO}(4.75 \times 10^2)$$

$$(\%S)/[\%S] = 130/P_{CO}$$

For 1 atmosphere pressure of CO, the distribution ratio for the sulfur is

$$(\%S)/[\%S] = 130$$

and for the pressure of CO at 2.5 atmospheres,

$$(\%S)/[\%S] = 130/2.5 = 52$$

To calculate the %S in the metal the amount of sulfur entering the furnace with the burden must be calculated.

Weight of ore per ton of hot metal (assuming 92.9% Fe in the hot metal) = (2000)0.929/0.5524 = 3370 lbs

Per cent S in the ore	0.009
Total sulfur in the ore	0.30 lbs

Weight of coke per ton of hot metal 1416.0 lbs

Per cent S in the coke 0.86

Total sulfur in coke 12.2 lbs

Total sulfur per ton hot metal 12.2+0.3=12.5 lbs

Let x=weight of sulfur in the hot metal and (12.5-x)=weight of sulfur in the slag.

$(\%S)/[\%S]=[(12.5-x)/905]/(x/2000)=130/p_{CO}$

For 1 atmosphere CO pressure

$(27.6-2.21x)/x=130$

$130x+2.21x=27.6$

$132.21x=27.6$

$x=0.208$ lbs in the metal

$(100)(0.208)/2000=0.0104\%$ S in the metal

For the slag, 12.50-0.208=12.3 lbs S in the slag

$(100)12.3/905=1.36\%$ S in the slag

For 2.5 atmospheres CO pressure

$(27.6-2.21x)/x=52$

$52x+2.21x=27.6$

$54.21x=27.6$

$x=0.51$ lbs in the metal

$(100)(0.51)/2000=0.0255\%$ S in the metal

For the slag, (12.50-0.51)=11.99 lbs in the slag

$(100)11.99/905=1.32\%$ S in the slag

TABLE IIb

	p_{CO}=1 atm	p_{CO}=2.5 atm
x, lbs of S in metal	0.208	0.51
[%S]=(100)x/2000	0.0104	0.0255
(%S)=(12.5)100/905	1.36	1.32

Manganese Distribution

Using the data of Bodsworth the equilibrium constant for the reaction $MnO+C \rightleftharpoons Mn+CO$ must be determined along with the activity coefficient of Mn, γ_{Mn}, in the hot metal.

The standard free energy change and the equilibrium constant are calculated from the following expression

$MnO+C=Mn+CO\uparrow$ $\quad K=a_{Mn}p_{CO}/a_{MnO}a_{C}$

$MnO \rightarrow Mn+1/2O_2$ $\quad \Delta G^\circ=95,400-19.7T$

$C+1/2O_2=CO$ $\quad \Delta G^\circ=-26,700-20.95T$

$MnO+C=Mn+CO$ $\quad \Delta G^\circ=68,700-40.65T$

$\Delta G^\circ=-RT\ln K=68,700-40.65T$

At 1800°K,

$\ln K=-[68,700/(1.987)(1800)-40.65/(1.987)]$

$\ln K=-[19.2-20.45]=1.25$

$K=3.5$

The γ_{Mn} can be determined from the interaction parameters that have been experimentally determined (see reference 2)

$\varepsilon_{Mn}^{C}=-0.5$ $\quad \varepsilon_{Mn}^{P}=-2.8$ $\quad \varepsilon_{Mn}^{S}=-5.9$

$\varepsilon_{Mn}^{Si}=0.0$ $\quad \varepsilon_{Mn}^{Mn}=0.0$ $\quad \gamma_{Mn}^{\circ}=1.0$

and the $\ln \gamma_{Mn}$ is expressed as

$$\ln\gamma_{Mn}=\ln\gamma^{\circ}_{Mn}+\varepsilon^{Mn}_{Mn}X_{Mn}+\varepsilon^{C}_{Mn}X_{C}+\varepsilon^{Si}_{Mn}X_{Si}+\varepsilon^{P}_{Mn}X_{P}+\varepsilon^{S}_{Mn}X_{S}$$

$$\text{or } \ln\gamma_{Mn}=-0.5X_{C}-2.8X_{P}-5.9X_{S}$$

For the metal composition at 1 atmosphere pressure-3.74% C, 4.90% Si, 0.102% P, and 0.0105% S- the mole fraction of each of the components is approximately 0.77Fe, 0.147C, 0.0826Si, 0.00155P, and 0.00015S, and γ_{Mn} becomes

$$\ln\gamma_{Mn}=-0.5(0.147)-2.8(\ 0.00155)-5.9(0.00015)$$

$$\ln\gamma_{Mn}=-0.0735-0.00436-0.00089=-0.07875$$

$$\gamma_{Mn}=0.924$$

Because Bodsworth calculated the γ_{MnO} assuming a value of γ_{Mn} in the metal of 0.80, the values of γ_{MnO} taken from Fig. 7.5 of reference 2 are increased to compensate for the higher calculated values of γ_{Mn}. For the problem under consideration the ratio of wt% CaO/wt% SiO_2 is 45.0/36.3=1.24 and the corresponding value of γ_{MnO} from Fig. 7.5 of reference 2 is 0.82. Correcting this value to compensate for the increased value of γ_{Mn}, we have

$$\gamma_{MnO}/0.924=0.82/0.80$$

$$\gamma_{MnO}=0.946$$

Assuming that the mole fractions of MnO and Mn can be approximated by % MnO and % Mn, the manganese distribution becomes

$$K=(a_{Mn})p_{CO}/(a_{MnO})(a_{C})=(\gamma_{Mn})(\%_{Mn})(p_{CO})/(\gamma_{MnO})(\%_{MnO})(a_{C})$$

$$[\%Mn]/(\%MnO)=K(\gamma_{MnO})/(\gamma_{Mn})(p_{CO})=(3.5)(0.946)/(0.924)(1.0)=3.59$$

The total amount MnO entering the furnace per ton of hot metal is 30.6 lbs which produces 23.7 lbs of Mn.

Let x be the weight of Mn in the hot metal, and (23.7-x)71/55/905 be the weight of MnO in the slag.

For 1 atmosphere pressure

$(x/2000)/[(23.7-x)71/(55\ 905)]=3.59$

$x=21.6$ lbs of Mn in the hot metal

The MnO in the slag is $30.6-1.29x=2.7$ lbs

For the metal composition at 2.5 atmospheres pressure-4.85% C, 1.25% Si, 0.102% P, and 0.0255% S-the mole fraction of each of the components is approximately 0.788 Fe, 0.189 C, 0.021 Si, 0.00155 P, and 0.00038 S. γ_{Mn} for these conditions becomes

$\ln\gamma_{Mn}=-0.5(0.189)-2.8(0.00155)-5.9(0.00038)$

$\ln\gamma_{Mn}=-0.0945-0.0043-0.00224=-0.10104$

$\gamma_{Mn}=0.904$

Correcting the value of γ_{MnO}, we have

$\gamma_{MnO}/0.904=0.82/0.80$

$\gamma_{MnO}=0.925$

The manganese distribution for $p_{CO}=2.5$ atmospheres becomes

$[\%Mn]/(\%MnO)=K(\gamma_{MnO})/(\gamma_{Mn})(p_{CO})=(3.5)(0.925)/(0.904)(2.5)=1.44$

$(x/2000)/[(23.7-x)71/(55\ 905)]=1.44$

$x=19$ lbs

The MnO in the slag is $30.6-1.29x=6.1$ lbs

TABLE IIIb

	p_{CO}=1 atm	p_{CO}=2.5 atm
x, lbs of Mn in the hot metal	21.6	19.0
[%Mn]=(100)x/2000	1.08	0.95
(%MnO)=(23.7-x)71/(55 905)	0.30	0.67

The predictions of the metal composition of Si, S, and Mn from the examples given above show that the assumption of equilibrium or a close approach to equilibrium produces much more reasonable compositions for 2.5 atmospheres pressure than for 1.0 atmosphere pressure. 1.25% Si, 0.026% S, and 0.95% Mn are all extremely acceptable values for the slag composition, temperature, and charge conditions considered. The distribution resulting from the consideration of 1 atmosphere are very unreasonable for silicon and sulfur-4.90% Si and 0.01% S, with manganese recovery being higher than that predicted at 2.5 atmospheres. In actual practice it has been found that manganese recoveries are smaller than those predicted by equilibrium at 1 atmosphere pressure of CO.

Metal and Slag Composition Prediction

Based on the earlier discussion of the furnace hearth conditions and the examples discussed above, the slag and metal compositions are predicted from the known furnace charge data such as charge rate of ore, coke, and stone, the chemical make-up of these materials, and the temperature of the slag phase in the furnace hearth. In this model all of the CaO, MgO, and Al_2O_3 that enter the furnace are assumed to enter the slag phase (very close

to actual furnace conditions in which the Al, Ca, and Mg contents of the hot metal are negligible) and for the most part the slag is considered to be composed of CaO, MgO, Al_2O_3, and SiO_2 only.

The silicon content of the metal is calculated first, assuming only an Fe-C-Si melt for the metal phase. A silicon composition is initially chosen for the metal and using a simple material balance on silicon, the resulting slag composition of silicon is determined. If the activities of the silicon in the metal and the silica in the slag are such that the equilibrium constant is satisfied,

$$K=(a_{Si})(p_{CO})/(a_{SiO_2})(a_C)$$

the model moves on to the sulfur prediction. However, if the equilibrium constant is not satisfied, a new value for the metal silicon is selected and the entire process repeated until the equilibrium constant at the temperature of interest is satisfied.

The metal is assumed to be saturated with carbon and a_C=1.0. The data of Turkdogan, Grieveson, and Beisler[35] are used for the γ_{Si} calculations. From their data $\ln\gamma_{Si}$ is found as a linear function of X_{Si} for carbon saturation of the metal and for a given temperature. The data of Rein and Chipman[39] are used to determine γ_{SiO_2} for $CaO-SiO_2-Al_2O_3$ slags with the data of γ_{SiO_2} being curve fit as a function of X_{CaO} for given $X_{AlO_{1.5}}$ values at 1550°C. For the slag, MgO is considered equivalent to CaO on a weight basis as suggested by Chipman and discussed earlier. Temperature corrections are allowed for in the calculations of

γ_{Si} and γ_{SiO_2}, but temperature corrections for γ_{SiO_2} are considerably more approximate than for γ_{Si}.

The sulfur distribution between slag and metal is obtained by the method described previously, using Eq. (28),

$$[\%S]/(\%S)=K_5\ p_{CO}/f_s\ C_s\ K_4$$

for which the values of f_s, C_s, K_4, and K_5 are determined. The sulfur capacity, C_s, is calculated from page 601 of reference 28, vol. II, and is a linear function of the slag basicity ratio (where the basicity ratio, R_n, is defined as (moles CaO+moles MgO)/(moles SiO_2+moles Al_2O_3) per 100 pounds of slag).

$$\ln C_S=2.3(1.215(R_n-1.0)-4.031).$$

f_S is determined by the method of Sherman and Chipman and the data from Fig. 16-19 of reference 28. K_4 and K_5 are determined from the data of Tables 16-5 and 16-6 of reference 42.

$$K_5=\exp\ 31{,}520/(R)(T°K)-5.27/R$$

$$K_4=\exp\ 28{,}200/(R)(T°K)+20.16/R$$

where R is the universal gas constant and T is the temperature in °K. With these values and a simple material balance on S between slag and metal the sulfur distribution ratio is easily determined.

It must be noted that the value of f_S is determined for 1600°C and the C_S value determined from data for 1500°C. The corrections for temperature are not known exactly, and Philbrook and Manning concluded that the errors resulting from the temperature difference are probably not very large.

All of the phosphorus that enters the furnace in the solid

burden is assumed to enter the metal. Therefore, the phosphorus content of the hot metal is simply a matter of determining the total amount of phosphorus entering the furnace per unit measure of time or weight of metal produced.

The data collected by Bodsworth for the $\ln\gamma_{MnO}$ is employed in the model. It has been found for a number of examples that the data of Neumann and Schenck[51] and of Filer and Darken[24] predict hot metal manganese compositions that are consistently too high, while the method using the data of Bodsworth[52-54] give very reasonable manganese compositions for the metal.

γ_{MnO} is a linear function of wt % CaO/SiO_2 for values of CaO/SiO_2 greater than 1.0 for 1540°C. The values of γ_{MnO} were computed by Bodsworth assuming a value of $\gamma_{Mn}=0.8$ as mentioned in the example above. These values of γ_{MnO} are corrected for the calculated values of γ_{Mn} which are approximately 0.90 for all the blast furnace metal considered. The equilibrium constant is found from the free energy of the reaction as given by Kubaschewski and Evans[57]

$$\Delta G^\circ=-RT\ln K=68{,}700-40.65T$$

γ_{Mn} for the metal is determined from the expression

$$\ln\gamma_{Mn}=\ln\gamma^\circ_{Mn}+\varepsilon^{Mn}_{Mn}X_{Mn}+\varepsilon^{C}_{Mn}X_C+\varepsilon^{S}_{Mn}X_S+\varepsilon^{P}_{Mn}X_p+\varepsilon^{Si}_{Mn}X_{Si}$$

with the interaction coefficients taken from Bodsworth. The Fe-Mn binary is assumed to exhibit ideal behavior, and as a result γ°_{Mn} is equal to 1.0. The effects of the MgO and Al_2O_3 contents of the

slag on the value of γ_{MnO} are neglected as their behavior is not clearly known although the effects on γ_{MnO} appear to be very small. Although the interaction coefficients used for γ_{MnO} calculations correspond to a temperature of 1600°C, and the data for γ_{MnO} correspond to 1540°C, no corrections are made for different temperatures.

The carbon composition for the metal droplets in the slag is calculated from Eq. (24) mentioned earlier with the temperature being that of the slag phase. The final C composition of the metal at tapping is also calculated from Eq. (24), but the temperature is taken as that of the metal, which is always assumed to be 30°K less than that of the slag.

REFERENCES

1. Making, Shaping, and Treating of Steel, Edited by H. E. McGannon, United States Steel Corporation, 1964.

2. C. Bodsworth, Physical Chemistry of Iron and Steel Manufacture, Toronto, Longmans, 1963.

3. Blast Furnace-Theory and Practice, Volumes 1 and 2, Edited by J. H. Strassburger, New York, Gordon and Breach Science Publishers, 1969.

4. R. G. Ward, An Introduction to the Physical Chemistry of Iron and Steel Making, London, Edward Arnold Publishers Ltd., 1962.

5. A. Poos and A. Decker, "Heat Balances and Coke-Consumption in the Blast Furnace", Revue Universelle des Mines, 1959, 15, 19-32.

6. R. Sevrin, A. Poos, and A. Decker, "The Application of a Digital Computer to the Calculation of Material and Heat Balances in the Blast-Furnace", Journal of the Iron and Steel Institute, 1962, 200, 34-37.

7. W. E. Marshall, "A Method of Estimating Blast Furnace Production and Coke Consumption", AISI Year Book, 1947, 379-404.

8. R. V. Flint, "Multiple Correlation of Blast Furnace Variables", AIME Proceedings on Blast Furnace, Coke Oven, and Raw Materials Conference, 1952, 11, 49-73.

9. R. V. Flint, "Effect of Burden Materials and Practices on Blast Furnace Coke Rate", Blast Furnace and Steel Plant, 1962, 50, 47-58.

10. A. N. Pokvisnev and I. F. Kurunov, "Criterion of Thermal State of the Hearth in Connection with the Thermal State of a Blast Furnace". Stal in English, 1965, April, 257-260.

11. A. F. Rebeko, L.S. Mkrtchan, and V. V. Besfamil'nyi, "Silicon Content of Pig Iron as a Criterion of the Thermal State of a Blast Furnace", Stahl in English, 1966, April, 260-262.

12. J. M. Ridgion, "Blast-Furnace Heat Balance in Stages: Development of a Computer Program" Journal of the Iron and Steel Institute, 1962, 200, 389-394.

13. J. Michard, P. Dancoisne, and G. Chanty, "Blast Furnace Practice with 100% Low Grade Self-Fluxing Sinter", AIME Proceedings on Blast Furnace, Coke Oven, and Raw Materials Conference, 1961, 20, 329-351.

14. E. Schurmann, W. Zischkale, P. Ischebeck, and G. Heynert, "Reduktionsablauf und Temperaturprofil im Hochofen", Stahl und Eisen, 1960, 80, 854-861.

15. H. N. Lander, H. W. Meyer, and F. D. Delve, "A Thermochemical Model of the Blast Furnace", Transactions of the Metallurgical Society of AIME, 1961, 221, 485-492.

16. A. L. Hodge and E. R. Wyczalek, "A Mathematical Model for Analyzing and Predicting Changes in Blast Furnace Operation", Linde Company Report, 1961.

17. P. Dancoisne, "Mathematical Model of the Blast Furnace", Canadian Metallurgical Quarterly, 1963, 2, 197-219.

18. C. Staib and J. Michard, "On Line Computer Control for the Blast Furnace", (Two Parts), Journal of Metals, 1965, 17, 33-39, and 17, 165-170.

19. V. Koump, R. H. Tien, R. G. Olsson, and T. F. Perzak, "Mathematical Simulation of the Stack Region of the Blast Furnace", Process Simulation and Control in Iron and Steel Making, Edited by J. M. Uys and H. L. Bishop, New York, Gordon and Breach Science Publishers, 1966.

20. A. K. Lahiri and V. Seshadri, "An Analysis of the Blast Furnace Process Based on a Dynamic Model", Journal of the Iron and Steel Institute, 1969, 207, 293-307.

21. I. Muchi, "Mathematical Model of the Blast Furnace", Transactions of the Iron and Steel Institute of Japan, 1967, 7, 223-237.

22. C. Staib, N. Jusseau, J. Vigliengo, and J. C. Cochery, "Blast Furnace Dynamic Behavior and Automatic Control", IRSID Report RE 189, Nov. 1967.

23. C. J. Fielden and B. I. Wood, "A Dynamic Digital Simulation of the Blast Furnace", Journal of the Iron and Steel Institute, 1968, 206, 650-658.

24. E. W. Filer and L. S. Darken, "Equilibrium Between Blast-Furnace Metal and Slag as Determined by Remelting", Journal of Metals, 1952, 4, 253-257.

25. A. J. Burgess and B. G. Balwin, "Influence of Slag Properties on Pig-Iron Composition", Journal of the Iron and Steel Institute, 1957, 186, 227-235.

26. G. G. Hatch and J. Chipman, "Sulfur Equilibria Between Iron Blast Furnace Slags and Metal", Transactions of the Metallurgical Society of the AIME, 1949, 185, 274-284.

27. W. O. Philbrook and F. S. Manning, "Rate Phenomena", Chapter 27, Blast Furnace-Theory and Practice, volume 2.

28. J. F. Elliott, M. Gleiser, and V. Ramachrishna, Thermochemistry for Steelmaking, Vol II, Reading, Mass., Addison-Wesley, 1963, 558, 600-602.

29. F. Neumann and H. Schenck,"Die durch zusatzelemente bewirkte Aktivitatsanderung von Kohlenstoff in flussigen Eisenlosunger nahe der Kohlenstoffsattigung", Archiv Eisenhuttenw, 1959, 30, 477-483.

30. H. Schenck, G. Frohberg, and E. Steinmetz, "Untersuchungen uber wechselseitige Aktivitatseinflusse in homgenen metallischen Mehrstofflosungen", Archiv Eisenhuttenw, 1963, 34, 37-42.

31. U. Feldman, "Zur Thermodynamik flussiger eisenreicher und kohlenstoffhalliger ternarer Legierungen", Archiv Eisenhuttenw, 1963, 34, 49-54.

32. U. Feldman, "Uber einige thermodynamische Eigenschaften des Systems Eisen-Silizium Kohlenstoff bei den Temperaturen der Stahlerzeugung", Ibid, 109-113.

33. O. Skiredj and J. F. Elliott, "Carbon Content of Graphite-Saturated Fe-Si-Mn Alloys, 1400-1650°C", Transactions of the Metallurgical Society of the AIME, 1963, 227, 536-538.

34. J. Chipman and R. Baschwitz, "The Activity of Silicon in Liquid Fe-Si-C Alloys", Transactions of the Metallurgical Society of the AIME, 1963, 227, 473-478.

35. E. T. Turkdogan, P. Grieveson, and J. F. Beisler, "Kinetic and Equilibrium Considerations for Silicon Reaction Between Silicate Melts and Graphite-Saturated Iron Part 1: Reaction Equilibria", Transactions of the Metallurgical Society of the AIME, 1963, 227, 1258-1264.

36. P. J. Boules, H. F. Ramstad, and F. D. Richardson, "Activities of Silicon in Metals and Alloys", Journal of the Iron and Steel Institute, 1964, 202, 113-121.

37. G. Smith and J. Taylor, "Activity of Silicon in Liquid-Iron Solutions", Journal of the Iron and Steel Institute, 1964, 202, 577-580.

38. D. Schroeder and J. Chipman, "The Influence of Carbon on the Activity Coefficient of Silicon in Liquid Iron-Carbon-Silicon", Transactions of the Metallurgical Society of the AIME, 1964, 230, 1492-1494.

39. R. H. Rein and J. Chipman, "The Distribution of Silicon Between Fe-Si-C Alloys and SiO_2-CaO-MgO-Al_2O_3 Slags", Transactions of the Metallurgical Society of the AIME, 1963, 227, 1193-1203.

40. D. A. R. Kay and J. Taylor, "Activities of Silica in the Lime + Alumina + Silica System", Transactions of the Faraday Society, 1960, 56, 1372-1386.

41. C. B. J. Fincham and F. D. Richardson, "Sulfur in Silicate and Aluminate Melts", Proceedings of the Royal Society, 1954, A223, 40-62. (See also Journal of the Iron and Steel Institute, 1954, 178, 4-15.)

42. Physical Chemistry of Steelmaking Committee (AIME), Electric Furnace Steelmaking, Vol II, Theory and Fundamentals, New York, Interscience Publishers, 1963, Chapter 16.

43. F. D. Richardson, "The Climate of Extractive Metallurgy in the 1960's", Transactions of the Metallurgical Society of the AIME, 1964, 230, 1212-1228.

44. H. Flood and J. M. Toguri, "The Application of the Mass Action Law to Metal-Slag Equilibria", Transactions of the Metallurgical Society of the AIME, 1963, 227, 525-529.

45. S. S. Wise and J. L. Margrave, "The Heats of Formation of Silicon Tetrafluoride and Silica", Journal of Physical Chemistry, 1963, 63, 815-821.

46. K. K. Kelley, "Contributions to the Data on Theoretical Metallurgy XIII. High Temperature Heat Content, Heat Capacity, and Entropy Data for the Elements and Inorganic Compounds", Bureau of Mines Bulletin-584, 1960.

47. C. E. Wicks and F. E. Block, "Thermodynamic Properties of 65 Elements-Their Oxides, Halides, Carbides, and Nitrides", Bureau of Mines Bulletin-605, 1963.

48. J. F. Elliott and M. Gleiser, Thermo-Chemistry for Steelmaking, Vol I, Reading, Mass., Addison-Wesley, 1960.

49. J. Chipman, Physical Chemistry of Process Metallurgy, Part I, New York, Interscience, 1960, 27.

50. W. O. Philbrook, Private communication to S. K. Tarby.

51. F. Neumann and H. Schenck, "Der Einflub der Oxyde von Magnesium und Aluminium auf die Reaktionsgleichgewichte des Mangans zewischen kohlenstoffgesattigtem siliziumhaltigem Eisen und Kalk-Kieselsaure-Schlacken bei 1500°C", Archiv Eisenhuttenw, 1960, 31, 83-87.

52. N. J. Grant, J. W. Dowding, and R. J. Murphy, "Manganese as an Indicator of Blast Furnace Slag Oxidation and Desulphurizing Power", Transactions of the Metallurgical Society of the AIME, 1953, 197, 1451-1454.

53. J. E. Stukel and J. Cocubinsky, "Distribution of Manganese Between Slag and Metal Under Reducing Conditions", Transactions of the Metallurgical Society of the AIME, 1954, 200, 353-356.

54. C. W. Sherman and J. Chipman, "Activity of Sulfur in Liquid Iron and Steel", Transactions of the Metallurgical Society of the AIME, 1952, 194, 597-602.

55. J. Taylor, "Silica Reduction Reaction in the Blast Furnace", Journal of the Iron and Steel Institute, 1964, 202, 420-423.

56. Tables of Thermal Properties of Gases, U. S. Department of Commerce, National Bureau of Standards-Circular 564, November, 1955.

57. O. Kubaschewski and L. L. Evans, Metallurgical Thermochemistry, 3rd Edition, Pergamon Press Ltd., 1958.

VITA

John Donald Oakey was born on October 13, 1943 in Newark, New Jersey to Douglas F. and Betty Lou Oakey. In June of 1961 Mr. Oakey graduated from Dunmore High School, Dunmore, Pennsylvania and in September of 1961 he matriculated at Lehigh University. He graduated with high honors from Lehigh in June 1965 with the degree of Bachelor of Science in Metallurgical Engineering. While an undergraduate, Mr. Oakey was elected to Tau Beta Pi and Alpha Sigma Mu and served as the president of the student metallurgical society.

In September of 1965 Mr. Oakey initiated a program of graduate study in the Department of Metallurgy and Materials Science at Lehigh University. He received a Master of Science degree in Metallurgy and Materials Science in October 1967, the title of the thesis being "The Effects of Magnesium Additions on the Electrical Resistivity Behavior of Lithium-Doped Cobalt Oxide (CoO)". From the fall of 1967 to the present he has served as an instructor in the Department of Metallurgy and Materials Science.

In August 1965 Mr. Oakey was married to the former Patricia Jean Peacock. They are the parents of a daughter, Jennifer Lynn, born in February 1969.